



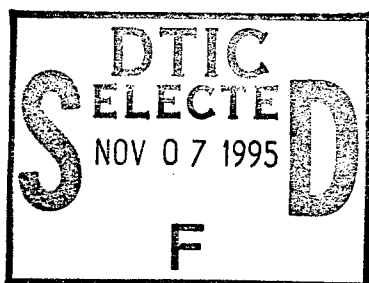
**US Army Corps
of Engineers**

Waterways Experiment
Station

Miscellaneous Paper GL-95-4
September 1995

Full Waveform Inverse Modeling of Ground Penetrating Radar Data: An Initial Approach

by Janet E. Simms, Dwain K. Butler, WES
Michael H. Powers, U.S. Geological Survey



19951106 016

Approved For Public Release; Distribution Is Unlimited

DTIC QUALITY INSPECTED 5

Prepared for Discretionary Research Program
U.S. Army Engineer Waterways Experiment Station

The contents of this report are not to be used for advertising, publication, or promotional purposes. Citation of trade names does not constitute an official endorsement or approval of the use of such commercial products.



PRINTED ON RECYCLED PAPER

Full Waveform Inverse Modeling of Ground Penetrating Radar Data: An Initial Approach

by Janet E. Simms, Dwain K. Butler

U.S. Army Corps of Engineers
Waterways Experiment Station
3909 Halls Ferry Road
Vicksburg, MS 39180-6199

Michael H. Powers

U.S. Geological Survey
Box 25046, MS 964
Denver, CO 80225-0046

Accession For	
NTIS CRA&I	<input checked="checked" type="checkbox"/>
DTIC TAB	<input type="checkbox"/>
Unannounced	<input type="checkbox"/>
Justification	
By	
Distribution /	
Availability Codes	
Dist	Avail and/or Special
A-1	

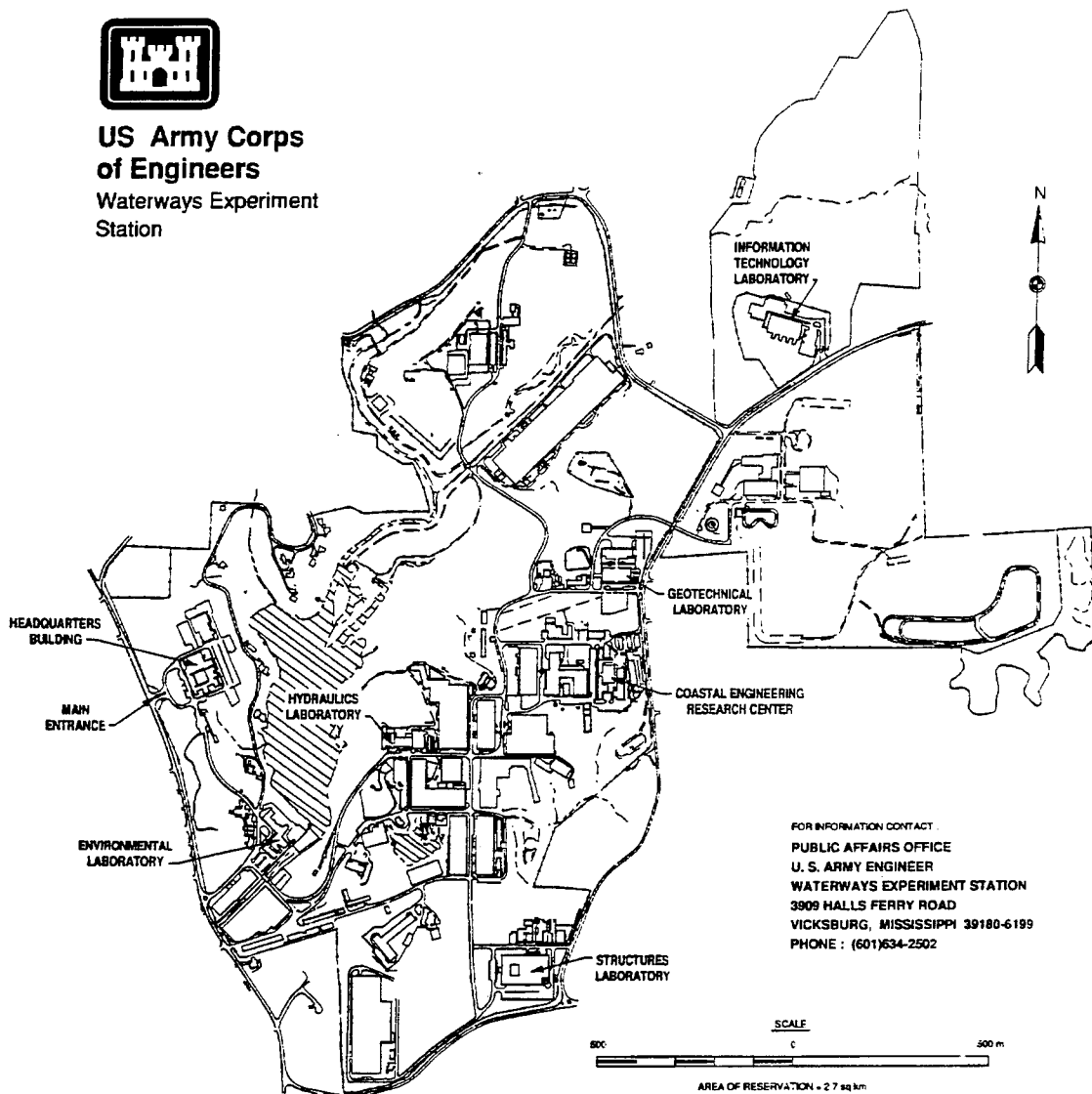
Final report

Approved for public release; distribution is unlimited

Prepared for Discretionary Research Program
U.S. Army Engineer Waterways Experiment Station
3909 Halls Ferry Road, Vicksburg, MS 39180-6199



**US Army Corps
of Engineers**
Waterways Experiment
Station



Waterways Experiment Station Cataloging-in-Publication Data

Simms, Janet E.

Full waveform inverse modeling of ground penetrating radar data : an initial approach / by Janet E. Simms, Dwain K. Butler, Michael H. Powers ; prepared for Discretionary Research Program, U.S. Army Engineer Waterways Experiment Station.

133 p. : ill. ; 28 cm. — (Miscellaneous paper ; GL-95-4)

Includes bibliographic references.

1. Ground penetrating radar. 2. Radar in earth sciences. I. Butler, Dwain K. II. Powers, Michael H. III. United States. Army. Corps of Engineers. IV. U.S. Army Engineer Waterways Experiment Station. V. Geotechnical Laboratory (U.S. Army Engineer Waterways Experiment Station) VI. Laboratory Discretionary Research Program (U.S. Army Engineer Waterways Experiment Station) VII. Title. VIII. Series: Miscellaneous paper (U.S. Army Engineer Waterways Experiment Station) ; GL-95-4.

TA7 W34m no.GL-95-4

Contents

Preface	iv
Conversion Factors, Non-SI to SI Units of Measurement	v
1—Introduction	1
Background and Applications	1
Justification and Relevance	2
Scope of Work	2
2—Electromagnetic Wave Theory	4
Propagation Velocity, Attenuation, and Wavelength	4
Reflection and Transmission at Boundaries	9
3—Forward Modeling of GPR Data	12
Forward Modeling Example	14
4—Full Waveform GPR Forward Modeling Investigations	16
Modeling Problem Selection and Details	16
Scope and Results of the Modeling Study	21
5—GPR Inverse Modeling	25
Parameter Considerations	25
Manual Inversion of GPR Data	28
6—Conclusions	30
References	31
Figures 1-18	
Appendix A: Table of Cases for Forward Modeling Problem Sets	A1
Appendix B: GPRMODv2 Forward Modeling Results for Problem Set 1	B1
Appendix C: GPRMODv2 Forward Modeling Results for Problem Set 2	C1
SF298	

Preface

This report describes the work performed under the U.S. Army Engineer Waterways Experiment Station (WES) Laboratory Discretionary Research Program titled "Full Waveform Inverse Modeling of Ground Penetrating Radar Data." The research was performed by Drs. Janet E. Simms and Dwain K. Butler, Earthquake Engineering and Geosciences Division (EEGD), Geotechnical Laboratory (GL). Outside technical assistance was provided by Mr. Michael H. Powers, United States Geological Service, Denver, CO. Ms. Lori Davis assisted in preparing this report. The work was performed under the direct supervision of Mr. Joseph R. Curro, Jr., Chief, Engineering Geophysics Branch, EEGD. The work was performed under the general supervision of Drs. A. G. Franklin, Chief, EEGD, and William F. Marcuson III, Director, GL.

At the time of publication of this report, Director of WES was Dr. Robert W. Whalin. Commander was COL Bruce K. Howard, EN.

The contents of this report are not to be used for advertising, publication, or promotional purposes. Citation of trade names does not constitute an official endorsement or approval of the use of such commercial products.

Conversion Factors, Non-SI to SI Units of Measurement

Non-SI units of measurement used in this report can be converted to SI units as follows:

Multiply	By	To Obtain
feet	0.3048	meters
feet per second	0.3048	meters per second
millimho per foot	3.28	millisiemen per meter

1 Introduction

Background and Applications

Ground penetrating radar (GPR) is an electromagnetic (EM) geophysical method that has emerged as a versatile high resolution tool for a variety of applications. When GPR systems became commercially available in the 1970's, the capabilities of GPR were easily oversold to a market eager for "high-tech" solutions to difficult subsurface problems. In certain geologic settings, even the very early GPR systems could produce real time graphic records (i.e., no processing required) which resembled snapshots of the subsurface. This tendency to oversell the method led to frequent application of GPR to inappropriate sites and objectives. Another problem was the use of GPR by inexperienced personnel. Fortunately, the capabilities and limitations of GPR are now better understood by geophysicists and the geotechnical and geoscience community as a whole, and the method is being more rationally exploited. In cases where GPR has a sufficient depth of investigation capability to address a specific problem, it has the greatest horizontal and vertical resolution of any geophysical method that can be applied to the problem.

GPR is applicable to a broad spectrum of interests and problems in geotechnical engineering and geoscience (Butler 1992). Some of the areas of application include the following: geological mapping (Butler et al. 1990; Davis and Annan 1989), foundation investigations (Butler et al. 1989), cavity and sinkhole mapping in karst areas (Ballard 1983), ground water investigations (Bohling et al. 1989), archaeological studies (Butler et al. 1994), detection and mapping of buried cultural features, e.g., waste disposal trenches, utilities, barrels, underground storage tanks, unexploded ordnance, etc. (Sharp et al. 1990; Llopis and Simms 1993), contaminant detection and mapping in the subsurface (Brewster and Annan 1994), and structural studies of buildings, bridges, dams, etc. In a military context, key areas of application are pavement assessment and evaluation (Maser and Scullion 1992), airfield evaluation, tunnel detection, concrete structure investigations, installation restoration, and foundation investigations.

Most commercially available GPR's are short pulse, time domain, EM wave propagation systems. The GPR systems use closely spaced EM transmitters (Tx) and receivers (Rx), and the common graphic data display of GPR waveforms side-by-side resembles a common depth point (CDP) seismic section (Figure 1). In the cartoon in Figure 1a, the Tx and Rx are both contained in the box indicated as "antennae"; for many GPR systems the Tx and Rx are separate, and the spacing

between them can be varied. When interpreting the GPR record, however, factors must be considered which are not relevant in seismic reflection: scattering from gravel, cobbles, microcrack clusters, and other small geologic inhomogeneities; backscatter signatures from overhead powerlines and surface structures which can masquerade as subsurface features in the GPR record; and minor changes in the dielectric properties of soil, rock or water which can appear as major GPR signatures but do not affect other physical properties, such as seismic velocity. Advantages of GPR are high vertical and horizontal resolution, rapid survey capability, and near-real time data interpretation in many cases. Major disadvantages are the site specific applicability and limited depth of investigation capability (generally less than 15 m).

Justification and Relevance

Ground penetrating radar surveys are often interpreted in a qualitative manner to identify anomalies. This method of interpretation is used to determine the existence of a feature, when specific properties of the feature are of no interest. For example, in the case of the hypothetical GPR cross-section in Figure 1a, the extent of the interpretation typically is limited to (1) identification of radar events corresponding to subsurface reflectors (interfaces) and (2) determination of depths to the interfaces assuming an average EM wave propagation velocity. However, GPR data can also be interpreted quantitatively to give more definitive depths, geometry, and EM (physical) properties of the subsurface material. Existing analysis procedures are simplistic, making use of only a small amount of the information contained in the received GPR waveforms, and do not consider electromagnetic wave attenuation, dispersion, scattering, geometric spreading, and interface reflection/transmission losses. The aim of this research is to develop interpretation procedures which utilize the full GPR waveform (Figure 1b) for determining layer thicknesses and the EM properties of subsurface materials.

Scope of Work

This work consisted of three phases: 1) review existing capability for full waveform forward modeling of GPR signals, 2) develop a catalog of theoretical GPR receiver waveforms for representative layered models (pavements, concrete with air- and water-filled cavities, etc.) of interest using typical physical property values, and 3) examine the feasibility of developing an inverse modeling procedure to determine physical properties by comparing full waveform forward solutions to measured GPR signatures.

The first phase involved identifying available GPR modeling programs and determining which, if any, are suitable for performing full waveform forward modeling of GPR signals for use in an inverse modeling program or procedure. The primary criteria are that the model assumptions must be realistic and defensible and that the major EM phenomena (spreading, attenuation, dispersion, reflection/transmission, scattering, multiples) be included. One GPR forward modeling program met the requirements, "GPRMODv2" (Powers and Olhoeft

1995). Since this project began, GPRMODv2 underwent a major revision and the authors were cooperative in incorporating special program features to facilitate this research. The concepts of GPR surveying and the key theoretical aspects of EM wave propagation in a layered media are developed in Chapter 2. The major assumptions and conditions of the forward modeling program will be examined in Chapter 3.

For Phase 2 of this project, the forward modeling program GPRMODv2 was used to generate models representative of pavement structure and concrete with air- or water-filled cavities. Parameters were varied for both two and three layer models to investigate their affect on the resulting GPR waveform.

Finally, for Phase 3, the requirements of developing an inverse GPR modeling capability are surveyed. First the procedures for manually adjusting the parameters of a subsurface model in an iterative manner to match model output with field GPR records is considered. Next the possibilities and advantages of simplifying the inversion process by constraining and/or reducing the number of model parameters is addressed. The number of model parameters can be reduced by simply eliminating some parameters from consideration in the inversion or by determining some parameters in advance by other means. If some parameters are known or assumed for the subsurface model, then they can be fixed or constrained during the inversion, thereby simplifying the inversion process. Parameters can be independently determined by laboratory testing on soil/rock samples in the laboratory, from drilling logs, from the results of electrical resistivity and electromagnetic soundings, from wide-angle GPR reflection/refraction surveys, and from push probe time domain reflectometry (TDR). The possibility of cross-correlation of the GPR waveform with the transmitter waveform or deconvolution of the GPR waveform to determine number and location of interfaces as the first phase of inversion is studied. Finally, the type of inversion procedure most likely to succeed will be determined: global inverse solution, such as typically used for electrical resistivity and frequency- and time-domain EM inversion, or a "layer-stripping" inversion process.

2 Electromagnetic Wave Theory

Ground penetrating radar is an electromagnetic (EM) method which operates in the megahertz (MHz) or gigahertz (GHz) frequency range. At these high frequencies displacement currents (currents associated with charges which are constrained from moving continuously) dominate and energy propagates into the ground as a wave. An electromagnetic pulse transmitted into the earth undergoes refraction, reflection, scattering, and dispersion. Contrast in the dielectric permittivity at layer boundaries causes the EM wave to be reflected and refracted. The dielectric permittivity is the proportionality factor relating the displacement current to energy. Since electromagnetic fields consist of both electric and magnetic fields, any property of the geologic material which affects either of these fields will also affect the propagation of the EM wave in the subsurface. Generally, the electrical properties of the soil and rock have a greater variation than the magnetic properties and, therefore, a greater influence on the EM wave propagation. Soil conductivity, which is usually controlled by the moisture content, is a major factor in determining if GPR can be used successfully at a site. High conductivity soils, such as those with high clay content, can significantly attenuate the EM signal and render GPR virtually useless.

Propagation Velocity, Attenuation, and Wavelength

The governing wave equation appropriate for ground penetrating radar is derived from Maxwell's equations (Balanis 1989, chapters 1 and 3). For a plane wave moving through a source-free material it is

$$\nabla^2 \mathbf{E} = -k^2 \mathbf{E} \quad \text{or} \quad \nabla^2 \mathbf{E} = \gamma^2 \mathbf{E},$$

where k is the complex wave vector, γ is known as the propagation vector, \mathbf{E} is the electric field vector, and ∇^2 is the Laplacian operator. Both k and γ are used in the literature, and the relationship between them is simply $\gamma = ik$ where $i = \sqrt{-1}$. The material can be dispersive (velocity varying with frequency) and lossy, inhomogeneous, anisotropic, or none of these, depending on how the wave vector (or number) or propagation vector (or constant) is characterized. In the most general terms, a solution to this equation, which describes the plane wave moving through the material, is

$$\mathbf{E}(\mathbf{r}) = \mathbf{e}_r E_0 e^{\pm i(\mathbf{k} \cdot \mathbf{r})}$$

where \mathbf{r} is the position vector, \mathbf{e}_r is a unit vector in the direction of the electric field, and E_0 is an initial amplitude of the electric field. If a harmonic time-dependence is assumed, as in a propagating EM wave, this general solution becomes

$$\mathbf{E}(\mathbf{r}) = \mathbf{e}_r \text{Real} [e^{i\omega t} E_0 e^{\pm i(\mathbf{k} \cdot \mathbf{r})}].$$

If the material is assumed to be homogeneous, then its properties do not vary as a function of position. Almost all rocks and soils have some heterogeneities, but on a scale similar to the GPR wavelength, they can generally be divided into volumes of homogeneous materials with the property differences occurring at defined boundaries. If the material is isotropic, then the properties are not direction dependent. Anisotropy is not uncommon in rocks, as most crystalline structures show distinct anisotropy, but again on the scale of most GPR wavelengths an assumption of isotropy is not unrealistic. The material can also be assumed linear, meaning its properties do not vary with the amplitude of the electric or magnetic field. This is true at the low magnitudes of the fields produced by ground penetrating radar systems. See Keller (1987) or Balanis (1989, chapter 2) for more information on these material property assumptions.

As an EM wave moves through a material, a given location experiences an electric and magnetic field that reverses polarity with time. When the material is in the presence of an electric field, some energy is lost as charge transport takes place according to the conductivity. Some energy is stored by charge polarization processes according to the measure of dielectric permittivity. However, different polarization processes take different amounts of time to complete, and the frequency of the EM wave will determine how much energy is stored for a given polarity cycle. This results in a frequency dependent dielectric permittivity. Each polarization process also involves some amount of energy loss through brief conductive losses while the charges are moving to their polarized state. This is the displacement current loss, sometimes called an alternating conductivity, or a dielectric relaxation loss, and can be characterized by making the dielectric permittivity complex (Olhoeft 1981). The magnetic permeability of most rocks and soils is not much different from the magnetic permeability of free space, but when iron is present it can also be frequency dependent and complex with magnetic relaxation effects (Olhoeft and Strangway 1974; Olhoeft and Capron 1994).

For isotropic, homogeneous materials, the wave vector or propagation vector reduce to complex, frequency dependent values called the wavenumber or propagation constant. Depending on the properties of the material, the wavenumber and propagation constant may be further reduced. In free space, where the conductivity is zero and propagation exists with no material losses, the wavenumber is

$$k = \omega \sqrt{\mu_0 \epsilon_0}$$

where ω is the angular frequency, μ_0 is the magnetic permeability of free space ($4\pi \times 10^{-7}$ Henries/meter), and ϵ_0 is the dielectric permittivity of free space

(8.854×10^{-12} Farads/meter). The solution for a plane wave traveling in the z direction reduces to

$$E(z) = e_x E_0 \cos[\omega(t-z/c)]$$

where the propagation velocity is

$$V = \frac{1}{\sqrt{\mu_0 \epsilon_0}} = c = 3 \times 10^8 \text{ meters/second,}$$

which is the speed of light in free space.

It is often necessary for simplification to assume that the rocks and soils being investigated with GPR are homogeneous, isotropic, linear, and source-free. However, they may be dispersive and lossy, which can be handled without too much complexity. The wavenumber can be written as

$$k(\omega) = \sqrt{\frac{\omega^2}{c^2} (\mu_r' - i\mu_r'') (\epsilon_r' - i\epsilon_r'') - i\omega \mu_0 (\mu_r' - i\mu_r'') \sigma_s}$$

where μ_r and ϵ_r are the complex, frequency dependent relative permeability and permittivity, and σ_s is the static (zero frequency) conductivity. Relative permittivity and permeability are ratios of the real property value with respect to the value of free space as in

$$\epsilon_r = \frac{\epsilon}{\epsilon_0} = \epsilon_r' - i\epsilon_r'' \quad \text{and} \quad \mu_r = \frac{\mu}{\mu_0} = \mu_r' - i\mu_r''$$

where ϵ_r' , ϵ_r'' , μ_r' , and μ_r'' are the real and imaginary parts of the relative, complex permittivity and permeability, respectively. For this case, the wavenumber, k , is a complex, frequency dependent value. It can be expressed in terms of its real and imaginary parts as

$$k(\omega) = \beta(\omega) - i\alpha(\omega)$$

where β is the real part of the wavenumber and α is the imaginary part. Both of these terms vary with frequency. In these terms, the propagation constant is simply

$$\gamma(\omega) = \alpha(\omega) + i\beta(\omega).$$

At this point the terminology choice between k and γ is irrelevant, as β is the phase parameter and α is the attenuation parameter for either choice. The wave equation solution for a plane wave moving through this material in the z direction is

$$E(z) = e_x E_0 e^{-\alpha z} \cos(\omega t \pm \beta z).$$

This wave is characterized by a velocity of

$$V = \frac{\omega}{\beta(\omega)}$$

a wavelength of

$$\lambda = \frac{2\pi}{\beta(\omega)}$$

and an amplitude change in decibels per meter of

$$a(\omega) = -8.686 \alpha(\omega)$$

due to conductive and relaxation losses. The frequency dependent parameters α and β can be expressed in terms of the material properties as

$$\alpha = \left(\frac{\omega}{c} \right) \sqrt{\left[\frac{\sqrt{A^2 + B^2} - A}{2} \right]} \quad \text{and} \quad \beta = \left(\frac{\omega}{c} \right) \sqrt{\left[\frac{\sqrt{A^2 + B^2} + A}{2} \right]}$$

where

$$A = \mu_r' \epsilon_r' - \mu_r'' \left(\epsilon_r'' + \frac{\sigma}{\omega \epsilon_0} \right) \quad \text{and} \quad B = \mu_r'' \epsilon_r' + \mu_r' \left(\epsilon_r'' + \frac{\sigma}{\omega \epsilon_0} \right)$$

A convenient way to handle both the frequency dependent and complex nature of the permittivity and permeability is through the Cole-Cole expression (Cole and Cole 1941; Keller 1987; Olhoeft and Capron 1994). The formulas are

$$\epsilon_r' - i \epsilon_r'' = \epsilon_\infty + \frac{(\epsilon_l - \epsilon_\infty)}{(1 + (i\omega\tau_e)^{\alpha_e})} \quad \text{and} \quad \mu_r' - i \mu_r'' = \mu_\infty + \frac{(\mu_l - \mu_\infty)}{(1 + (i\omega\tau_\mu)^{\alpha_\mu})}$$

where ϵ_∞ , μ_∞ , and ϵ_l and μ_l are the high and low frequency limits of permittivity and permeability, respectively; τ_e and τ_μ are time constants of relaxation, and α_e and α_μ are Cole-Cole time constant distribution parameters (Cole and Cole 1941). In each layer, for both permittivity and permeability, four values are given (low frequency limit, high frequency limit, time constant, and distribution parameter). If the high and low limits are equal to each other, the property value is real and independent of frequency (and the time constant and distribution parameter are irrelevant). When the high and low frequency limits are different, the functions behave as shown in Figure 2. The time constant of relaxation, τ_e or τ_μ , controls where in frequency the decrease in the real part steps from ϵ_l to ϵ_∞ , which is also the frequency where the imaginary part is at a maximum. The slopes on the step down in the real part and the flanks of the imaginary part are controlled by the distribution parameter, α_e or α_μ , which varies from 1.0 to 0.0 for steepest to smoothest slope. When either α_e or α_μ is zero the corresponding permittivity or permeability is a constant value midway between the high and low frequency limits.

Using the Cole-Cole functions means ten parameters are required to describe each earth material, four each for the complex magnetic permeability and the

complex dielectric permittivity, plus a static conductivity and a thickness. In the frequency range from above 100 MHz to less than 1 GHz, soils and rocks often have very small relaxation losses (Olhoeft and Capron 1994). By disregarding the complex nature of the material properties and assuming that no iron-bearing materials are present, which are reasonable assumptions for many cases, the number of parameters can be reduced to three per material. They are a real, relative dielectric permittivity, a real, static conductivity, and a thickness. The imaginary parts of the permittivity and permeability are assumed to be zero, and the real relative magnetic permeability is assumed to be one. For this case, the wavenumber is

$$k(\omega) = \left(\frac{\omega}{c} \right) \sqrt{\epsilon_r - i \frac{\sigma_s}{\epsilon_0 \omega}}$$

and its real and imaginary parts become

$$\alpha = \left(\frac{\omega}{c} \right) \sqrt{\frac{1}{2} \left[\sqrt{\epsilon_r^2 + \left(\frac{\sigma}{\omega \epsilon_0} \right)^2} - \epsilon_r \right]} \quad \text{and} \quad \beta = \left(\frac{\omega}{c} \right) \sqrt{\frac{1}{2} \left[\sqrt{\epsilon_r^2 + \left(\frac{\sigma}{\omega \epsilon_0} \right)^2} + \epsilon_r \right]}$$

Note that because α and β are still functions of frequency, the wave traveling through this material is still dispersive, but only through conductive losses. However, when $\sigma/\omega \epsilon_0$ is on the order of one or less, which it will be for conductivities less than 5 millisiemen/meter (mS/m) at 100 MHz and less than 55 mS/m at 1 GHz, then a reasonable approximation for β is

$$\beta = \left(\frac{\omega}{c} \right) \sqrt{\epsilon_r}$$

Because the velocity of the wave is ω/β , this results in a frequency independent velocity of

$$V = \frac{c}{\sqrt{\epsilon_r}}$$

which is commonly used in ground penetrating radar. The wavelength according to this approximation is simply

$$\lambda = \frac{c}{f \sqrt{\epsilon_r}}$$

where f is the frequency in cycles per second. An approximation that can be made for α (Von Hippel 1954, page 28) where

$$\alpha(\omega) = \frac{\sigma}{2c\epsilon_0\sqrt{\epsilon_r}}$$

results in a formula for a change in amplitude in decibels per meter according to:

$$a(\omega) = -1637 \frac{\sigma}{\sqrt{\epsilon_r}}$$

The vectors **E**, **J**, **H**, and **B** are the electric field, the electric current density (including displacement currents), the magnetic field, and the magnetic induction, respectively. The loss tangent is commonly used as a measure of the loss mechanisms in a material with regard to EM wave propagation. However, separate loss tangents are often defined for different combinations of loss mechanisms. The total electromagnetic loss tangent is α/β , or the ratio of the imaginary to the real part of the wavenumber. Physically, this is the phase difference between the vectors **E** and **H** (Lorrain and Corson 1970). The total electromagnetic loss tangent is

$$\tan \delta_{em} = \tan \left(\frac{\delta_e + \delta_m}{2} \right) = \frac{\alpha}{\beta}$$

The total electrical loss tangent includes conductive and dielectric relaxation losses, but not magnetic relaxation losses, and is defined as

$$\tan \delta_e = \frac{\epsilon_r'' + \frac{\sigma}{\omega\epsilon_0}}{\epsilon_r'}$$

Physically, this is the phase difference between **E** and **J**. The magnetic loss tangent is

$$\tan \delta_m = \frac{\mu_r''}{\mu_r'}$$

and represents the phase angle between **B** and **H**.

Reflection and Transmission Boundaries

When an EM wave encounters an interface between two media, the contrast in material properties, the radius of curvature of the interface, and the incident angle, polarization, and radius of curvature of the arriving energy will determine the amplitudes, directions, and polarizations of the reflected and transmitted energy. This encounter can be very complex without some simplifying assumptions. Generally, these assumptions include making the incident wavefront and the material boundary be planar surfaces, and assuming only uniform plane waves. The polarization effects can be eliminated by considering the problem in only two

dimensions, where the incident wave is linearly polarized along the third dimension. This is called a horizontal, perpendicular or E polarization (Balanis 1989, chapter 5).

Figure 3 shows a planar boundary between two media, and the rays associated with the planar wavefronts for the incident, reflected, and transmitted energy. The electric field is oriented in and out of the page in this figure. For a specular reflector, where the surface roughness consists of height variations that are small compared to the wavelength, the angle of reflection is equal to the angle of incidence:

$$\theta_r = \theta_i$$

The transmitted angle can be calculated from the incident angle and the material properties through Snell's Law (Balanis 1989; Lorrain and Corson 1970; Ulaby, Moore and Fung 1981). The formula is:

$$\sin \theta_t = \left(\frac{\mu_2 k_1}{\mu_1 k_2} \right) \sin \theta_i$$

where k_1 and μ_1 are the wavenumber and magnetic permeability of the incident layer, and k_2 and μ_2 are the wavenumber and magnetic permeability of the transmitted layer.

When the wavenumber of either material is complex, the transmitted angle becomes complex. Physically, this means for the transmitted wave the planes of constant phase (direction of β , the real part of the wavenumber) and the planes of constant amplitude (direction of α , the imaginary part of the wavenumber) are not parallel (see Balanis 1989, page 214, or Von Hippel 1954, page 64). This means the wave is no longer linearly polarized. However, in the case of normal incidence, where θ_i is equal to zero, the transmitted and reflected waves are also normal to the interface with no polarization changes.

The amplitudes of the transmitted and reflected waves are dependent on the incident wave amplitude, the material properties of the two media, and the angle of incidence (and the polarization which is still assumed to be horizontal, E, or perpendicular to the plane of the incident and reflected rays). The Fresnel equations (Lorrain and Corson 1970, page 508; Kline and Kay 1965, page 179) describe these relationships and the formulas are

$$E_r = R E_i \quad \text{and} \quad E_t = T E_i$$

where R and T are the reflection and transmission coefficients, respectively, and are as follows:

$$R = \frac{\mu_2 k_1 \cos \theta_i - \mu_1 k_2 \cos \theta_t}{\mu_2 k_1 \cos \theta_i + \mu_1 k_2 \cos \theta_t} \quad \text{and}$$

$$T = \frac{2\mu_2 k_1 \cos\theta_i}{\mu_2 k_1 \cos\theta_i + \mu_1 k_2 \cos\theta_t}$$

For normal incidence ($\theta_i=0^\circ$), these reduce to

$$R = \frac{\mu_2 k_1 - \mu_1 k_2}{\mu_2 k_1 + \mu_1 k_2} \quad \text{and}$$

$$T = \frac{2\mu_2 k_1}{\mu_2 k_1 + \mu_1 k_2}$$

Note that for complex media, these coefficients will also be complex, resulting in amplitude and phase changes in the reflected and transmitted waves.

3 Forward Modeling of GPR Data

Only within the past five years have serious efforts been made to model full waveform GPR data. These efforts have concentrated solely on the forward modeling process. The forward modeling routine must include the physical parameters introduced in the GPR theory section (complex relative dielectric permittivity, complex relative magnetic permeability, electrical conductivity, layer thickness, and time relaxation and distribution parameters) and model the effects these parameters have on the transmitted waveform. The processes a GPR wave undergoes as it passes through a material are reflection and transmission at interfaces or boundaries, attenuation, geometric spreading, dispersion, and scattering. The GPR forward modeling program GPRMODv2 (Powers and Olhoeft 1995) employed in this research compensates for all of these effects except scattering. The program makes several assumptions to simplify the modeling process: zero source-receiver offset; normal incidence; horizontal, layered, homogeneous, isotropic media; and no three dimensional electric or magnetic polarization, near-field, or scattering loss effects. The assumption of zero source-receiver offset and normal incidence are interrelated and will be discussed later. Assuming a horizontally layered media simplifies the wave propagation path and is a reasonable assumption for obtaining an initial model response or approximation to field data. The absence of electric or magnetic polarization is a direct result of assuming normal incidence and a horizontal interface. In reality, the electric field probably does not maintain its linearity at an interface, but becomes polarized in some elliptical form. However, what is measured at the receiver is only the component of the field that is in the same direction as the transmitted field.

Reflection and transmission of the GPR signal occur at boundaries of contrasting dielectric properties. With each boundary encountered, the amplitude of the original signal is attenuated and only a small fraction of the originally transmitted signal is measured by the receiver. In addition to the primary reflection which occurs at an interface and is detected by the receiver, reflection multiples are also generated at interfaces. These multiples are reflections off more than one interface as the transmitted signal travels through the subsurface. It is important to differentiate the primary reflections from multiple reflections since multiples do not represent true interfaces at depth (if a single reflection traveltime is assumed).

The conductivity of a material is a major factor in determining the degree of signal attenuation. The higher the conductivity value, the greater the amount of signal energy that is absorbed by the medium, thus reducing the amplitude of the signal measured at the receiver. Soils having a high clay and moisture content can absorb so much of the transmitted signal that the GPR will not be able to "see" below that layer. If identification of the clay layer is the objective, then loss of signal at depth would be a good marker for identifying the clay. However, if the layer of interest is below the clay layer, then another technique would be required to locate it.

There are two types of geometric spreading. The first is caused by the antenna radiation pattern and the other is a result of spherical spreading of the initial energy output. The radiation pattern of a GPR antenna varies the amount of energy output as a function of angle from the normal to the antenna. In addition, the radiation pattern varies with the electromagnetic properties of the near surface material. The coupling effects between the antenna and ground surface are generally ignored, however the forward modeling routine used in this research does provide an option for fitting the model response to the field data by compressing or stretching the model waveform. The effect of the incident angle of energy output on the reflection and transmission coefficients was investigated using the Fresnel equations (chapter 2). Assuming a magnetic permeability of free space and positive, real propagation constants that increase with depth, plots of the reflection coefficient and transmission coefficient as a function of incident angle θ were constructed (Figure 4). It can be seen that the curves are relatively flat for incident angles $\theta < 20^\circ$. The effect of geometrical spreading caused by the angle of incidence of the energy output is related to the separation distance between the transmitter (Tx) and receiver (Rx) antenna. A general rule of thumb given by Annan and Cosway (1992) states that the separation between the transmitter and receiver should be approximately equal to 20% of the target depth (Figure 5). Based on this assumption, the ratio between one half the Tx-Rx distance ($s=2x$) and the target depth y should be $x/y=0.1$. This corresponds to an incident angle of $\theta \approx 6^\circ$, which is much less than the 20° limit. Thus, if the general rule of Annan and Cosway (1992) is adhered to, normal incidence can be assumed. For very shallow investigations, high frequency antennae are required which have very small source-receiver offset and thus virtually normal incidence.

The second type of geometric spreading occurs when the transmitted energy propagates into the earth and expands over an ever increasing spherical surface. The spreading wavefront is only truly spherical when the velocity profile of the material is isotropic and homogeneous. The forward modeling program corrects for geometric spreading using an algorithm based on May and Hron (1978) and Balanis (1989).

Dispersion occurs when the velocity of a material varies with frequency. Both dielectric, magnetic, and conductive losses can cause dispersion. It is often assumed that the velocity of a layer is constant, although in reality the velocity is generally frequency dependent over at least some frequency range. Mathematically, dispersion is represented by the imaginary components of the dielectric permittivity and magnetic permeability. As discussed earlier, the complex parameters are introduced via the Cole-Cole model. Dispersion is simulated in the forward

modeling program by computing a separate time delay for each frequency for the traveltime to a particular reflection event (Powers and Olhoeft 1995).

Scattering occurs on a small scale (scale of the wavelength) and can be classified as either volume scattering or surface scattering. Volume scattering is caused by objects dispersed in the media, such as gravel or rocks, which scatter the signal in multiple directions when the electromagnetic wave encounters it. Surface scattering occurs when the traveling wave hits a rough interface which causes the wave to spread in various directions. The primary effect of scattering is the reduction of signal strength (Olhoeft 1984). Neither type of scattering is considered in the forward modeling program.

Forward Modeling Example

The forward modeling process begins by choosing the number of layers in the model and specifying the parameter values for each layer. The parameters include layer thickness, electrical conductivity, relative dielectric permittivity, relative magnetic permeability, and the Cole-Cole relaxation and distribution parameters for the permittivity and permeability. Generally, both the inexperienced and experienced modeler do not have an intuitive feeling for the parameters required for modeling GPR data. The low and high frequency limits for both the real relative dielectric permittivity and real relative magnetic permeability are required as input. The default values for the magnetic permeability are generally suitable for modeling most GPR data; only in cases where the soil has a significant iron content will these values need adjusting. Values for the relative dielectric permittivity and electrical conductivity can be obtained from publications of laboratory measurements on similar materials. For the Cole-Cole parameters, the default values are good initial values. The distribution parameter α governs the slope of the relaxation curve whereas the relaxation parameter τ shifts the curve laterally. These parameters can be determined from laboratory measurements or, for sand/clay mixtures, GPRMODv2 includes an option for estimating the Cole-Cole parameters based on the sand/clay/water ratio (Olhoeft 1986).

An example of the forward modeling output is shown in Figure 6. The model is for a two layer rigid pavement structure consisting of concrete and gravel base overlaying a sandy soil. The primary reflections A and B in the output trace are caused by the concrete/gravel interface at 0.2m depth and the gravel/sand interface at 0.6m depth, respectively. The reflection at about 10ns (a) is a first multiple (i.e. wave that traveled same path as primary reflection A) of the concrete/gravel interface, whereas reflection b is the first multiple of the gravel/sand interface. Reflections c and d are multiples that traveled a more complex path. The thickness of layer 1 (concrete) dictates how far in time the primary reflection A is shifted from zero; as thickness increases, two-way traveltime increases. The separation between primary reflectors A and B is controlled by the thickness of the gravel base (layer 2). As this thickness decreases, it becomes more difficult to distinguish the location in time of the concrete/gravel interface (B) because the onset of the reflection event gets mixed in with the arrivals of the primary reflection A and multiple reflection a. The ability to differentiate reflection events is a major concern in the inversion of GPR data.

Forward modeling is a useful aid in determining if it is feasible to use GPR at a particular site, what frequency antenna is required to detect layers of varying thickness, and what type of response should be expected for various combinations of conductivity, dielectric permittivity, and magnetic permeability. Although forward modeling is a valuable learning aid, one is often in the situation where the GPR data has been collected and it is necessary to determine the layer structure and dielectric properties based solely on the radar data; this is when the inversion of GPR data is required. The inverse modeling of GPR data is discussed in Chapter 5.

4 Full Waveform GPR Forward Modeling Investigations

Modeling Problem Selection and Details

Problem selection and justification

The concepts of EM wave propagation theory and full waveform forward modeling are discussed in the preceding chapters. In this chapter a common geotechnical problem is selected for a detailed modeling study to illustrate the use of full waveform GPR modeling and to investigate key concepts of detectability and resolution. Included in the modeling study are effects of reflection from interfaces between different materials, changes in propagation path length, transmitter frequency, and material properties, multiple reflection events, and attenuation caused by finite conductivity. The effects of dispersion are not considered in the present study and are likely not significant in most materials over the frequency range 100 MHz to 1 GHz (Olhoeft and Capron 1994).

Detection of air- and water-filled cavities in concrete structures or behind concrete layers is the problem selected for study. This is a frequently occurring problem that can threaten the integrity and safe operation of critical structures and an application for which GPR is commonly considered. Cavities can occur in concrete used as structural components (pillars, walls and monoliths) for a variety of reasons, e.g., as an artifact of the construction process, a result of concrete degradation, and as a result of delamination or debonding from other structural components. Concrete is also used in the form of layers or slabs for building floors and walls, flow channels, soil and rock slopes, and tunnel liners. Cavities also occur behind concrete layers or slabs due to a variety of processes, such as differential settlement or piping. Application of GPR to detection of cavities within or behind concrete is always a tradeoff between the requirement for high frequencies for resolution of cavity thickness or of thin concrete layers and lower frequencies for achieving the required depth of investigation.

Model problem sets

Three transmitter center frequencies, 300, 500, and 900 MHz, are selected for the model calculations, and are representative of commercially available GPR

systems and typical of frequencies which might be selected for investigation of concrete structures. The Ricker waveform is used for all three frequencies; thus the shape of the pulse is the same for all three frequencies, with only the duration varying to produce the variation in center frequency. One major GPR manufacturer maintains that the Ricker waveform is an extremely close approximation to the actual waveform for their antennae. Duke (1990) investigated the antennae of a second major GPR manufacturer and produced calibrated transmitter waveforms; these actual calibrated waveforms are compared to the ideal Ricker waveforms in Figure 7 for the same designated, nominal center frequencies. Both the actual and the Ricker waveforms are scaled to the same arbitrary maximum amplitude. The actual 300 MHz transmitter waveform and spectra are very similar to the corresponding Ricker waveform and spectra. The actual 500 and 900 MHz transmitter waveforms are different from the Ricker waveforms in various aspects, due to transmitter ringing and noise.

Two problem sets are considered for the modeling investigation. Problem Set 1 consists of models of concrete over air or water. For the concrete over air cases, the thickness of concrete is systematically varied from 0.1 to 4 m, while for the concrete over water cases a fixed concrete thickness is selected. Problem Set 2 consists of models of a concrete layer over a water layer over "sand". Cases in Problem Set 2 have a fixed concrete thickness, while the thickness of the water layer is systematically varied. Also, for some of the cases in Problem Set 2, GPR forward models are conducted with and without multiple events.

Concrete is not a simple material to characterize generically. The EM properties for concrete used for this investigation were deduced from Buyukozturk and Rhim (1993) for three concrete water contents (w.c.), 9.5%, 6.7%, and 0%, as shown in Table 1, which also includes the properties for air, water and sand. A small frequency dependence of the relative dielectric permittivity is included for concrete. For purposes of this study, this representative set of EM properties is selected based on published information, without consideration of the relevance of specific concrete mix design, i.e., type of cement, sand/gravel/cement/water mix, type and size distribution of aggregate, etc. The concrete is considered massive and unreinforced. The concrete specimens used for the measurements by Buyukozturk and Rhim were cast with a water/cement/sand mix ratio of 1:2:4 by weight, with no coarse aggregate. A portland cement of Type I was used. Specimen age was 4 weeks at the time of measurements. The effect reinforced concrete has on the penetration of a transmitted GPR signal was not studied in this investigation.

Table 1
EM Properties of Model Materials

Model Material	Relative Dielectric Permittivity (Real)			Conductivity mS/m
	300 MHz	500 MHz	900 MHz	
Concrete w.c. = 9.5%	8.4	8.3	8.1	40
w.c. = 6.7%	5.2	5.1	5.0	30
w.c. = 0.0%	3.5	3.55	3.6	10
Air	1	1	1	0
Water	80	80	80	20
Sand	25	25	25	5

Conceptual modeling considerations

A conceptual understanding of the GPR modeling process requires consideration of EM wave propagation velocities, two-way reflection times from interfaces in the model, reflection and transmission coefficients, effects of geometric spreading and attenuation on wave amplitudes, and multiple reflection events. An understanding of the modeling process also is extremely helpful if not necessary for formulating or deducing a subsurface model that explains or is consistent with the features observed in field GPR data. To illustrate the process of conceptual modeling, the model used in Problem Set 2, concrete over a water-filled cavity over sand, is utilized.

Consider the specific case of a 0.3 m thick concrete layer over a 0.05 m thick water cavity over a saturated sand, which is considered infinitely thick for purposes of the modeling investigation. The EM wave propagation velocity (speed) c_i and EM wavelength λ_i , where the subscript i refers to the i -th material in the model, and the amplitude reflection coefficients R_{ij} and transmission coefficients T_{ij} , where ij refers to the interface between the i -th and j -th materials in the model, are given by the following equations

$$c_i = c_0 / \epsilon_{n,i}',$$

$$\lambda_i = c_i / f,$$

$$R_{ij} = (\sqrt{\epsilon_i'} - \sqrt{\epsilon_j'}) / (\sqrt{\epsilon_i'} + \sqrt{\epsilon_j'}),$$

and

$$T_{ij} = 2\sqrt{\epsilon_{ni}'} / (\sqrt{\epsilon_{ni}'} + \sqrt{\epsilon_{nj}'}),$$

where c_0 is the EM wave speed in a vacuum (3×10^8 m/s), ϵ_n' is the real part of the relative dielectric permittivity of the i -th model material, and f is the frequency. The

above expressions for the reflection and transmission coefficients are simplifications for the full frequency dependent expressions (see Chapter 2) used in GPRMODv2. Using the subscripts c, w, and s for concrete, water and sand, respectively, Table 2 gives the values for wave speed, wavelength, reflection coefficient, and transmission coefficient for the model materials. The velocities for concrete are averages for the three frequencies for each water content value.

Table 2
EM Velocities, Wavelengths, Reflection and Transmission Coefficients

Model Material	Velocity, $\times 10^8$ m/s (m/ns)	Wavelength, m 300 500 900	Reflection Coefficient	Transmission Coefficient
Layer 1: Concrete			$R_{c,w}$	$T_{c,w}$
w.c. = 9.5%	1.04 (0.104)	.35 .21 .12	-0.515	0.485
w.c. = 6.7%	1.33 (0.133)	.44 .27 .15	-0.599	0.401
w.c. = 0.0%	1.59 (0.159)	.53 .32 .18	-0.654	0.346
Layer 2: Water	0.33 (0.033)	.11 .07 .04	$R_{w,s}$ 0.286	$T_{w,s}$ 1.286
Layer 3: Sand	0.6 (0.06)	.20 .12 .08		

With the wave velocities in Table 2, it is possible to determine the two-way travel times through the layers of the model. Figure 8 shows the results of the traveltimes calculations for selected GPR events in the model, where the terminology "event" refers to the arrival of energy at the receiver that has followed a distinct propagation path through the model (or the subsurface in the case of actual GPR data). Thus the GPR records, either field data or model calculations, consist of much more than just the primary reflection events from each interface. In some cases identification of the multiple events is helpful, but in most cases the multiples complicate the interpretation process by interfering (superimposing) with both the primary reflections and with other multiples. It is also possible that interfaces will be so close together (i.e., a thin layer) that the primary reflections will interfere with each other and the two interfaces will not be *resolved*. The numerical designation of the multiples refers to the interfaces where reflections occur along the multiple propagation path, where the top or air/layer 1 interface is assigned '0'. Thus the designation '101' refers to a event which reflects from interface 1, interface 0, and interface 1; this multiple event is shown as the third event from the top in Figure 8.

Whether or not events interfere with each other or a layer is resolved depends on the frequency and hence the duration and dominant wavelength of the propagating waveform. The dominant wavelengths of the nominal Ricker waveforms are shown in Table 2. Widess (1973) demonstrates that a layer is theoretically resolved for thicknesses greater than $\lambda/8$, where λ is the dominant wavelength of the waveform

within the layer. However, practical resolution is typically taken to occur at approximately $\lambda/4$ (Jol 1995), and “visual resolution,” i.e., the thickness for which the two primary reflections are visually obvious, occurs at approximately $\lambda/2$. Thus in the absence of interfering multiples, visual resolution of the water layer (see Table 2) should occur for layer thickness of approximately 0.06, 0.04, and 0.02 m for frequencies of 300, 500, and 900 MHz, respectively. Based on these considerations, the water layer in Figure 8 (thickness $h_w = 0.05$ m) should be visually resolved for 500 and 900 MHz but not for 300 MHz.

A useful way to visualize a GPR record is as the convolution of the propagating waveform with the impulse response of a model or the earth. The impulse response is constructed simply as a spike at the two-way reflection time for each event with amplitude and polarity equal to the reflection coefficient (see Table 2); this simplistic impulse response ignores transmission and propagation losses. In the convolutional model response, each event will have duration equal to duration of the propagating waveform. Interference will then occur when events occur closer in time than the duration of the propagating waveform. From Figure 7, a duration for the Ricker waveforms can be defined as the visually apparent time between zero departure (total duration) for the waveform or as the time between the negative peaks of the waveform. The approximate values for these definitions of duration are shown below:

	<u>300 MHz</u>	<u>500 MHz</u>	<u>900 MHz</u>
Total Duration, ns	6.3	3.7	2.15
Time between negative peaks, ns	2.5	1.5	0.85

Comparing these values for duration to the two primary reflection two-way times in Figure 8 indicates that the two primary events should be well resolved for 900 MHz, interfere slightly for 500 MHz (although the two negative peaks for each event should be resolved), and should significantly interfere for 300 MHz. The resolution assessment based on waveform duration is completely consistent with the assessment based on dominant wavelength in the preceding paragraph.

Results of GPRMODv2 calculations for the concrete/water/sand model of Figure 8 with concrete w.c. = 9.5% and 900 MHz Ricker waveform are shown in Figure 9; the top plot is for no multiples, and the bottom plot includes multiple events. The two primary events are labeled and are clearly resolved as predicted previously for 900 MHz based on waveform duration and dominant wavelength considerations. Two multiple events are indicated in the bottom plot. The first labeled multiple event is actually the superposition of two multiple events, 101 and 212, that arrive nearly simultaneously (see Figure 8 under w.c. = 9.5%). The multiple event 201 is attenuated significantly, and all other multiple events are not evident.

As an illustration of the effects of propagation velocity on the spacing of primary and multiple events, Figure 10 shows GPRMODv2 calculation results for concrete w.c. = 0.0% and 900 MHz, i.e., identical to the model for Figure 9 except for water content and hence propagation velocity (see Table 2). From the reflection times in Figure 8 under w.c. = 0.0% and dominant wavelength and duration considerations, it is evident that the primaries should still be resolved; however, multiple event 101

should now interfere with the 2nd primary, while multiple events 101 and 212 should be resolved. All of these predictions are evident in the calculated GPR model response and the events are identified in Figure 10. Multiple event 202 is also evident and identified for this case, because of the decreased attenuation for the lower conductivity associated with $w.c. = 0.0\%$ compared to the higher conductivity with $w.c. = 9.5\%$.

As a final example to illustrate forward modeling concepts, the GPRMODv2 results for the previous model with $w.c. = 9.5\%$ and using a 300 MHz propagating waveform are shown in Figure 11. Considering the arrival times in Figure 8 under $w.c. = 9.5\%$ and dominant wavelength and duration for 300 MHz, it is obvious that not only should the two primary events not be resolved but multiple events 101 and 212 should interfere with the primaries. The GPR model results in Figure 11 illustrate the lack of resolution of the two primaries and comparison of the calculation with no multiples (top plot) with the calculation with multiples (bottom plot) illustrates the interference of multiple events 101 and 212 with the primaries. None of the other multiples are evident, illustrating greater attenuation of the 300 MHz waveform relative to the 900 MHz case considered earlier. Although the complex waveforms in Figure 11 suggest superposition of events, *arrival times other than that of the 1st primary cannot be determined with confidence by visual inspection*. Application of data processing procedures, such as crosscorrelation and deconvolution, to detect event arrivals that are too closely spaced in time to be visually resolved is discussed in the next chapter.

Scope and Results of the Modeling Study

Scope of study

Appendix A contains tabulations of the cases included in the Problem Sets. Table A1 lists the 27 cases of Problem Set 1 for concrete over air for which GPR model responses were computed and reproduced for this report. Table A2 lists the cases of Problem Set 1 for concrete over water. The GPR model response calculations from GPRMODv2 for Problem Set 1 are contained in Appendix B. Table A3 lists the cases of Problem Set 2 for models of concrete over water over sand. Cases 37-144 in Table A3 are for calculations with multiples, while cases 145-252 are for calculations with no multiples. The GPR model response calculations for Problem Set 2 are contained in Appendix C.

Selected results and discussion: Problem set 1

Results of the GPRMODv2 model calculations for Problem Set 1 are presented in Appendix B. Figure 12 combines Figures B4 and B11 for a side-by-side comparison example. The three plots on the left side of Figure 12 are for concrete over air, while the three plots on the right are for concrete over water, with the same frequencies side-by-side and concrete thickness $h = 0.3$ m and $w.c. = 9.5\%$ for all cases. All of the concrete/air and concrete/water cases show the primary and first multiple event. From Table 2, the reflection coefficient for concrete over water is

-0.515, while the reflection coefficient for concrete over air is +0.485. Thus the first expected and observed difference in the concrete/air and concrete/water cases are the different polarities of the reflection events. For the concrete thickness 0.3 m, the primaries and multiples are well separated for all three frequencies. The concrete thickness for this problem can be determined from the model response by using the arrival time of the primary or the time difference between primary and multiple multiplied by the propagation velocity. The approximate two-way time difference between primaries and multiples is $t = 6$ ns; the concrete thickness h is given by $h = (t/2)(c/\sqrt{\epsilon_r})$,

$$h = 0.5 \times (6 \times 10^{-9}) \times (3 \times 10^8) / \sqrt{8.4} \text{ m} = 0.31 \text{ m},$$

in satisfactory agreement with the known model value.

Another more subtle feature of the cases in Figure 12 is the effect on amplitudes of the reflection process and total signal attenuation. For each plot, a "Display Gain" is shown (rounded to the nearest dB). This gain is a constant by which all values in the model calculation output values are multiplied to make the maximum amplitude in the output equal to 80% of the maximum value for the graphic display (Powers and Olhoeft 1995). Thus the Display Gain is directly related to the total signal loss as a result of attenuation, spreading, and reflection and transmission at boundaries for all cases. In fact, the total signal loss will always be greater than the display gain in dB, since the display gain will be determined by the amplitude of the first primary event rather than the amplitude of the initial transmitter waveform (the first primary amplitude will always be less than the initial transmitter waveform amplitude). Two features are apparent from Figure 12: (1) signal loss increases as frequency increases for both primaries and multiples as expected; (2) signal losses are greater by approximately 1 dB for the concrete/air cases than for the concrete/water cases. The second feature is understood by comparing the reflection coefficients for concrete/air and concrete/water. Only 48.5% of the incident amplitude is reflected at the air boundary, while 51.5% is reflected at the water boundary. This difference in reflected amplitude at the two boundaries amounts to 1 dB (by converting the reflection coefficients to dB and comparing) as shown by the model calculations.

In addition to the cases shown in Appendix B, for concrete thicknesses of 0.1, 0.3, and 0.75 m, the thickness h was systematically varied from 0.01 m to 4.0 m to determine signal loss as a function of thickness for the GPR model calculations. Signal loss in dB versus concrete thickness for concrete w.c. = 9.5% (top) and 0.0% (bottom) is plotted in Figure 13, where the "signal loss" is just set numerically equal to the display gain. The signal loss plots illustrate several important concepts regarding the interplay of electromagnetic parameters in determining total signal loss and achievable penetration depth in concrete. The plots in Figure 13 have the appearance of two linear regions joined by a transition region. The initial steeply sloping region of the plots corresponds to the region where geometric spreading dominates the total signal loss, while the second lesser sloping region corresponds to domination of the total signal loss by actual intrinsic propagation loss. Why the transition region is so abrupt, particularly for the w.c. = 9.5% cases, is not clear. The initial linear regions for the w.c. = 9.5% cases and for the w.c. = 0.0% cases are practically coincident, while the slope for the w.c. = 9.5% cases is steeper than for

the w.c. = 0.0% cases. The slopes within the second linear region for the three frequencies are approximately equal for each w.c.; although the curves for each frequency are separated by approximately 5 dB, i.e., signal loss for 500 MHz is 5 dB greater than 300 MHz and signal loss for 900 MHz is 5 dB greater than 500 MHz. The second linear region begins at approximately 0.75 m for w.c. = 9.5% and 1.75 m for w.c. = 0.0%. Slopes within the second linear region approximately equal 1.4 dB/m for concrete w.c. = 9.5% and approximately equal 1 dB/m for concrete w.c. = 0.0%, consistent with observed values for similar materials reported by others (Annan 1992).

A somewhat initially surprising result is that the plots predict greater signal loss at larger propagation distances (> 2 m) for the lower conductivity concrete. The explanation for this somewhat counterintuitive result is the role played by dielectric permittivity in signal loss and the geometric spreading formulation (see Chapter 3 and Powers and Olhoeft 1995). The factor of two decrease in dielectric permittivity plays a larger role in determining penetration than the factor of four decrease in conductivity; this relative effect may not be the same for other ranges of permittivity and conductivity.

A typical value for total loss that can occur from all propagation effects and still result in detection of the signal at the Rx is 100 dB (Annan 1992). Assuming that the signal loss plotted in Figure 13 is the actual total propagation loss, this will give a *conservative estimate* of achievable maximum concrete thickness penetration for each frequency at the thickness where each curve crosses the 100 dB loss value. It is assumed that the average of the maximum thicknesses for w.c. = 9.5% and 0.0% is the maximum thickness for an "average concrete"; these values are tabulated below:

	<u>300 Mhz</u>	<u>500 Mhz</u>	<u>900 MHz</u>
Maximum Penetration Thickness, m (For 'average concrete' at 100 dB total signal loss)	8	6.8	3.7

These values of 100 dB penetration *thickness* are consistent with values of 100 dB penetration *range* calculations reported elsewhere for similar conductivities and permittivities (Annan 1992).

Selected results and discussion: Problem Set 2

Problem Set 2 is a systematic investigation of the primary and multiple events associated with the concrete/water/sand model discussed in the "Conceptual modeling considerations" section. For this investigation, the water layer thickness is varied from 0.01 m to 0.4 m for three concrete water contents and three frequencies. The concrete thickness is fixed at 0.3 m for all cases in Problem Set 2. The complete GPRMODv2 calculation results of the investigation are presented in Appendix C which serves as a reference catalog for this type problem. For problems of this type, the key factors to be determined are concrete thickness, cavity thickness, and whether the cavity is water- or air-filled. Determination of the

concrete thickness was discussed in the preceding section. Determination of the cavity (water layer) thickness requires the arrival time of the second primary event. Thus the two primary events associated with the cavity must be resolved either visually or via data processing. Identification of the two primary events allows the determination of the concrete and cavity thicknesses. The propagation velocities within the concrete and cavity are also determined, and in turn the real part of the dielectric permittivity of the concrete and cavity-filling material, which will identify the cavity-fill material (air or water). The preceding discussion is a description of a manual inversion of GPR data. In the actual case of field GPR data, all the multiple events and noise will be present to complicate the identification of the second primary and determination of its arrival time. The value of the full waveform forward modeling capability is for iterative manual inversion or as the core of an automated inversion capability, since all primary and multiple events (as well as attenuation, spreading and dispersion effects) are included.

The cases for water layer thickness $h_w = 0.05$ m are discussed in detail in the "Conceptual modeling considerations" section. For this water layer thickness, the two primary reflections are just resolved for 900 MHz but not resolved for 300 MHz (see Figures 10 and 11). Examination of the results in Appendix C reveals the following approximate water layer thicknesses required for *visual resolution*:

	<u>300 MHz</u>	<u>500 MHz</u>	<u>900 MHz</u>
Minimum Resolvable Layer Thickness, m	0.1	0.05	0.03

Although there is a slight dependence on concrete properties affecting the resolution, the above visually resolvable thicknesses are good rules-of-thumb.

Considering the minimum water layer thickness required for visual resolution, as in the preceding paragraph, results in output from GPRMODv2 in which the primary and multiple events are closely spaced in time and superimposed to some extent. It is useful and instructional to consider a water layer thickness for which all the events are separated. Figure 14 reproduces Figure C54, Case 252, for water layer thickness $h_w = 0.4$ m. An additional display gain of 20 dB is applied to Figure 14 to enhance recognition of the events. Eight events are identified in Figure 14.

5 GPR Inverse Modeling

The numerical inversion of any geophysical data is basically an iterative process where a forward model is fit to the data and the parameters adjusted until an acceptable fit between the model and the data is achieved. The greater the number of parameters involved in the inversion, the more complex the inversion process. Since some GPR parameters are interrelated, a unique inversion solution cannot be obtained. Because of the large number of parameters involved and the nonuniqueness of the solution, the usual techniques for inverting geophysical data to obtain a global solution of all parameters simultaneously via an iterative least squares inversion procedure (Simms and Morgan 1992) is not practical for full waveform GPR data. However, experience and knowledge of typical values of parameters for a given material can aid in simplifying the GPR inversion requirements and in determining if the inversion result is reasonable.

Parameter Considerations

Based on the forward modeling program GPRMODv2 (Powers and Olhoeft 1995) discussed previously, a minimum of thirteen parameters are involved in the modeling of GPR data. Thus, a minimum of thirteen parameters would be required as input to the inversion. The parameters include three that pertain to the overall model (number of layers, coupling ratio, and zero time offset) and *ten that are required for each layer* (conductivity, thickness, and eight Cole-Cole parameters). The number of initial variable inversion parameters can be reduced to four if some simplifying assumptions are made. The parameter zero time offset is obtained from header information when the data were collected in the field; it is dependent on the GPR system used to acquire the data. A second parameter, coupling ratio, is determined from the expression $C_r = \sqrt{\epsilon_r}/2$. This relationship was obtained by assuming the antenna is designed for a material having a dielectric permittivity of $\epsilon_r = 4$ so the velocity $V_{\text{design}} = f_{\text{design}} \lambda_{\text{antenna}} = c/\sqrt{\epsilon_r} = c/2$. The interaction of the transmitted pulse with the ground surface tends to reduce the peak operating frequency of the antenna thus $V_{\text{field}} = (f_{\text{design}} \lambda_{\text{antenna}})/C_r = c/\sqrt{\epsilon_r}$. A permittivity of four is arbitrary but the expression for the coupling ratio provides an adequate initial approximation. The two parameters dealing with the magnetic permeability can assumed initially to be constant, their values governed by whether the material is or is not magnetic. However, if a material is thought to have a significant iron content then these parameters should be allowed to vary throughout the inversion. The four Cole-Cole relaxation and distribution parameters, two related to the

dielectric permittivity and two to the magnetic permeability, can also be initially taken as constant. If the material is dispersive or wet, then the default values will need to be adjusted. The five remaining parameters, number of layers, layer thickness, electrical conductivity, and high/low relative dielectric permittivities, are the major parameters involved in modeling GPR data. For the inversion though, the number of layers and layer conductivity (if measured in the field or laboratory) can be fixed, which leaves three parameters per layer that will vary throughout the inversion process, layer thickness and high/low relative dielectric permittivities, plus the coupling ratio.

The first step in the inversion process is to determine how many layers are represented in the GPR trace. Two methods were investigated to do this, crosscorrelation and deconvolution. Crosscorrelation compares two sequences to determine how similar one sequence is to the other. An example of using crosscorrelation to identify interface boundaries is shown in Figure 15. In Figure 15a, a 900 MHz Ricker waveform was crosscorrelated with the forward model response from a three layer model consisting of concrete, water, and sand (no multiples). A Ricker waveform is representative of the output signal for a commercially available GPR antenna system. The top plot is the Ricker waveform, the center plot is the model response, and the bottom plot is the result of the crosscorrelation. Figure 15b represents the same set of plots except the input wavelet (top plot) is that for a 900 MHz antenna of another GPR manufacturer. For both input waveforms, the crosscorrelation results in a replica of the input wavelet at each layer interface. The apparent discrepancy in the location of the interfaces relative to time (location of peaks on the model response and crosscorrelation curves) represents the time difference between the peak on the input wavelet and zero time. The crosscorrelation ignores any time offset of the input signal, thus time t' of peak B' on the crosscorrelation curve is equal to time t between peak A on the input wavelet and peak B on the model response curve.

Deconvolution was also tested as a method to identify layer interfaces. Deconvolution is a process designed to restore a waveshape to the form it had before it underwent a linear filtering action (Sheriff 1984). The same input and model response curves used above were deconvolved to obtain the location of the layer boundaries (Figure 16). Again, the input signal in Figure 16a is a Ricker waveform and Figure 16b is the other calibrated antenna waveform. The deconvolution is also relative to the input wavelet and ignores any initial time offset. Note that the deconvolution output is similar to that of an impulse rather than a replica of the input wavelet, as was the case in the crosscorrelation.

When the Ricker waveform is used as the input signal, both the crosscorrelation and deconvolution provide a relatively sharp response. However, as the input signal becomes more complex, as with the other input waveform, deconvolution provides a cleaner and sharper identification of the layer interface. The simplification of the output to an impulse-like response is desirable in order to obtain a clearer definition of the layer boundary and, in cases when thin layers are present, for separation (resolution) of the layers.

A rough estimate of the interface depth can be determined based on an estimate of the material velocity and the traveltime. This should provide an adequate initial value for the inversion routine.

The electrical conductivity can be obtained from a reference, which typically would report a range of values for a given material, laboratory measurements, or data collected in the field. However, it is preferable to measure the conductivity of the material since conductivity values can vary over a wide range and are dependent on site specific conditions.

Values for the relative dielectric permittivity are obtained from laboratory measurements performed on field samples or, more commonly, from publications of laboratory measurements on similar materials. The permittivity of the near surface soil layer can also be obtained using time domain reflectometry (TDR). This field measurement would correspond to the high frequency dielectric permittivity in the forward modeling program. The real dielectric permittivity tends to range between 4 and 25 for typical soils and pavements. In the higher frequency range, $f > 100$ MHz, the high frequency dielectric permittivity ϵ_{rh} dominates and the low frequency dielectric permittivity ϵ_{rl} can be set equal to ϵ_{rh} . However, if dispersion is a factor within the operating frequency range of the antenna, then ϵ_{rl} should be set greater than ϵ_{rh} .

A list of the thirteen inversion parameters and their general range of values is given below. The values for the relative dielectric permittivity are based on one author's experience whereas the values for relative magnetic permeability and the Cole-Cole parameters were obtained from forward modeling exercises using GPRMODv2 (Powers and Olhoeft 1995). Many of these parameter ranges are based on laboratory measurements of field samples (Olhoeft 1986, Olhoeft and Capron 1994). Note that the dielectric permittivity and magnetic permeability parameter values have -1 flags in the program to indicate a metallic or magnetic object.

<u>PARAMETER</u>	<u>RANGE</u>
Number of Layers	variable
Layer Thickness, h	variable
Conductivity, σ	0-50 mS/m
ϵ_{rh} , ϵ_{rl}	4-25, dry sand 4-10, metallic object -1
τ_e	dry 1.0, wet 10.0, iron in soil: dry 0.8, wet 10.0 ns
α_e	dry 1.0, wet 0.8, iron in soil: dry 0.7, wet 0.8
μ_{rl}	iron-free soil 1.0, iron in soil 1-16, magnetic object -1
μ_{rh}	iron-free soil 1.0, iron in soil 1-2, magnetic object -1
τ_μ	iron-free soil 1.0, iron in soil > 0.3 ns
α_μ	iron-free soil 1.0, iron in soil 0.75
Cr	1-2
Offset	dependent on antenna system

After the initial values of the parameters have been chosen, the inversion proceeds by calculating a model GPR trace and comparing it to the field trace. Usually some measure of fit is used to determine if the model trace is a satisfactory representation of the field trace, or if the parameters should be adjusted and a new model trace calculated. This process is repeated until a maximum number of iterations has been reached or the model fit is acceptable. The conventional methods for data inversion invert all parameters simultaneously. When the problem contains a large number of parameters, which could be the case with GPR data, the inversion becomes time consuming and problems with convergence arise. A possible inversion technique to avoid this problem is to use a layer stripping method. Layer stripping involves inverting for parameters one layer at a time and then removing that layer and proceeding downward through the subsurface. The number of parameters solved for at a given time are reduced, and therefore the time required to perform the inversion is greatly reduced. The layer stripping technique has been used to invert dc resistivity data (Pekeris 1940) and seismic reflection data (Yagle and Levy 1985).

Manual Inversion of GPR Data

To illustrate the procedure involved in a numerical inversion, the manual inversion of GPR field data is presented through the use of the forward modeling program GPRMODv2 (Powers and Olhoeft 1995). A plot of the field data is given in Figure 17. The hyperbolic reflection on the right side of the radar section is caused by a 4 feet diameter steel pipe. The initial parameter values chosen to invert the data are listed below. Only four of the parameters in the table were allowed to vary; all others were assumed constant. The thickness of the material overlaying the pipe was calculated based on an assumed velocity of 0.1m/s and a one-way travel time of 18ns (obtained from plot of field data).

<u>PARAMETER</u>	<u>VARY</u>	<u>VALUE</u>
Number of Layers	no	2
Layer Thickness	yes	$h_1=1.8\text{m}$
Conductivity	no	$\sigma_1=10\text{mS/m}$, $\sigma_2=10,000\text{mS/m}$
ϵ_{r1}	yes	$\epsilon_{r1}=8$, $\epsilon_{r12}=-1$
$\epsilon_{r\infty}$	yes	$\epsilon_{r\infty1}=8$, $\epsilon_{r\infty2}=-1$
τ_e	no	$\tau_{e1}=10\text{ns}$, $\tau_{e2}=0\text{ns}$
α_e	no	$\alpha_{e1}=0.8$, $\alpha_{e2}=1$
μ_{r1}	no	$\mu_{r11}=1$, $\mu_{r12}=-1$
$\mu_{r\infty}$	no	$\mu_{r\infty1}=1$, $\mu_{r\infty2}=-1$
τ_μ	no	$\tau_{\mu1}=0\text{ns}$, $\tau_{\mu2}=0\text{ns}$
α_μ	no	$\alpha_{\mu1}=1$, $\alpha_{\mu2}=1$
Cr	yes	$\sqrt{\epsilon_r}/2 = 1.41$
Offset	no	9.45 ns

Figure 18a is a plot showing the initial model fit (solid curve) to the field data (dotted curve). The field scan is the GPR trace at the apex of the pipe reflection. The GPR field data (Figure 17) show that the onset of the pipe reflection occurs at about 36ns and it is at this point where fitting of the model trace will begin. The initial model requires the curve to be expanded vertically and shifted to the left. To accomplish this, the dielectric permittivity is increased to 9.0, giving a $C_r=1.5$, and the layer thickness decreased to 1.34m for the first iteration (Figure 18b). The model curve is now in approximately the correct position laterally, however the curve still requires more vertical expansion. For the second iteration, the permittivity is increased to 10 with $C_r=1.58$ and the layer thickness must be decreased to 1.2m (Figure 18c). This iteration appears to have smoothed the variations present in the curve between 55ns and 70ns, which should be retained since the field scan shows the undulations and therefore should be modeled. In the next iteration, the permittivity is reduced to 9.2, $C_r=1.52$, and the layer thickness increased to 1.3m (Figure 18d). Now the model curve has basically the same shape as the field scan, so the dB is increased to 7 to vertically enhance the model response (Figure 18e). Further attempts to match the positive peaks in the model curve with those in the field scan were not successful so the model fit in Figure 18e is accepted and the inversion process terminated. The parameters used in each iteration step are summarized below.

<u>ITERATION</u>	<u>ϵ_{rl}</u>	<u>ϵ_{rm}</u>	<u>C_r</u>	<u>h</u>	<u>dB</u>
Initial	8.0	8.0	1.41	1.80	0
1	9.0	9.0	1.50	1.34	0
2	10.0	10.0	1.52	1.30	0
3	9.2	9.2	1.52	1.30	0
Final	9.2	9.2	1.52	1.30	7

Holding many of the parameters constant is not a bad practice if effects caused by dispersion are small and the remaining parameters can be reliably determined or estimated. Which parameters can be held fixed during the inversion depends on the soil properties at a site. The iterative procedure is considerably simplified when the number of varying parameters involved in the inversion is reduced.

6 Conclusions

In situations where ground penetrating radar has a sufficient depth of investigation capability to address a specific problem, it has the greatest horizontal and vertical resolution of any geophysical method that can be applied to the problem. Existing analysis procedures use only a small amount of the information contained in the received GPR waveform, and do not consider electromagnetic wave attenuation, geometric spreading, dispersion, scattering, and interface reflection/transmission losses. This research focused on the assumptions and considerations necessary for developing an interpretation procedure that utilizes the full GPR waveform for determining layer thicknesses and the EM properties of subsurface materials.

Forward modeling of GPR data is helpful in determining if it is feasible to use GPR at a particular site given certain physical properties of the soil, what frequency antenna is required to detect layers of varying thickness, and what type of response should be expected for various combinations of conductivity, dielectric permittivity, and magnetic permeability. The forward modeling study showed that, because of the superposition of primary arrival events and multiples, arrival times other than that of the first primary reflection cannot always be determined with confidence by visual inspection of the GPR record. The application of data processing techniques to detect event arrivals that are too closely spaced in time to be visually resolved is required.

An initial investigation of the inversion of GPR data was undertaken. There are many parameters involved in the inversion of full waveform GPR data. The inversion problem would be unmanageable without making certain assumptions and restraining some parameters with field measurements. Fortunately, in the high frequency range, $f \geq 100\text{MHz}$, dispersion often times is not a major concern so the imaginary component of the dielectric permittivity and magnetic permeability is zero. If the soil is relatively iron-free so the magnetic permeability can be assigned a fixed value, then the number of free parameters in the inversion is reduced to three per layer, the real dielectric permittivity ($\epsilon_r = \epsilon_{r\text{max}}$ in GPRMODv2), conductivity, and layer thickness, plus the coupling ratio ($C_r = \sqrt{\epsilon_r}/2$).

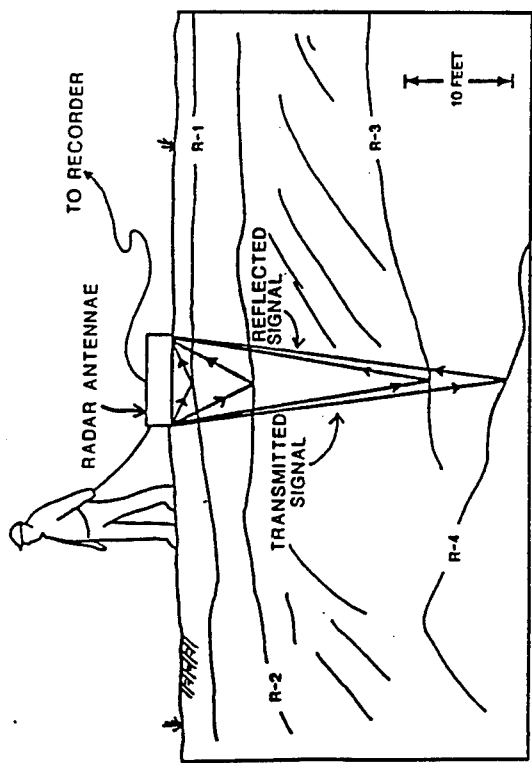
Both crosscorrelation and deconvolution were shown to be effective at delineating material interfaces, however deconvolution was better able to resolve interfaces for more complex transmitter waveforms. Identification of the number of interfaces (hence number of layers) and their approximate location in depth and/or time is an important first step in the inversion process.

References

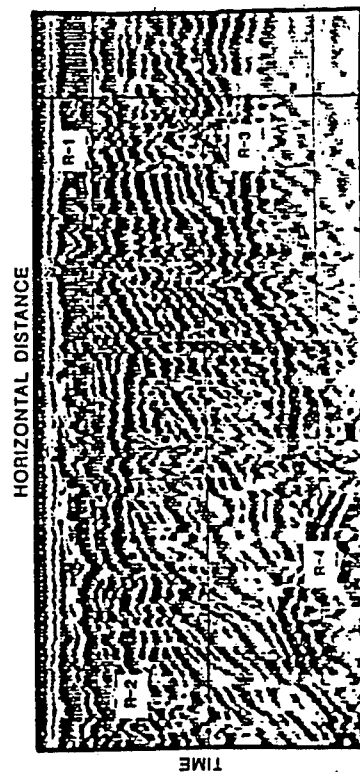
- Annan, A.P. (1992). "Ground penetrating radar workshop notes," Systems and Software, Inc., Mississauga, Ontario, Canada.
- Annan, A.P., and Cosway, S.W. (1992). "Ground penetrating radar survey design," Annual Meeting of SAGEEP.
- Balanis, C.A. (1989). *Advanced Engineering Electromagnetics*. John Wiley and Sons, New York.
- Ballard, Robert F. (1983). "Cavity detection and delineation research, Report 5, Electromagnetic (Radar) techniques applied to cavity detection," Technical Report GL-83-1, U.S. Army Engineer Waterways Experiment Station, Vicksburg, MS.
- Bohling, Geoffrey C., Anderson, Mary P., and Bentley, Charles R. (1989). "Use of ground penetrating radar to define recharge areas in the Central Sand Plain," Technical Report, Project No. G1458-03, University of Wisconsin, Madison, WI.
- Brewster, M.L., and Annan, A.P. (1994). "Ground-penetrating radar monitoring of a controlled DNAPL release: 200 MHz radar," *Geophysics*, 59(8), 1211-1221.
- Butler, Dwain K. (1992). "Proceedings of the government users workshop on ground penetrating radar applications and equipment," Miscellaneous Paper GL-92-40, U. S. Army Engineer Waterways Experiment Station, Vicksburg, MS.
- Butler, Dwain K., Yule, Donald E., Llopis, Jose L., and Sharp, Michael L. (1989). "Geophysical assessment of foundation conditions: Right abutment, Mill Creek Dam," Technical Report GL-89-12, U. S. Army Engineer Waterways Experiment Station, Vicksburg, MS.
- Butler, Dwain K., Llopis, Jose L., Dobecki, Thomas L., Corwin, Robert F., Wilt, Michael J., and Olhoeft, Gary. (1990). "Comprehensive geophysics investigation of an existing dam foundation: Engineering geophysics research and development," *Geophysics: The Leading Edge of Exploration*, 9(9); 44-53.

- Butler, Dwain K., Simms, Janet E., and Cook, Daryl S. (1994). "Archaeological geophysics investigation of the Wright Brothers 1910 Hangar Site: Wright-Patterson Air Force Base, Ohio," Technical Report GL-94-13, U. S. Army Engineer Waterways Experiment Station, Vicksburg, MS.
- Buyukozturk, Oral, and Rhim, Hong C. (1993). "Electromagnetic properties of concrete for nondestructive testing," *Proceedings of the International Conference on Nondestructive Testing of Concrete in the Infrastructure*.
- Cole, K.S. and Cole, R.S. (1941). "Dispersion and adsorption in dielectrics, I, alternating current characteristics," *J. Chem. Phys.* 9, 341-351.
- Davis, J.L., and Annan, A.P. (1989). "Ground penetrating radar for high-resolution mapping of soil and rock stratigraphy," *Geophysical Prospecting*, 37, 531-551.
- Duke, S.K. (1990). "Calibration of ground penetrating radar and calculation of attenuation and dielectric permittivity versus depth," M.S. Thesis T-3920, Colorado School of Mines, Golden, CO, 236p.
- Jol, Harry M. (1995). "Ground penetrating radar antennae frequencies and transmitter powers compared for penetration depth, resolution and reflection continuity," *Geophysical Prospecting*, 43, 693-709.
- Keller, G.V. (1987). "Rock and mineral properties." *Electromagnetic Methods in Applied Geophysics: Volume 1, Theory*. M.N. Nabighian ed., Society of Exploration Geophysics, Tulsa, OK, pp. 13-51.
- Kline, M., and Kay, I.W. (1965). *Electromagnetic theory and geometrical optics*. John Wiley and Sons, New York, p179.
- Llopis, Jose L., and Simms, Janet E. (1993). "Geophysical investigation at U.S. Army Materials Technology Laboratory, Massachusetts," Technical Report GL-93-29, U.S. Army Engineer Waterways Experiment Station, Vicksburg, MS.
- Lorrain, D., and Corson, D.R. (1970). *Electromagnetic fields and waves*. Freeman, San Francisco.
- Maser, Kenneth R., and Scullion, Tom. (1992). "Automated pavement subsurface profiling using radar: Case studies of four experimental field sites," *Transportation Research Record No. 1344*, National Academy Press, Washington, D.C.
- May, B.T., and Hron, F. (1978). "Synthetic seismic sections of typical petroleum traps," *Geophysics* 43(6), 1119-1147.
- Olhoeft, G.R. (1981). "Electrical properties of rocks." *Physical Properties of Rocks and Minerals*. Y.S.Touloukian, W.R.Judd, and R.F.Roy, eds., McGraw-Hill, NY, pp.257-330.

- Olhoeft, G.R. (1984). "Applications and limitations of ground penetrating radar," SEG Expanded Abstracts, 54th Ann. Int. Mtg., p147-148.
- Olhoeft, G.R. (1986). "Electrical properties from 10^{-3} to 10^{19} Hz -- physics and chemistry." *Proceedings of the 2nd International Symposium on the Physics and Chemistry of Porous Media*. J.R. Banavar, J. Koplik, and K.W. Winkler, eds., Am. Inst. Phys., Conf. Proc. 154.
- Olhoeft, G.R., and Strangway, D.W. (1974). "Magnetic relaxation and the electromagnetic response parameter," *Geophysics*, 39(3), 302-311.
- Olhoeft, G.R., and Capron, D.E. (1994). "Petrophysical causes of electromagnetic dispersion." *Proceedings of the Fifth International Conference on Ground Penetrating Radar*. June 12-16, Kitchener, Ontario, Canada, 145-152.
- Pekeris, C.L. (1940). "Direct method of interpretation in resistivity prospecting," *Geophysics* 5, 31-46.
- Powers, M.H., and Olhoeft, G.R. (1995). "GPRMODV2: One-dimensional full waveform modeling of dispersive ground penetrating radar data, version 2.0," U.S. Geological Survey Open File Report 95-58.
- Sharp, Michael K., Yule, Donald E., and Butler, Dwain K. (1990). "Geophysical Investigation of Burial Site 3-A, Defense Depot Ogden, Utah," Miscellaneous Paper GL-90-6, U.S. Army Engineer Waterways Experiment Station, Vicksburg, Ms.
- Sheriff, R.E. (1984). *Encyclopedic dictionary of exploration geophysics*. 2nd ed., Society of Exploration Geophysicists, Tulsa, OK.
- Simms, J.E., and Morgan, F.D. (1992). "Investigation of various least-squares inversion schemes for interpreting resistivity data," *Geophysics*, 57, 1282-1293.
- Ulaby, F.T., Moore, R.K., and Fung, A.K. (1981). *Microwave Remote Sensing Active and Passive, Volume 1: Microwave remote sensing fundamentals and radiometry*. Addison-Wesley Publishing, Reading, MA.
- Von Hippel, A.R. (1954). *Dielectrics and Waves*. The M.I.T. Press, Cambridge, MA, pp.28,64.
- Widess, M.B. (1973). "How thin is a thin bed?," *Geophysics*, 38, 1176-1180.
- Yagle, A.E., and Levy, B.C. (1985). "A layer-stripping solution of the inverse problem for a one-dimensional elastic medium," *Geophysics* 50(3), 425-433.



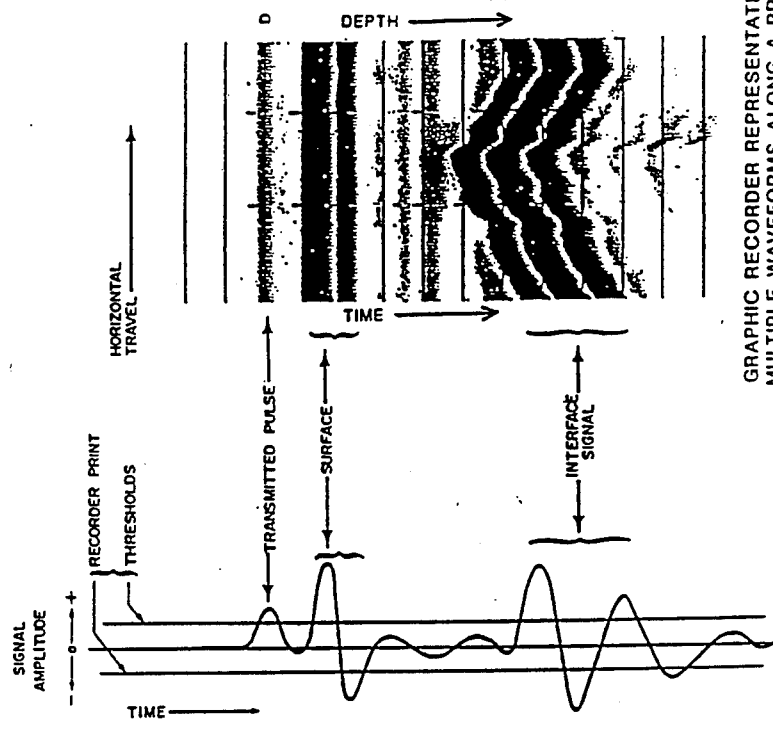
GPR SURVEY OVER GEOLOGIC SECTION, REFLECTORS R-1 -- R-4



GRAPHIC RADAR RECORD FOR ABOVE SECTION

1a. GPR survey concepts

GPR RECEIVED SIGNAL AND GRAPHIC PROFILE DISPLAY



SKETCH OF TYPICAL SINGLE WAVEFORM

1b. Typical, single GPR full waveform and graphic record

Figure 1. GPR surveying concepts, typical single full waveform, and graphic record

COLE-COLE DISTRIBUTION

$$\epsilon_l = 25 \quad \epsilon_\infty = 7 \quad \tau\epsilon = 8\text{ns} \quad \alpha\epsilon = 1.0$$

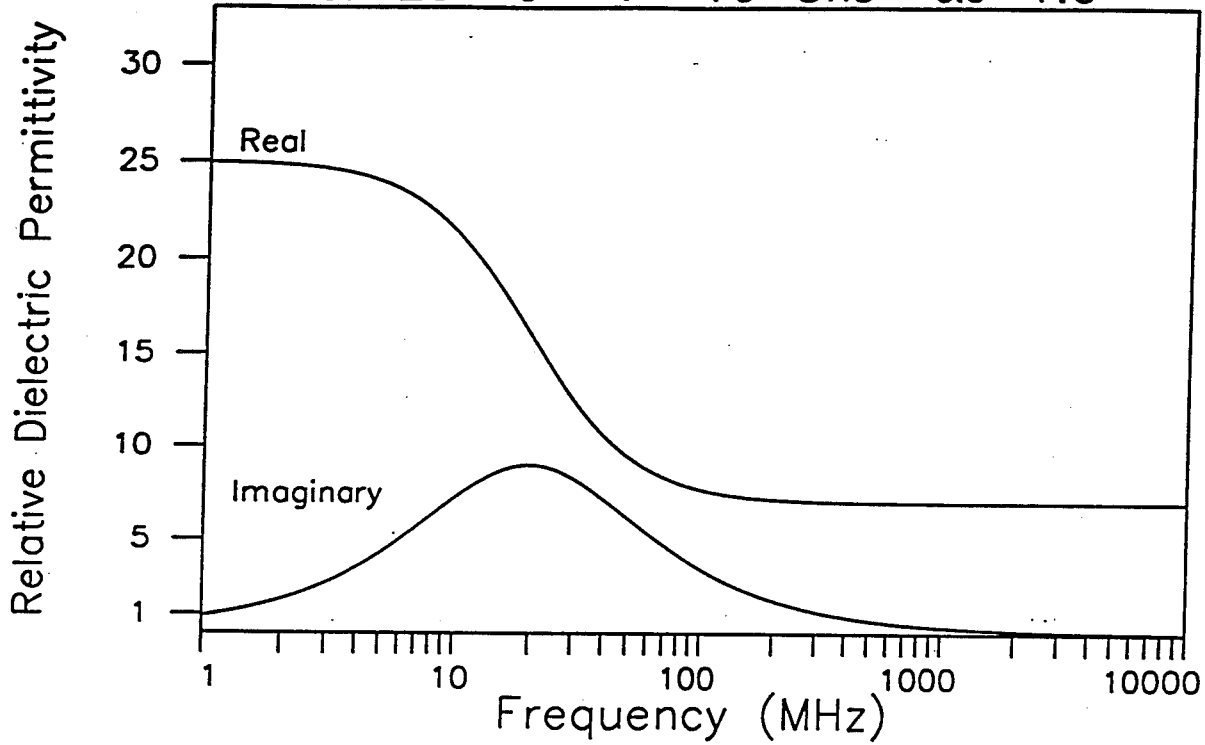


Figure 2. Cole-Cole plots of the real and imaginary parts of the dielectric permittivity as a function of frequency

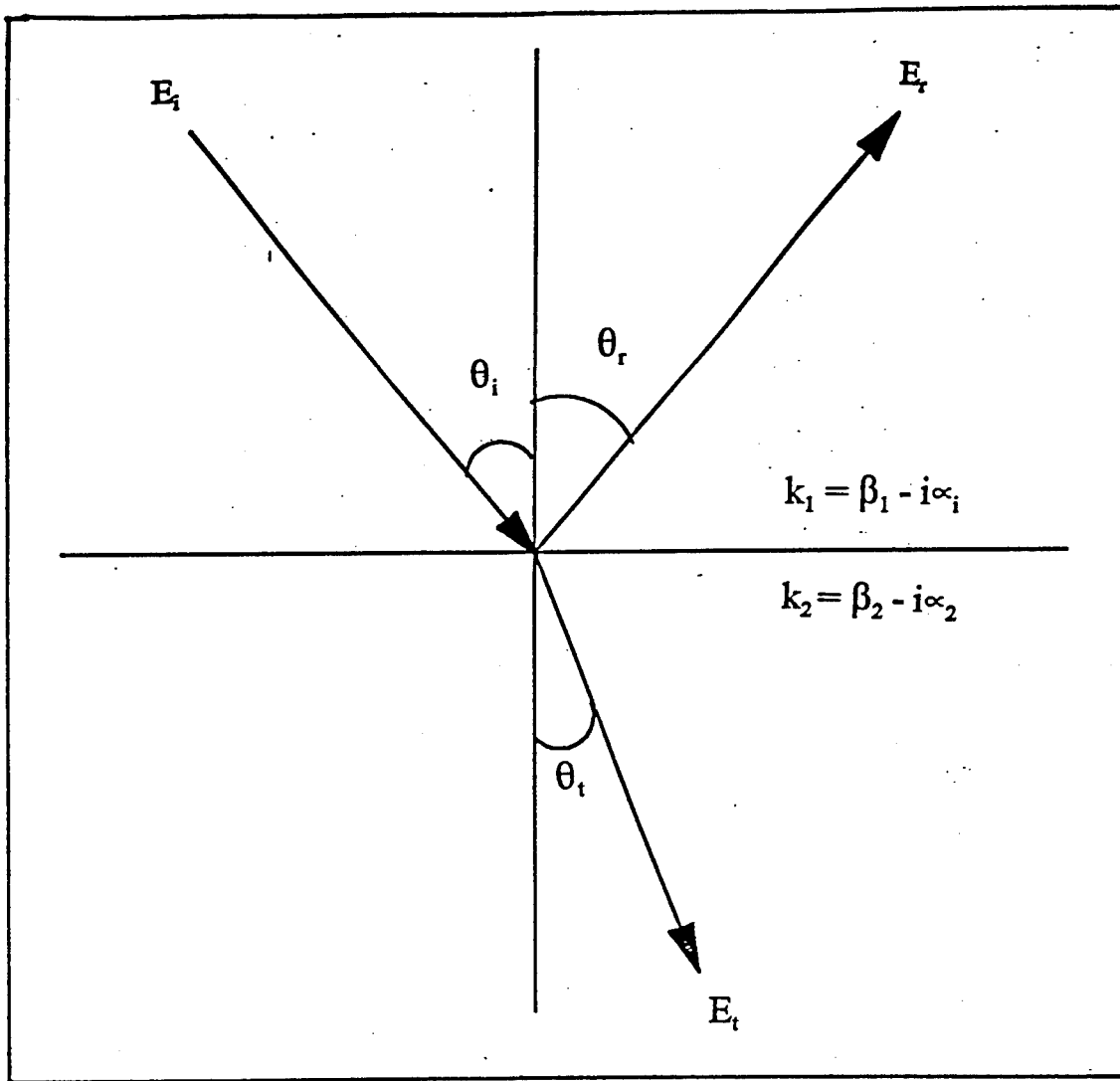


Figure 3. Incident, reflected, and transmitted rays, and their associated angles, at an interface

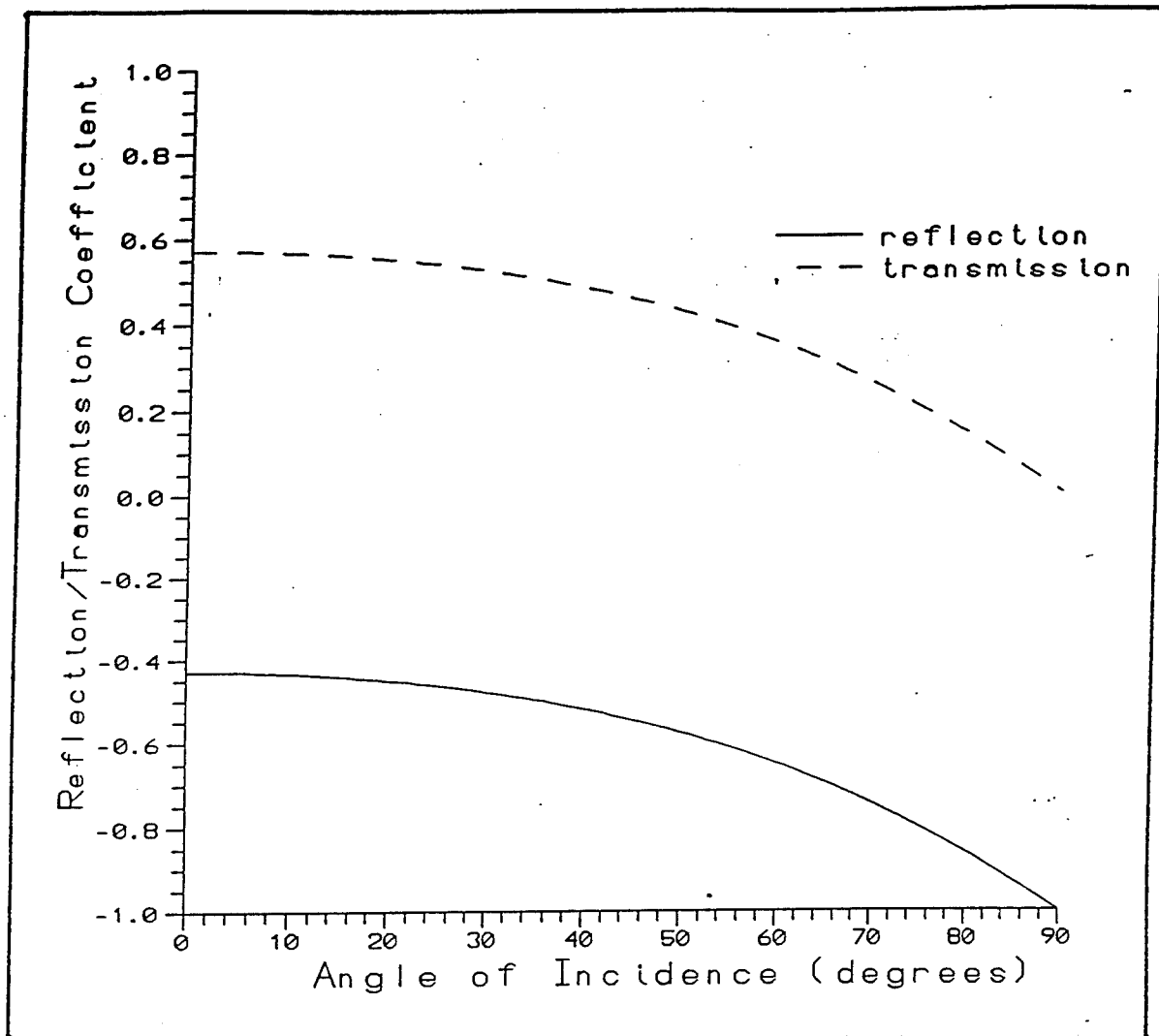


Figure 4. Effect of angle of incidence on reflection and transmission coefficients .
 $\mu_1 = \mu_2 = \mu_0$, propagation constant $\gamma_1 = 2$, $\gamma_2 = 4$

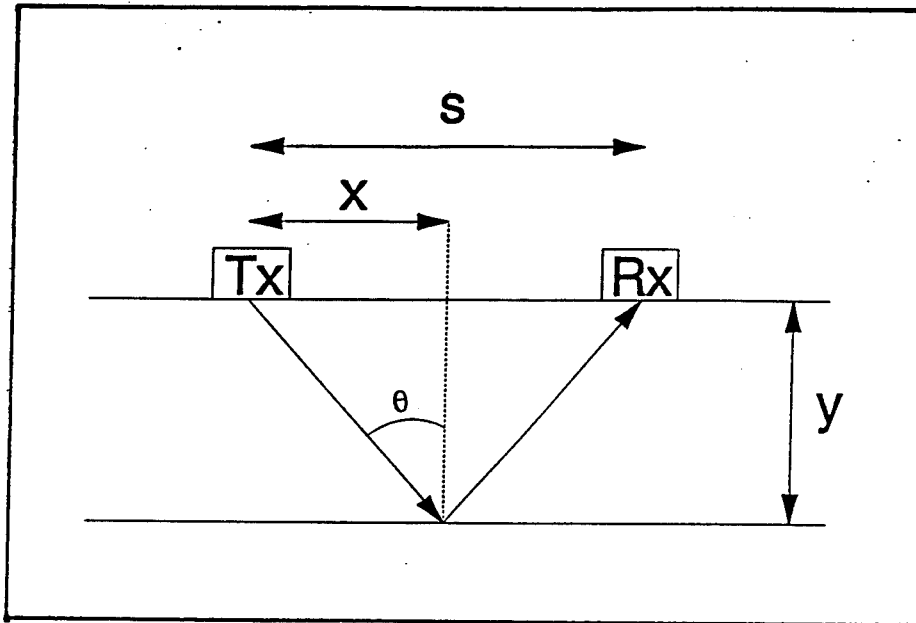


Figure 5. Illustration relating antenna separation (s) to target depth (y). Rule of thumb is $s=0.2y$ (Annan and Cosway 1992)

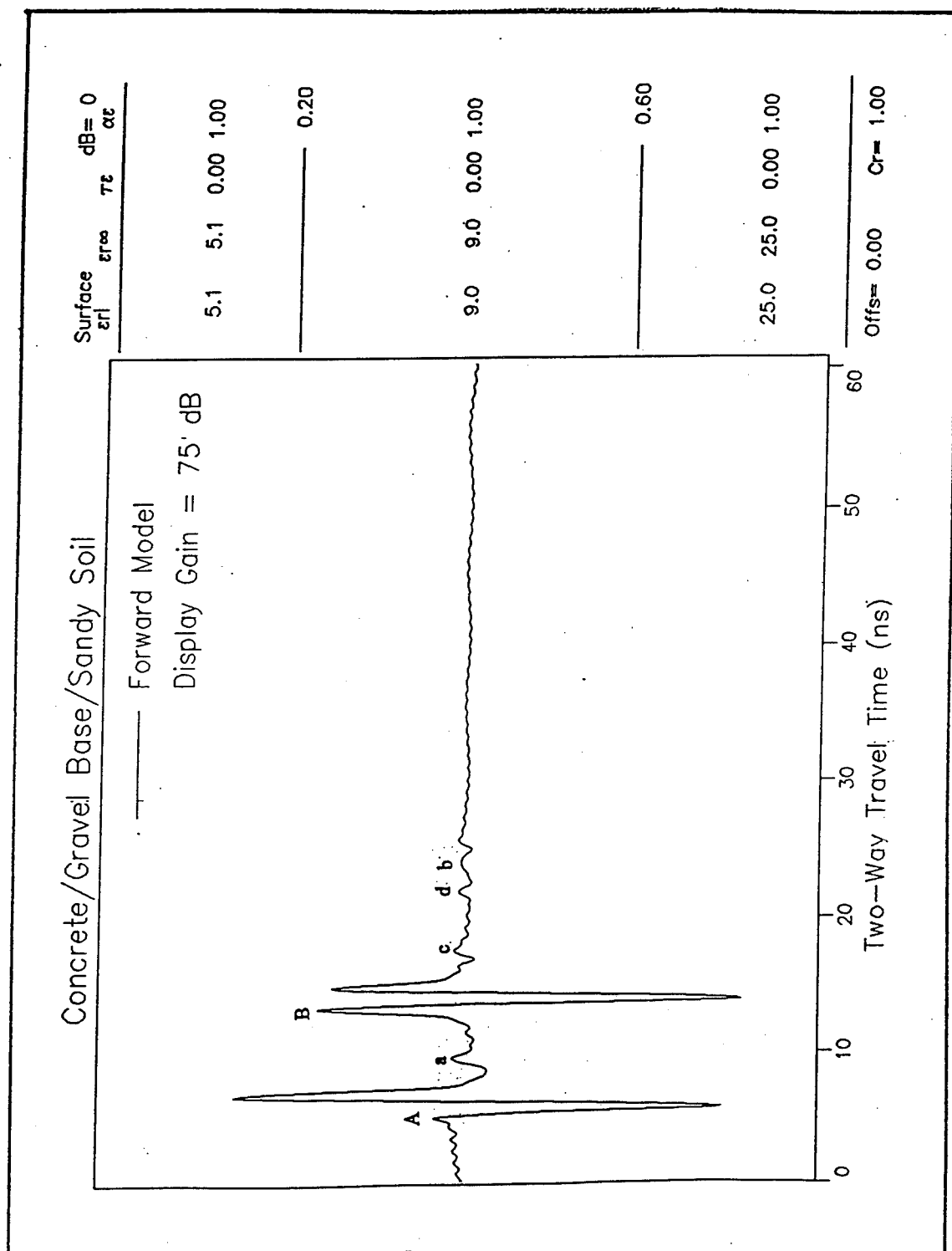


Figure 6. Example of forward model output for a two layer pavement structure

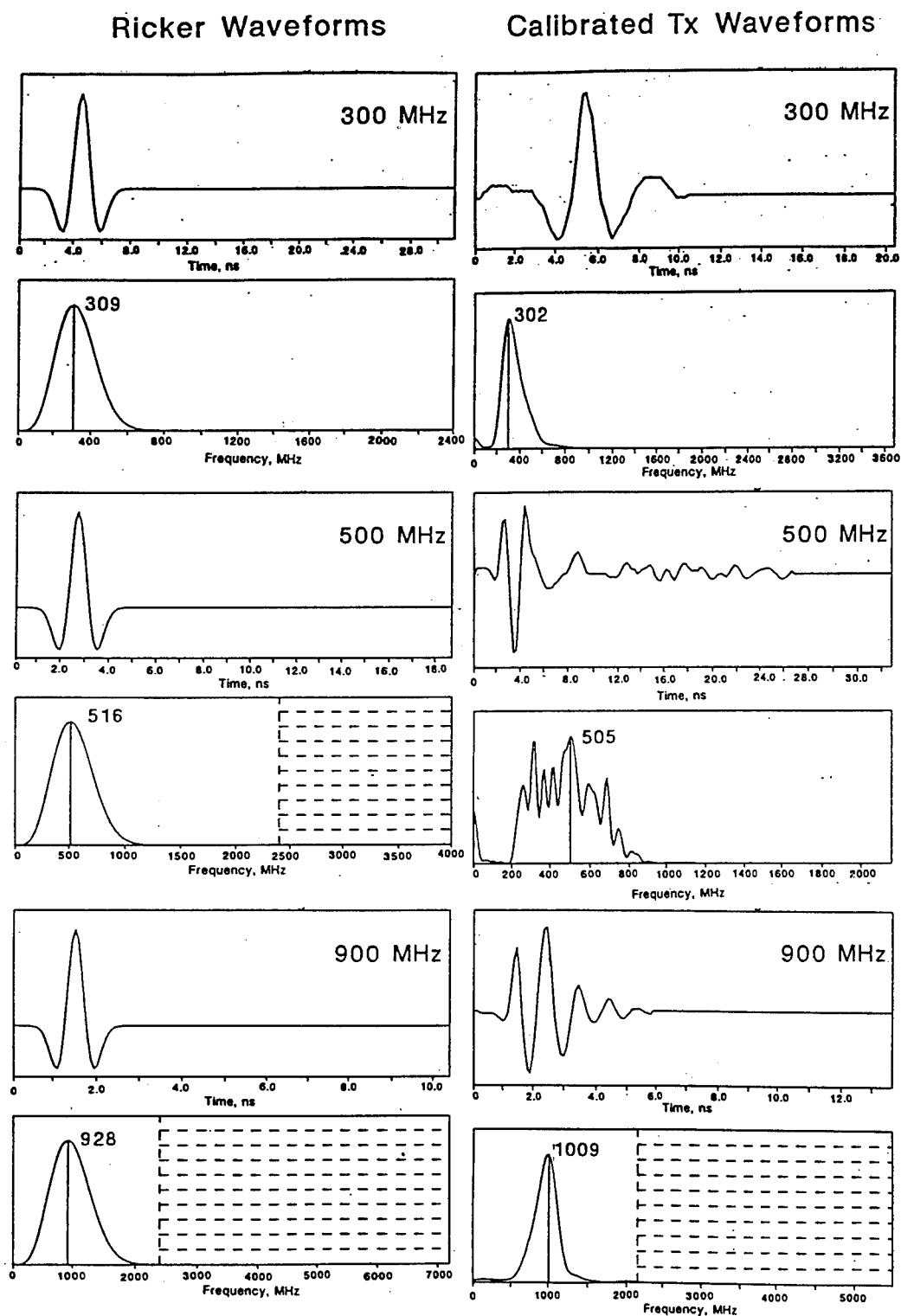


Figure 7. Comparison of 300, 500, and 900 MHz Ricker waveforms (left) with calibrated transmitter (Tx) waveforms (right)



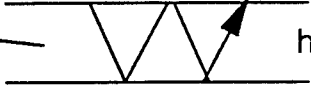

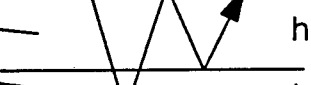
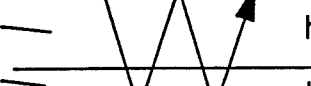
		Two-Way Reflection Times, ns			
		9.5%	6.7%	0.0%	
1st Primary					
Concrete		$h = 0.3 \text{ m}$	5.8	4.5	3.8
Water		$hw = 0.05 \text{ m}$			
Sand					
2nd Primary					
Concrete		$h = 0.3 \text{ m}$	8.8	7.5	6.8
Water		$hw = 0.05 \text{ m}$			
Sand					
Multiple (101)					
Concrete		$h = 0.3 \text{ m}$	11.6	9.0	7.6
Water		$hw = 0.05 \text{ m}$			
Sand					
Multiple (212)					
Concrete		$h = 0.3 \text{ m}$	11.8	10.5	9.8
Water		$hw = 0.05 \text{ m}$			
Sand					
Multiple (201)					
Concrete		$h = 0.3 \text{ m}$	14.6	12.0	10.6
Water		$hw = 0.05 \text{ m}$			
Sand					
Multiple (202)					
Concrete		$h = 0.3 \text{ m}$	17.6	15.0	13.6
Water		$hw = 0.05 \text{ m}$			
Sand					

Figure 8. Two-way reflection times for primary and selected multiple events in a concrete/water/sand model for three concrete water contents

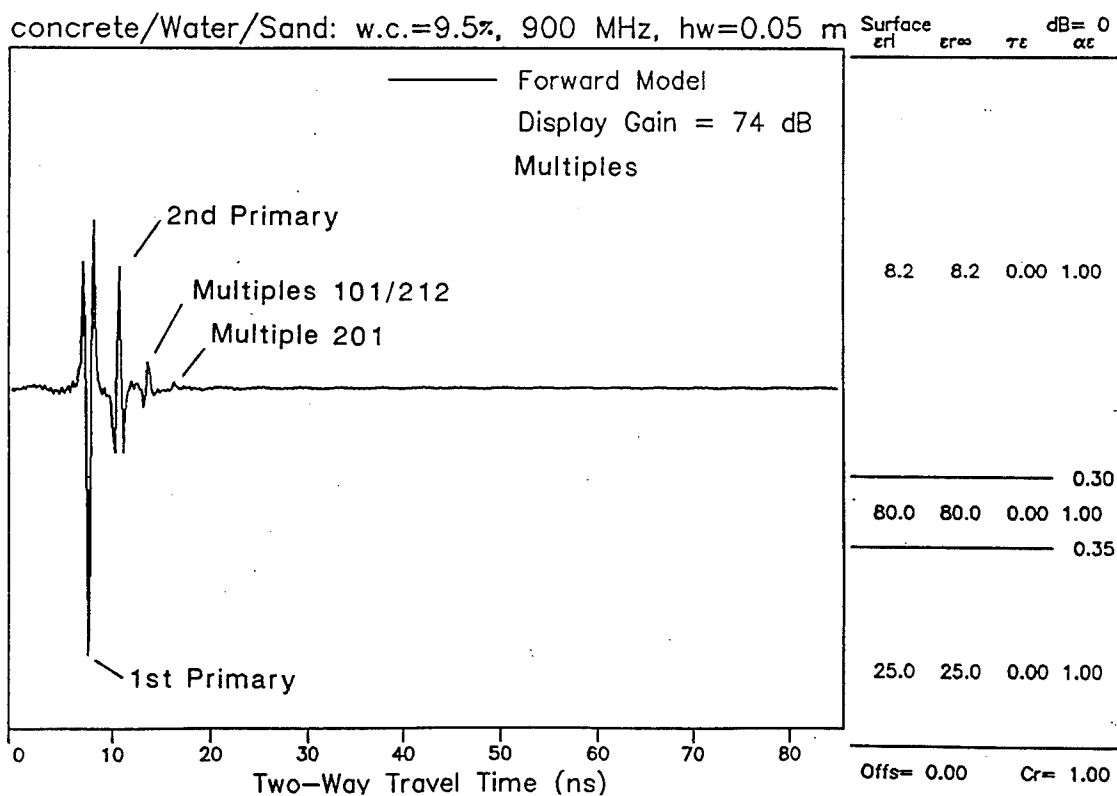
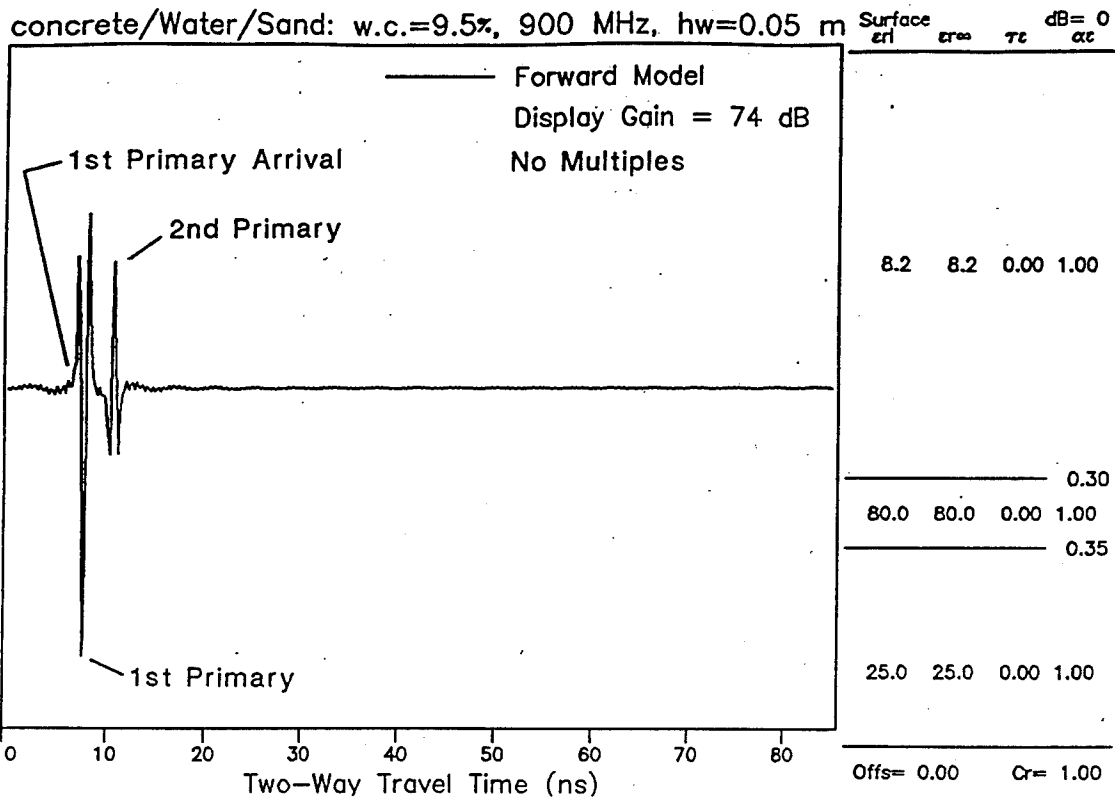


Figure 9. GPRMODv2 output for Case 172 (top) and Case 65 (bottom), concrete w.c. = 9.5% and 900 MHZ, with primary reflections (both plots) and multiples (bottom only) identified

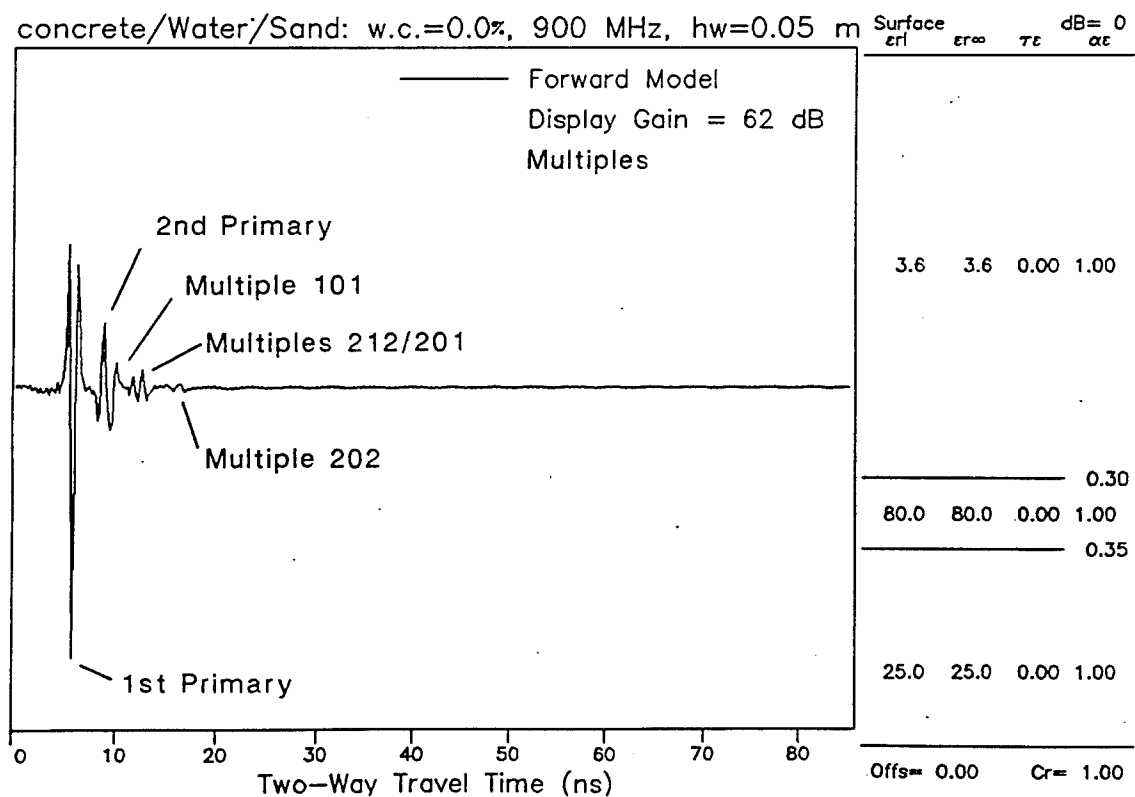
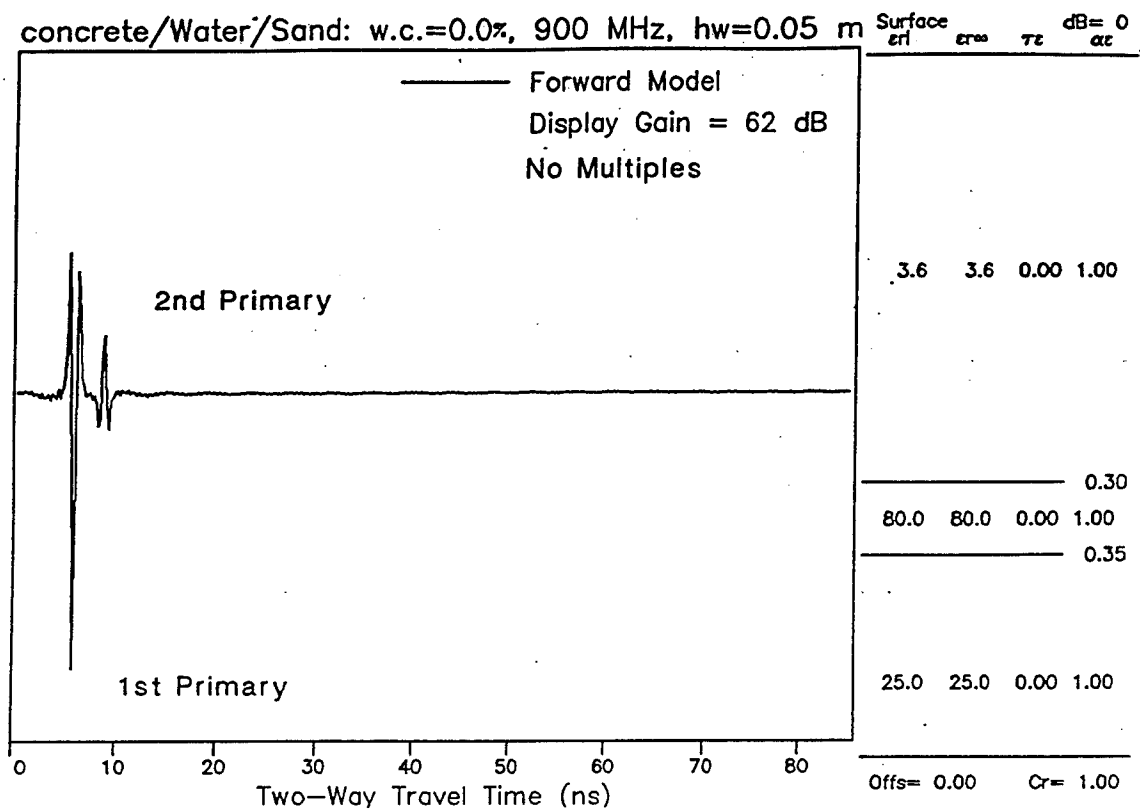


Figure 10. GPRMODv2 output for Case 245 (top) and Case 137 (bottom), concrete w.c. = 0.0% and 900 MHz, with primary reflections (both plots) and multiples (bottom only) identified

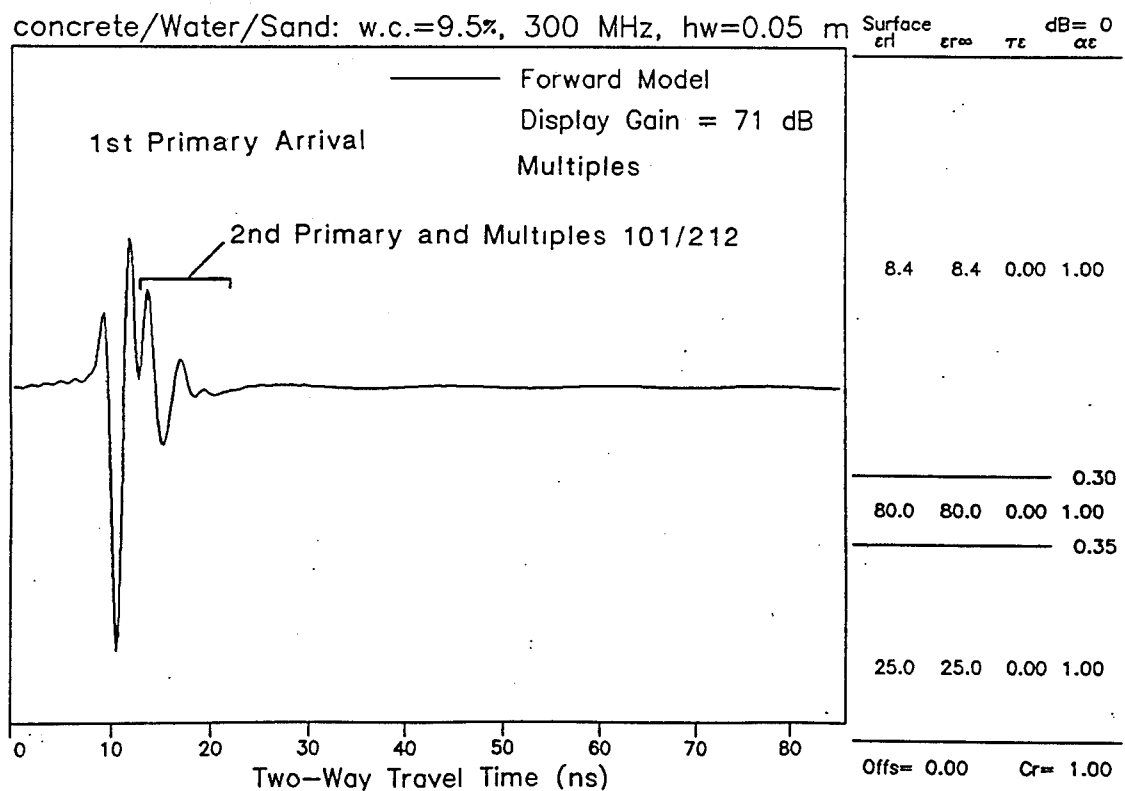
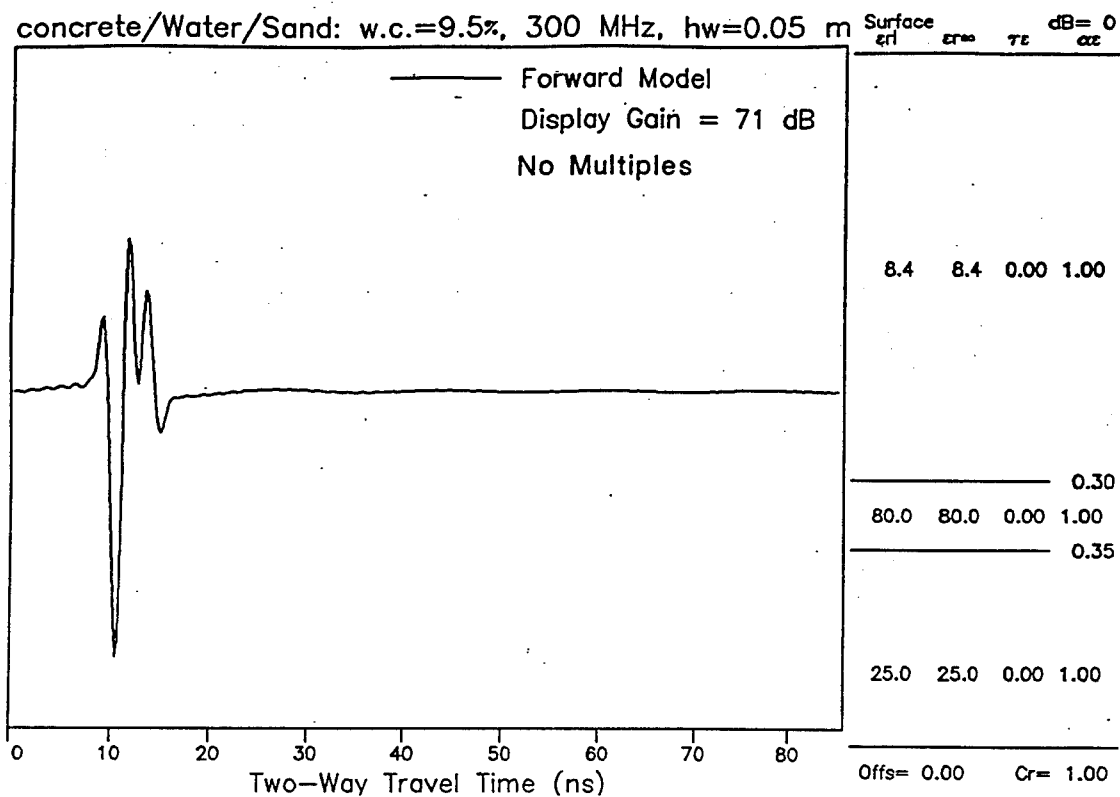


Figure 11. GPRMODv2 output for Case 149 (top) and Case 41 (bottom), concrete w.c. = 9.5% and 300 MHz, with primary reflections (both plots) and multiples (bottom only) identified

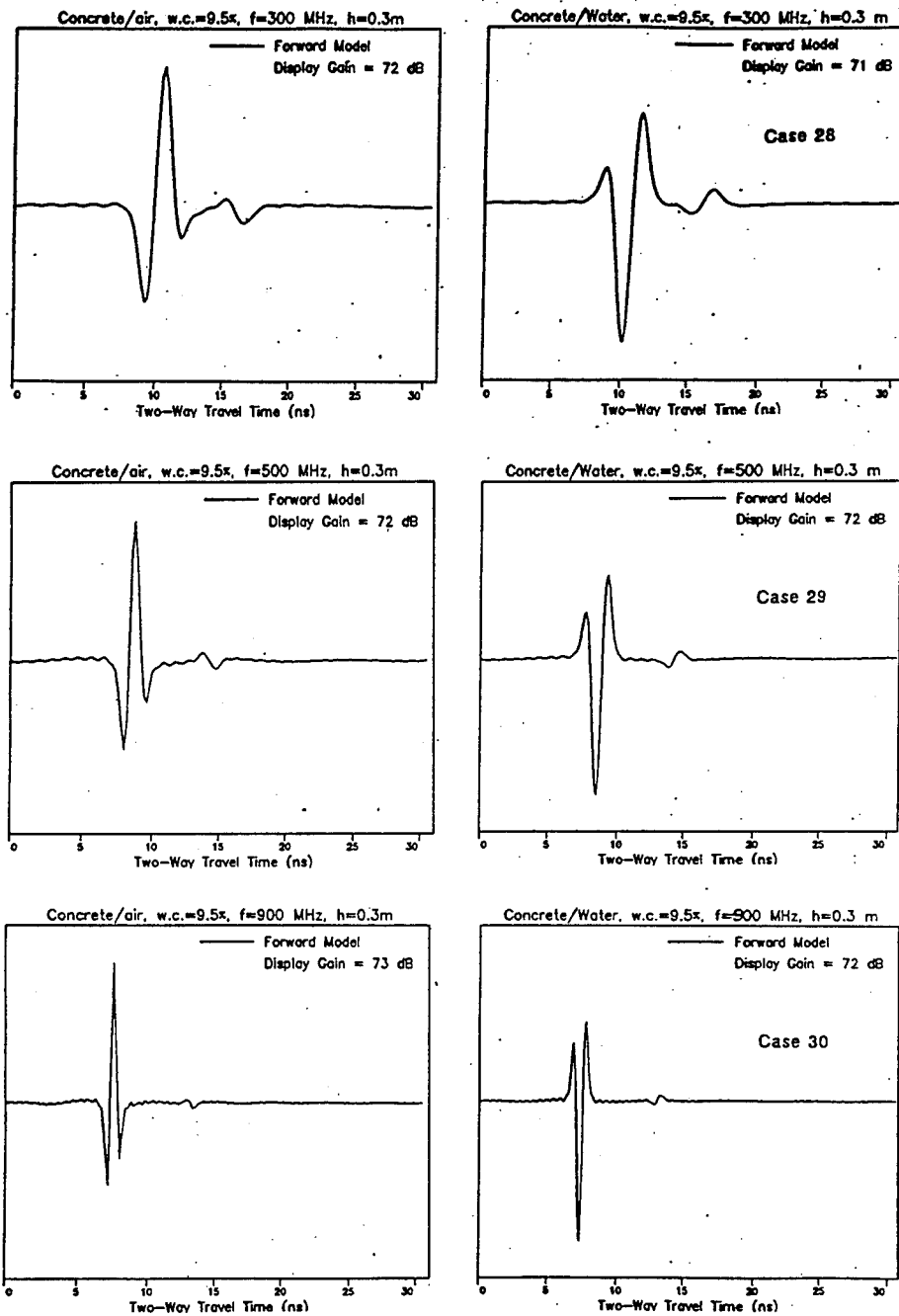


Figure 12. Comparison of concrete/air, Cases 10-12, with concrete/water reflections, Cases 28-30

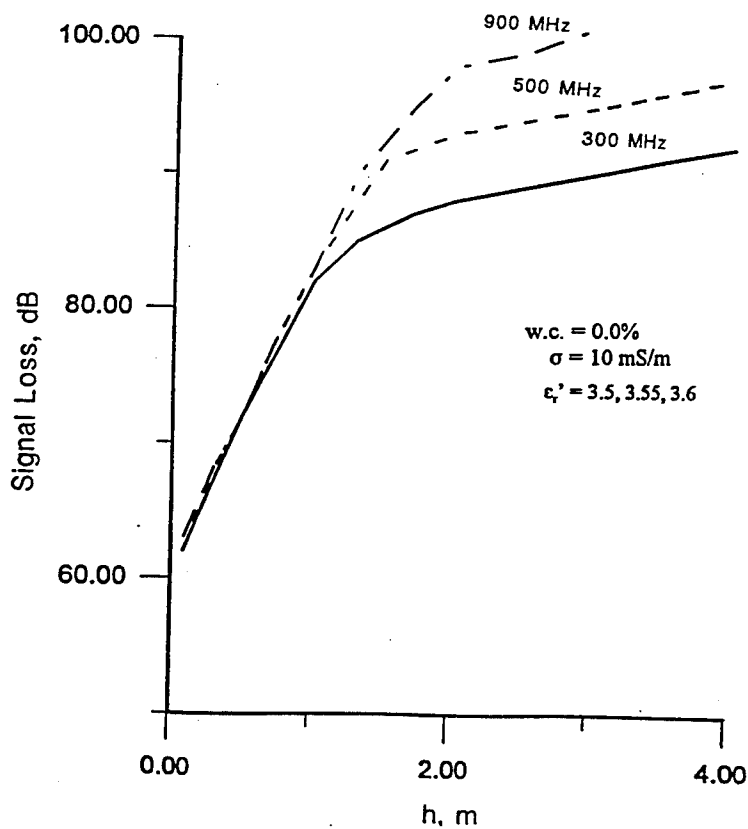
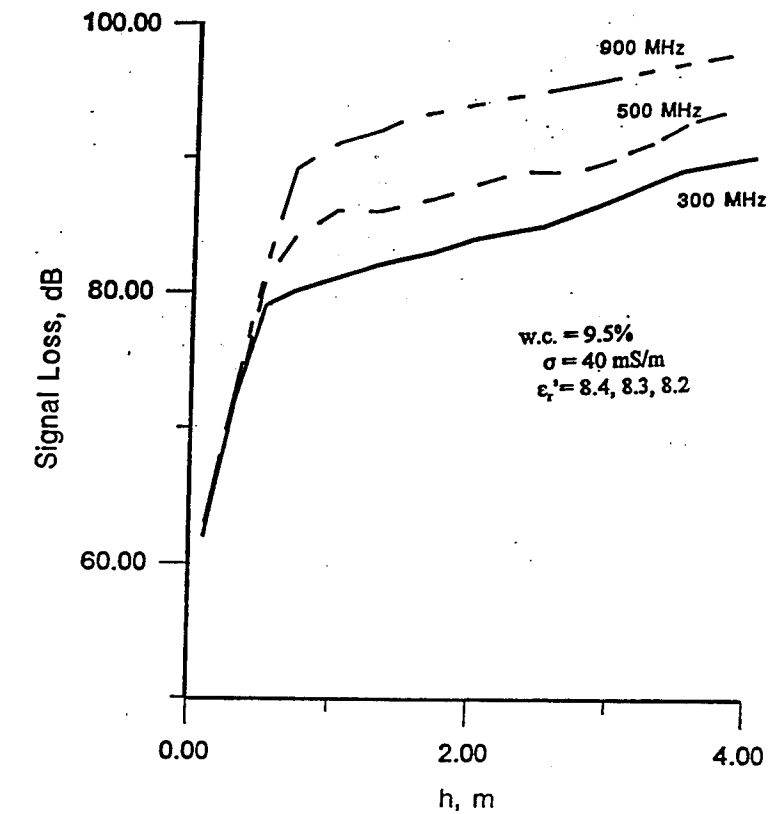


Figure 13. Signal loss versus concrete thickness for concrete w.c. = 9.5% (top) and concrete w.c. = 0.0% (bottom)

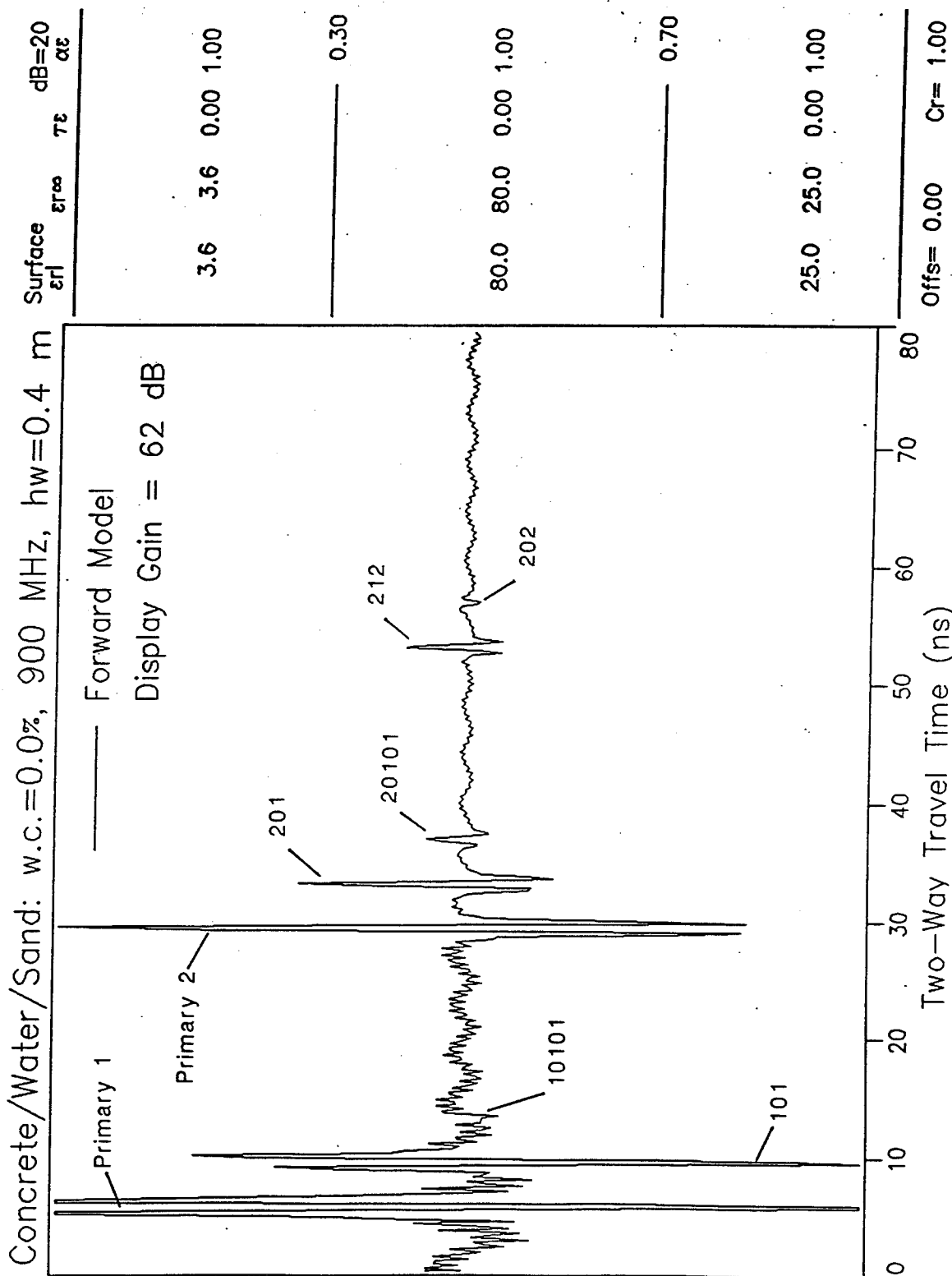


Figure 14. GPRMODv2 output for Case 252, identifying eight events: two primary reflections and six multiples

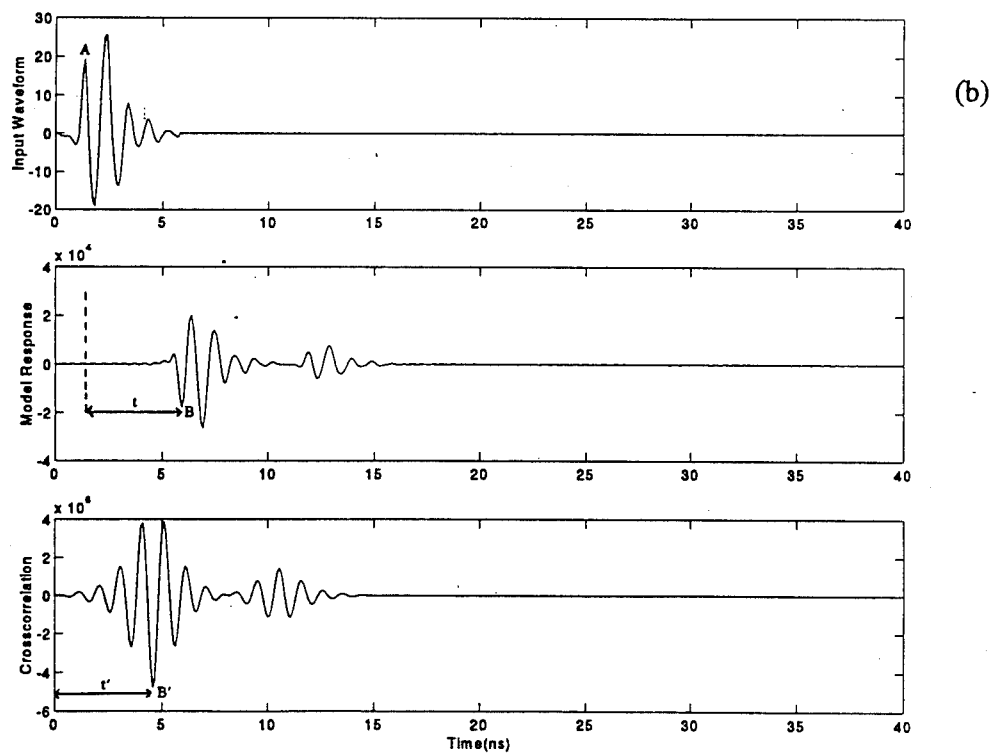
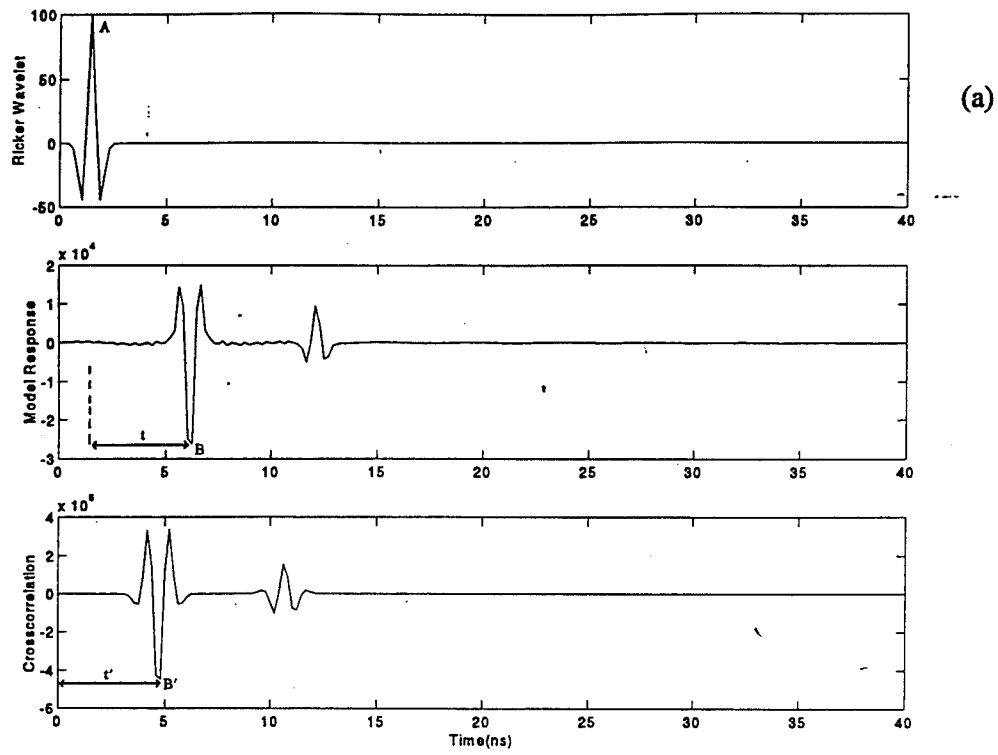


Figure 15. Results of crosscorrelation between transmitted antenna waveform and three layer model response. a) Ricker waveform, b) transmitter waveform of major GPR antenna manufacturer

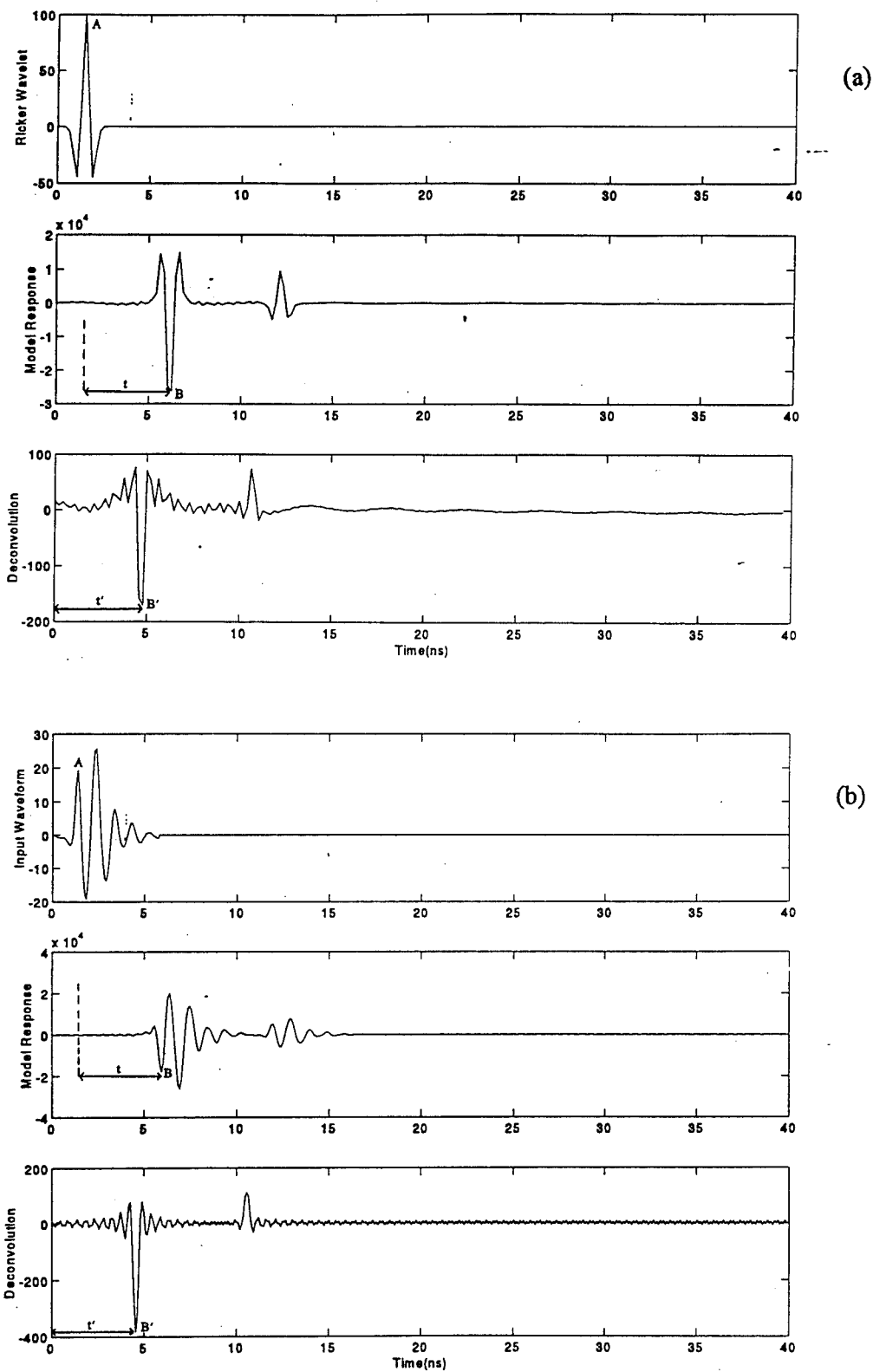


Figure 16. Results of deconvolution between transmitted antenna waveform and three layer model response. a) Ricker waveform, b) transmitter waveform of major GPR antenna manufacturer

pulseEKKO HEADER PARAMETERS

FILE = b:\w1521a
 JOB# =
 TITLE = w-152-1 side 1 line 1
 DATE = 17/10/94
 NUMBER OF TRACES = 83
 NUMBER OF PTS/TRC = 125
 TIMEZERO AT POINT = 12
 TOTAL TIME WINDOW = 100
 STARTING POSITION = 0.000
 FINAL POSITION = 8.200
 STEP SIZE USED = 0.100
 POSITION UNITS = metres
 NOMINAL FREQUENCY = 100.00
 ANTENNA SEPARATION = 1.000
 PULSER VOLTAGE = 400
 NUMBER OF STACKS = 32
 SURVEY MODE = Reflection

PROCESSING SELECTED

FILTERS:
 TRACE STACKING: 1
 POINT STACKING: 1
 TRACE DIFFERENCING: N
 SELECTION TIME: -9 to 91
 TRACE: 1 to 83
 GAINS: GAIN TYPE: CONSTANT
 MULTIPLIER: 0.100

PLOT LAYOUT PARAMETERS

TRACE SPACING AND WIDTH: 0.0300 and 0.1000
 TRACE BOTTOM AND TOP: 1.0000 and 6.0000
 MARGIN LEFT AND RIGHT: -0.5000 and 1.0000
 PAGE WIDTH: 7.0000
 BORDER SIZE: 0.000
 PRINTER NAME: LAS300
 SCALE BAR: Name:color1 Type:EA Expansion:0.500 Contour:0

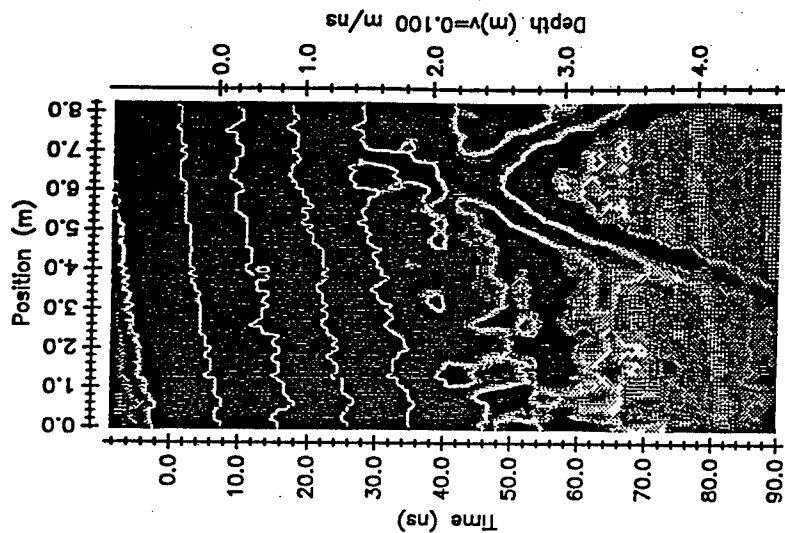
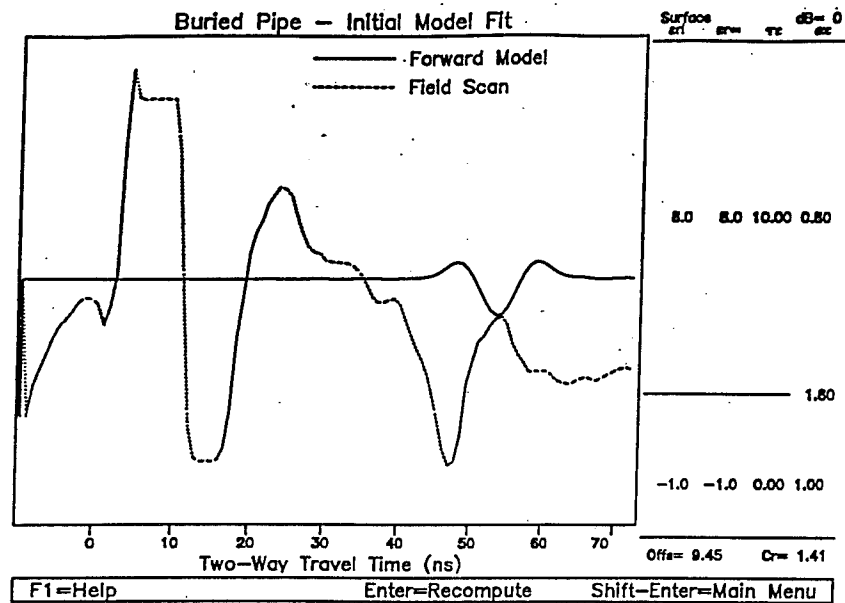
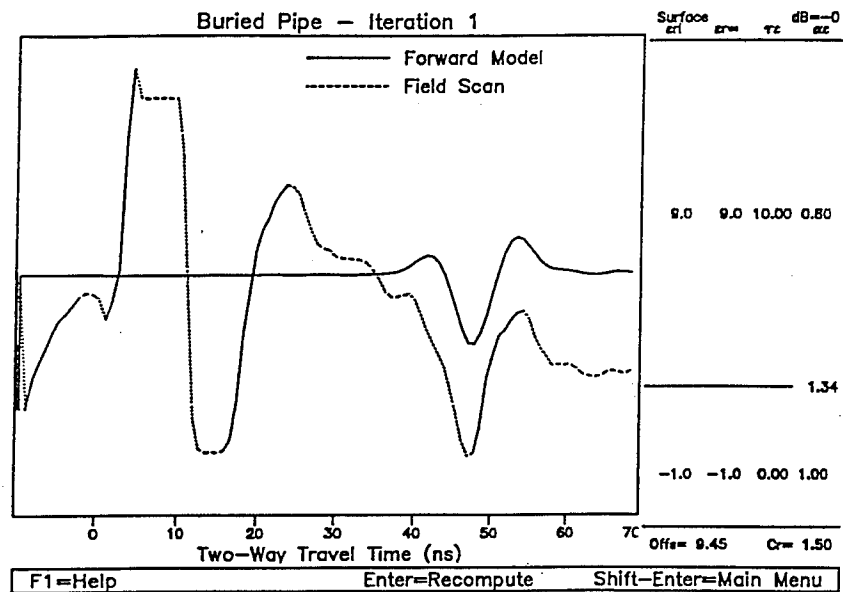


Figure 17. GPR field data collected over 4 ft diameter steel pipe

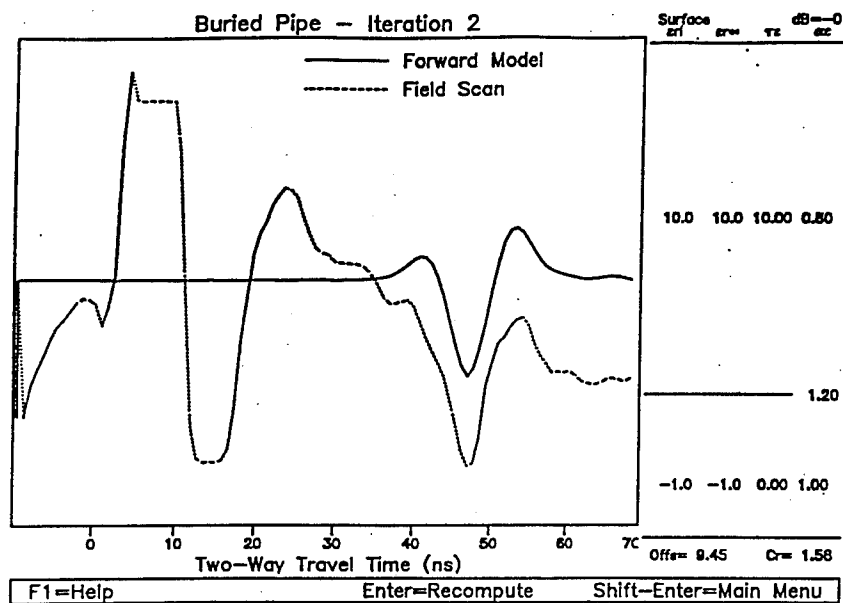


(a)

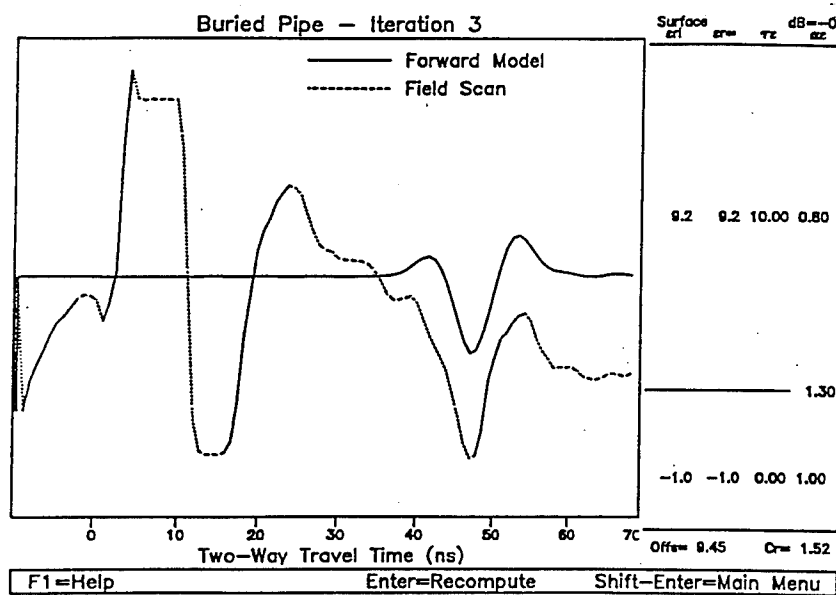


(b)

Figure 18. Illustration of manual inversion of GPR data. a) initial model fit (solid curve) to field data (dotted curve), b) model fit after Iteration 1, c) model fit after Iteration 2, d) model fit after iteration 3, e) model fit obtained by increasing dB level

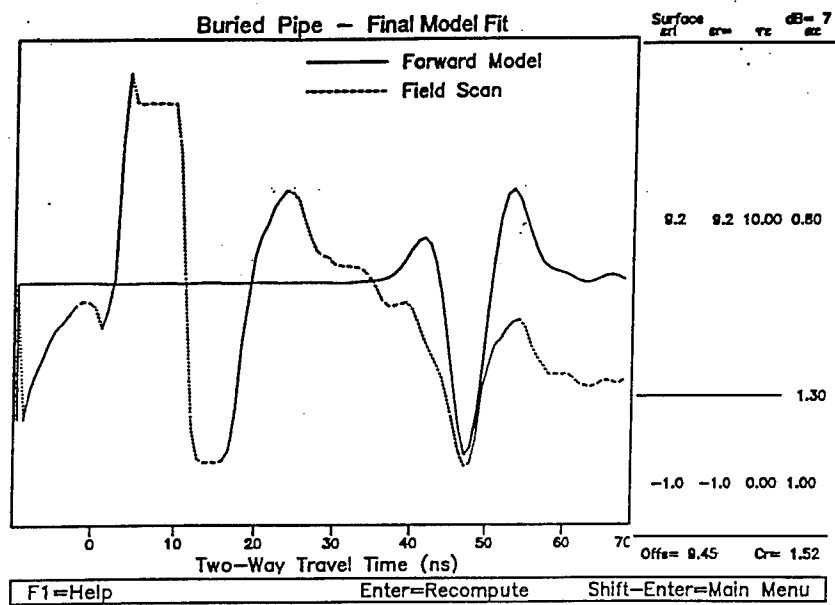


(c)



(d)

Figure 18. (Continued)



(e)

Figure 18. (Concluded)

Appendix A

Tables of Cases for Forward Modeling Problem Sets

Table A1--Concrete/Air: Cases 1-27

Table A2--Concrete/Water: Cases 28-36

Table A3--Concrete/Water/Sand: Cases 37-252

Table A1 Concrete/air: Cases 1-27								
Water Content	Frequency (Mhz)	Layer	Material	ϵ_d	ϵ_r	σ (S/m)	Thickness (m)	Case
9.5%	300	1	concrete	8.4	8.4	.04	.1	1
		2	air	1	1	0	∞	
	500	1	concrete	8.3	8.3	.04	.1	2
		2	air	1	1	0	∞	
	900	1	concrete	8.2	8.2	.04	.1	3
		2	air	1	1	0	∞	
6.7%	300	1	concrete	5.2	5.2	.03	.1	4
		2	air	1	1	0	∞	
	500	1	concrete	5.1	5.1	.03	.1	5
		2	air	1	1	0	∞	
	900	1	concrete	5.0	5.0	.03	.1	6
		2	air	1	1	0	∞	
0%	300	1	concrete	3.5	3.5	.01	.1	7
		2	air	1	1	0	∞	
	500	1	concrete	3.55	3.55	.01	.1	8
		2	air	1	1	0	∞	
	900	1	concrete	3.6	3.6	.01	.1	9
		2	air	1	1	0	∞	

Table A1 (Continued) Concrete/air: Cases 1-27								
Water Content	Frequency (Mhz)	Layer	Material	ϵ_d	ϵ_r	σ (S/m)	Thickness (m)	Case
9.5%	300	1	concrete	8.4	8.4	.04	.3	10
		2	air	1	1	0	∞	
	500	1	concrete	8.3	8.3	.04	.3	11
		2	air	1	1	0	∞	
	900	1	concrete	8.2	8.2	.04	.3	12
		2	air	1	1	0	∞	
	300	1	concrete	5.2	5.2	.03	.3	13
		2	air	1	1	0	∞	
	500	1	concrete	5.1	5.1	.03	.3	14
		2	air	1	1	0	∞	
	900	1	concrete	5.0	5.0	.03	.3	15
		2	air	1	1	0	∞	
0%	300	1	concrete	3.5	3.5	.01	.3	16
		2	air	1	1	0	∞	
	500	1	concrete	3.55	3.55	.01	.3	17
		2	air	1	1	0	∞	
	900	1	concrete	3.6	3.6	.01	.3	18
		2	air	1	1	0	∞	

Table A1 (Continued) Concrete/air: Cases 1-27								
Water Content	Frequency (Mhz)	Layer	Material	ϵ_a	ϵ_m	σ (S/m)	Thickness (m)	Case
9.5%	300	1	concrete	8.4	8.4	.04	.75	19
		2	air	1	1	0	∞	
	500	1	concrete	8.3	8.3	.04	.75	20
		2	air	1	1	0	∞	
	900	1	concrete	8.2	8.2	.04	.75	21
		2	air	1	1	0	∞	
6.7%	300	1	concrete	5.2	5.2	.03	.75	22
		2	air	1	1	0	∞	
	500	1	concrete	5.1	5.1	.03	.75	23
		2	air	1	1	0	∞	
	900	1	concrete	5.0	5.0	.03	.75	24
		2	air	1	1	0	∞	
0%	300	1	concrete	3.5	3.5	.01	.75	25
		2	air	1	1	0	∞	
	500	1	concrete	3.55	3.55	.01	.75	26
		2	air	1	1	0	∞	
	900	1	concrete	3.6	3.6	.01	.75	27
		2	air	1	1	0	∞	

Table A2 Concrete/Water: Cases 28-36								
Water Content	Frequency (Mhz)	Layer	Material	ϵ_r	ϵ_i	σ (S/m)	Thickness (m)	Case
9.5%	300	1	concrete	8.4	8.4	.04	.3	28
		2	water	80	80	.02	..	
	500	1	concrete	8.3	8.3	.04	.3	29
		2	water	80	80	.02	..	
	900	1	concrete	8.2	8.2	.04	.3	30
		2	water	80	80	.02	..	
6.7%	300	1	concrete	5.2	5.2	.03	.3	31
		2	water	80	80	.02	..	
	500	1	concrete	5.1	5.1	.03	.3	32
		2	water	80	80	.02	..	
	900	1	concrete	5.0	5.0	.03	.3	33
		2	water	80	80	.02	..	
0%	300	1	concrete	3.5	3.5	.01	.3	34
		2	water	80	80	.02	..	
	500	1	concrete	3.55	3.55	.01	.3	35
		2	water	80	80	.02	..	
	900	1	concrete	3.6	3.6	.01	.3	36
		2	water	80	80	.02	..	

Appendix A Tables of Cases for Forward Modeling Problem Sets

Table A3
Concrete/Water/Sand Variable Water Layer Thickness Test Cases

Concrete Properties:

Water Content	Frequency (MHz)	ϵ_d	ϵ_m	σ (S/m)	Thickness (m)
9.5%	300	8.4	8.4	.04	.3
	500	8.3	8.3	.04	.3
	900	8.2	8.2	.04	.3
6.7%	300	5.2	5.2	.03	.3
	500	5.1	5.1	.03	.3
	900	5.0	5.0	.03	.3
0%	300	3.5	3.5	.01	.3
	500	3.55	3.55	.01	.3
	900	3.6	3.6	.01	.3

Water Properties That Remain Constant:

ϵ_d	ϵ_m	σ (S/m)
80	80	.02

Sand Properties:

ϵ_d	ϵ_m	σ (S/m)	Thickness (m)
25	25	.005	∞

Table A3 (Continued)**Concrete/Water/Sand: Variable Water Layer Thickness Test Cases 37-252**

Water Content	Frequency (MHz)	Thickness of Water (m)	Case (with mult.)	Case (no mult.)
9.5%	300	.01	37	145
		.02	38	146
		.03	39	147
		.04	40	148
		.05	41	149
		.10	42	150
		.15	43	151
		.20	44	152
		.25	45	153
		.30	46	154
		.35	47	155
		.40	48	156
	500	.01	49	157
		.02	50	158
		.03	51	159
		.04	52	160
		.05	53	161
		.10	54	162
		.15	55	163
		.20	56	164
		.25	57	165
		.30	58	166
		.35	59	167
		.40	60	168
	900	.01	61	169
		.02	62	170
		.03	63	171
		.04	64	172
		.05	65	173
		.10	66	174
		.15	67	175
		.20	68	176
		.25	69	177
		.30	70	178
		.35	71	179
		.40	72	180
6.7%	300	.01	73	181
		.02	74	182
		.03	75	183
		.04	76	184
		.05	77	185
		.10	78	186
		.15	79	187
		.20	80	188
		.25	81	189
		.30	82	190
		.35	83	191
		.40	84	192

Table A3 (Continued)
Concrete/Water/Sand: Variable Water Layer Thickness Test Cases 37-252

6.7%	500	.01	85	193
		.02	86	194
		.03	87	195
		.04	88	196
		.05	89	197
		.10	90	198
		.15	91	199
		.20	92	200
		.25	93	201
		.30	94	202
		.35	95	203
		.40	96	204
	900	.01	97	205
		.02	98	206
		.03	99	207
		.04	100	208
		.05	101	209
		.10	102	210
		.15	103	211
		.20	104	212
		.25	105	213
		.30	106	214
0%	300	.35	107	215
		.40	108	216
	500	.01	109	217
		.02	110	218
		.03	111	219
		.04	112	220
		.05	113	221
		.10	114	222
		.15	115	223
		.20	116	224
		.25	117	225
	900	.30	118	226
		.35	119	227
		.40	120	228
		.01	121	229
		.02	122	230
		.03	123	231
		.04	124	232
		.05	125	233
		.10	126	234
		.15	127	235
		.20	128	236
		.25	129	237
		.30	130	238
		.35	131	239
		.40	132	240

Table A3 (Continued)				
Concrete/Water/Sand: Variable Water Layer Thickness Test Cases 37-252				
0%	900	.01	133	241
		.02	134	241
		.03	135	243
		.04	136	244
		.05	137	245
		.10	138	246
		.15	139	247
		.20	140	248
		.25	141	249
		.30	142	250
		.35	143	251
		.40	144	252

Appendix B

GPRMODv2 Forward Modeling Results for Problem Set 1

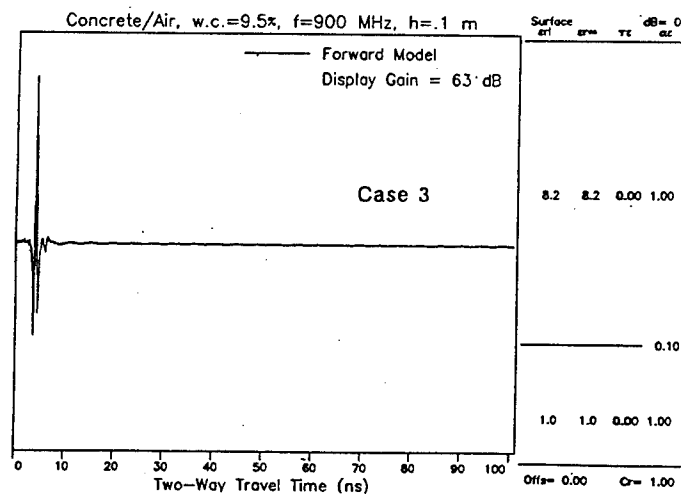
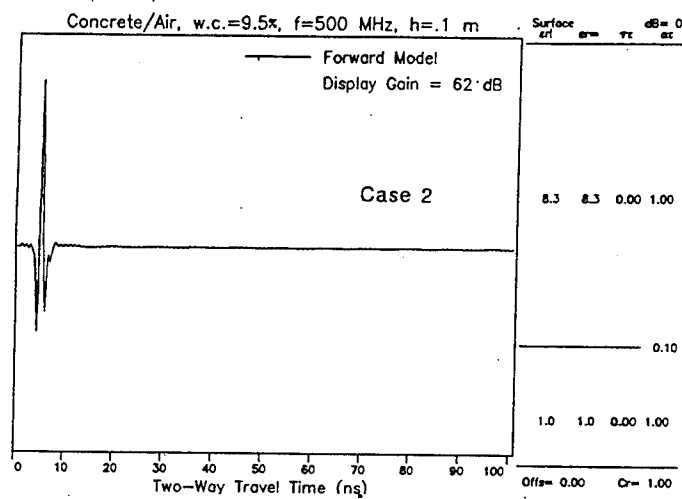
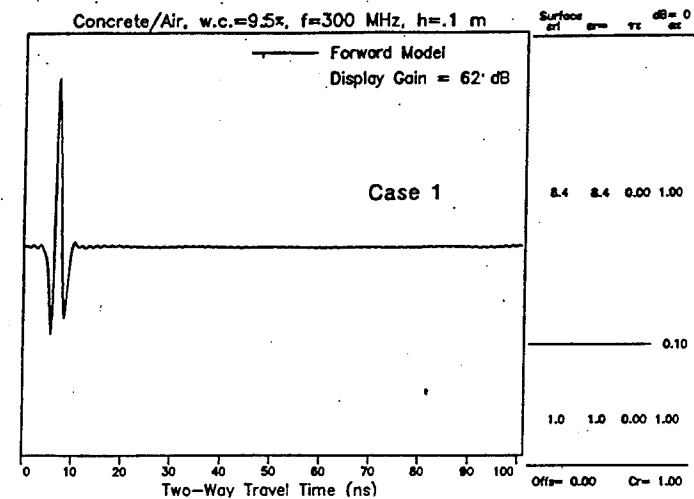


Figure B1. GPR model calculation results, Cases 1-3

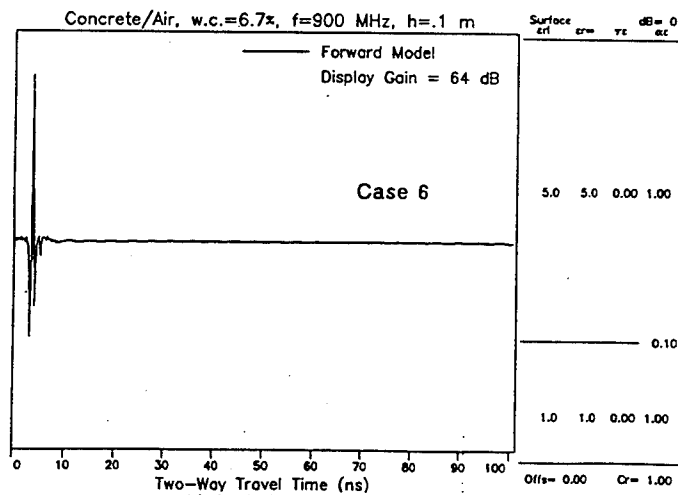
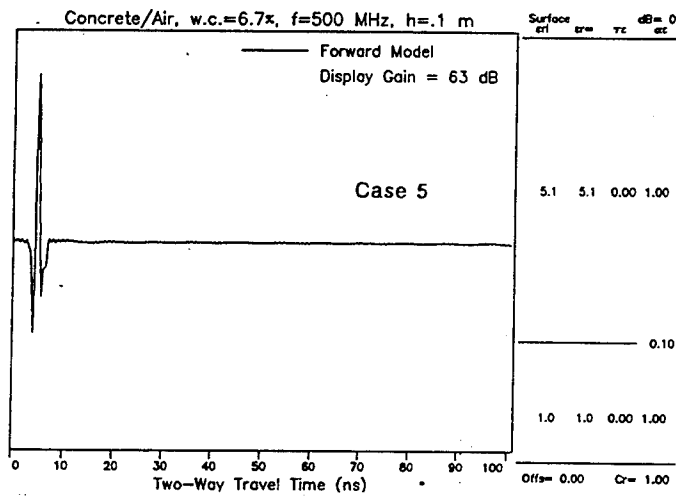
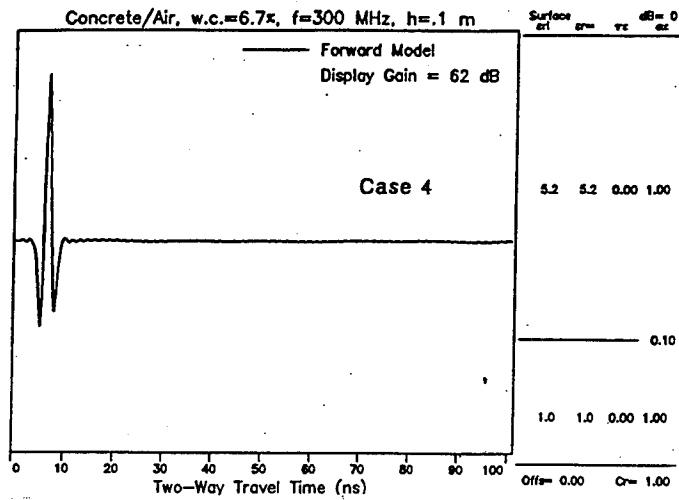


Figure B2. GPR model calculation results, Cases 4-6

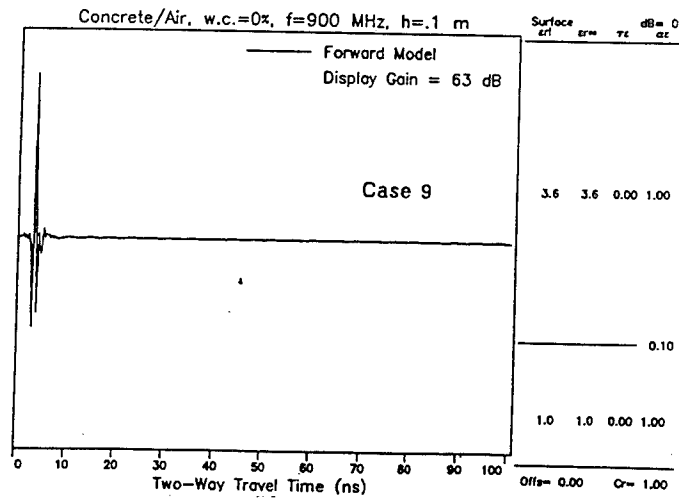
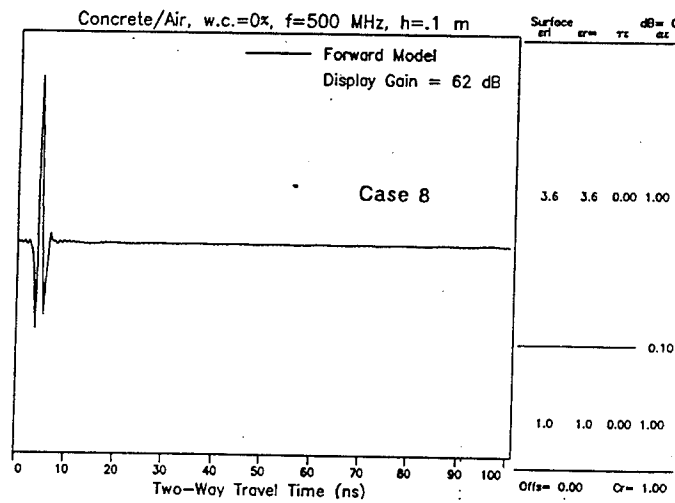
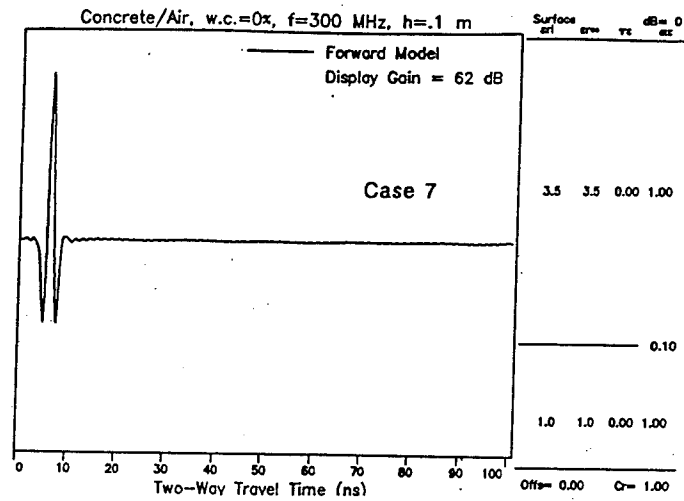


Figure B3. GPR model calculation results, Cases 7-9

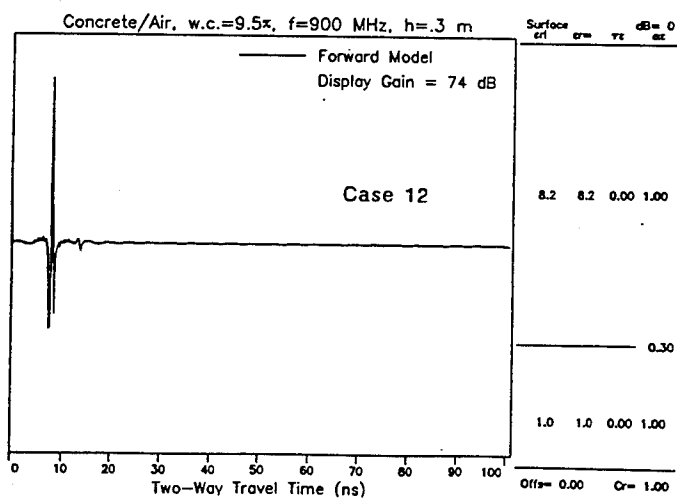
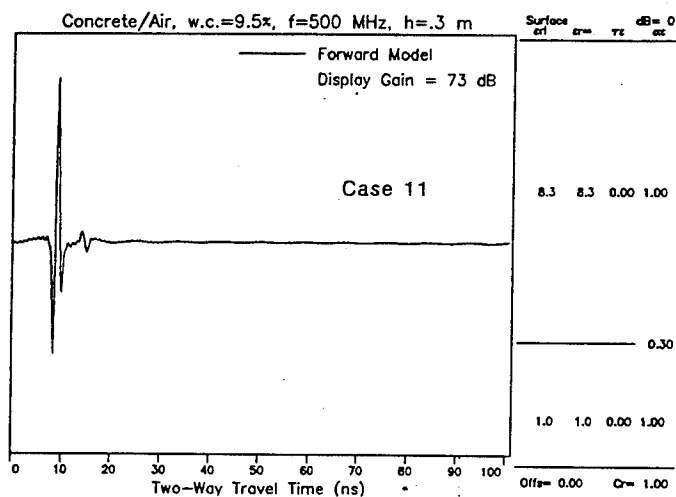
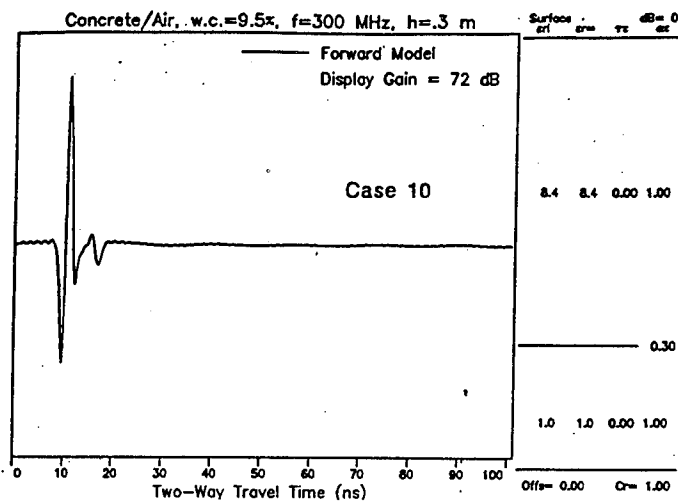


Figure B4. GPR model calculation results, Cases 10-12

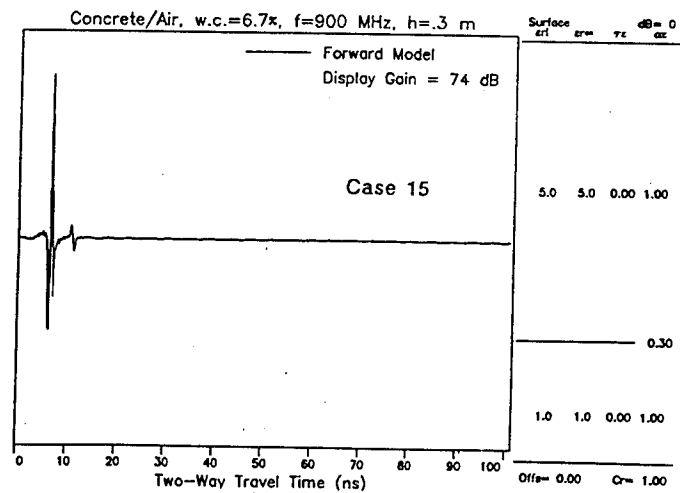
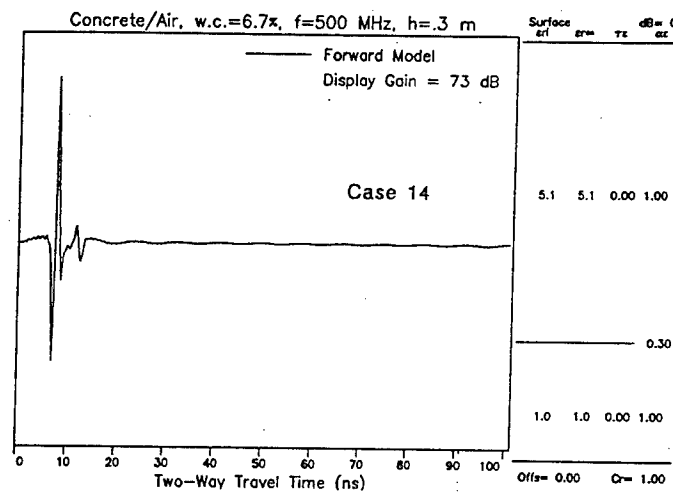
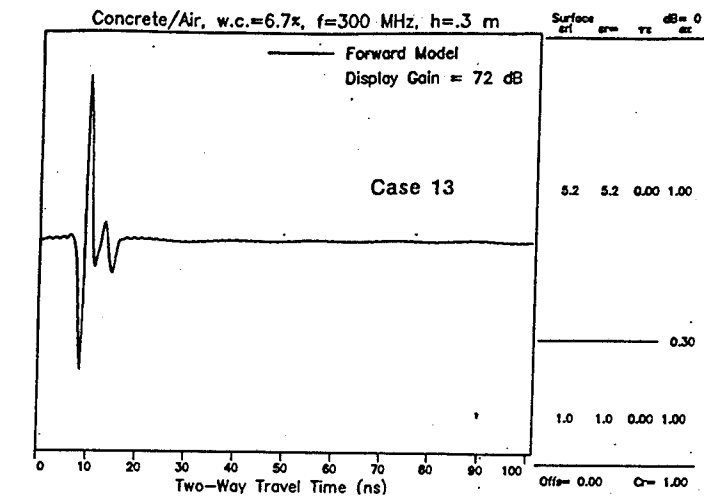


Figure B5. GPR model calculation results, Cases 13-15

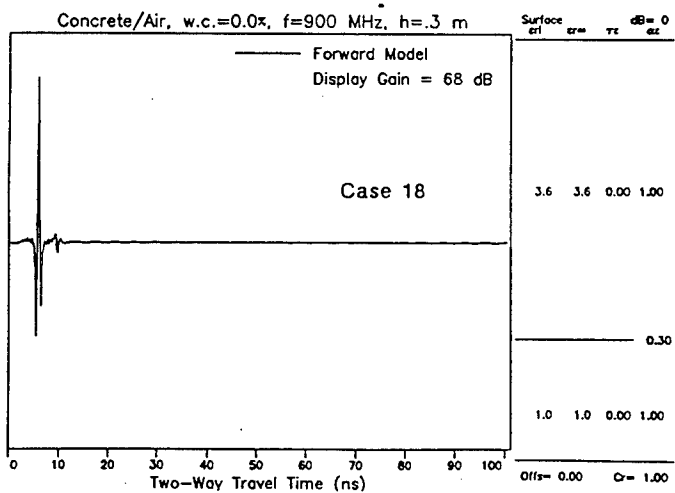
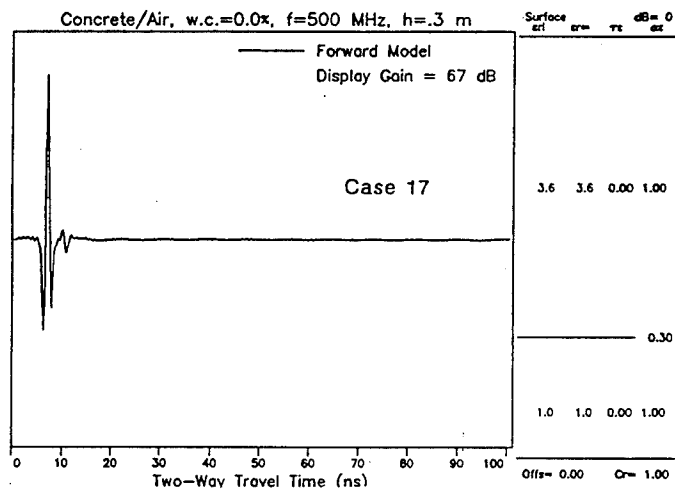
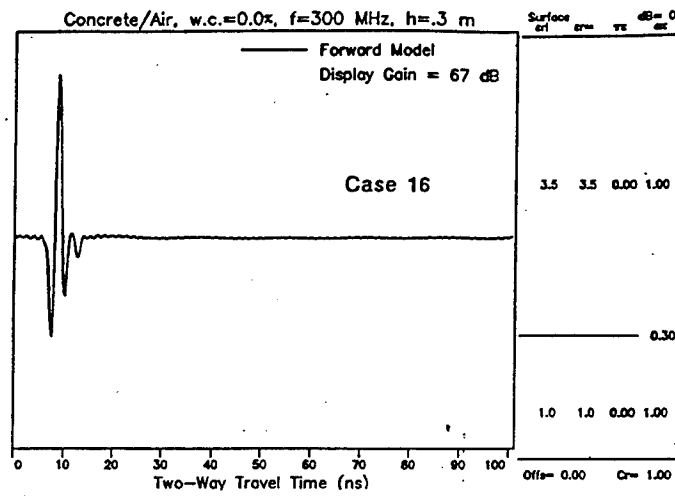


Figure B6. GPR model calculation results, Cases 16-18

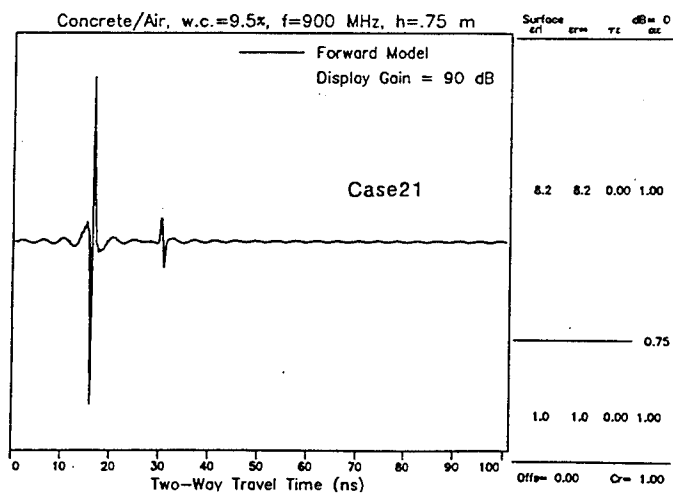
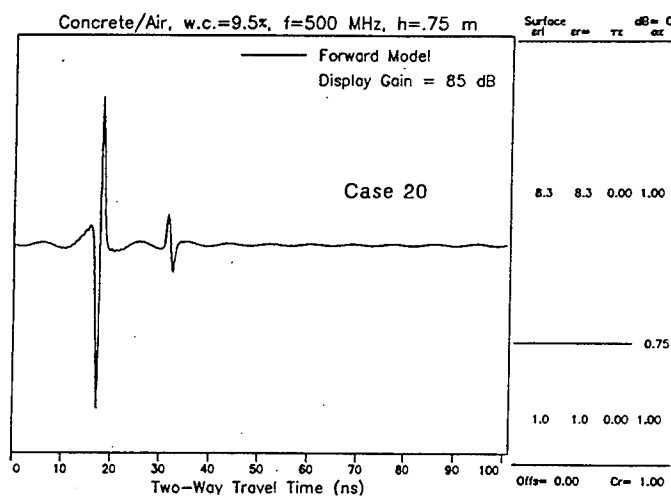
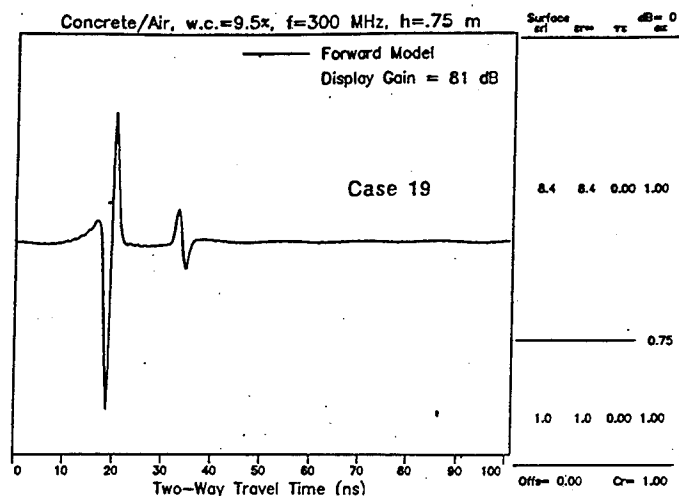


Figure B7. GPR model calculation results, Cases 19-21

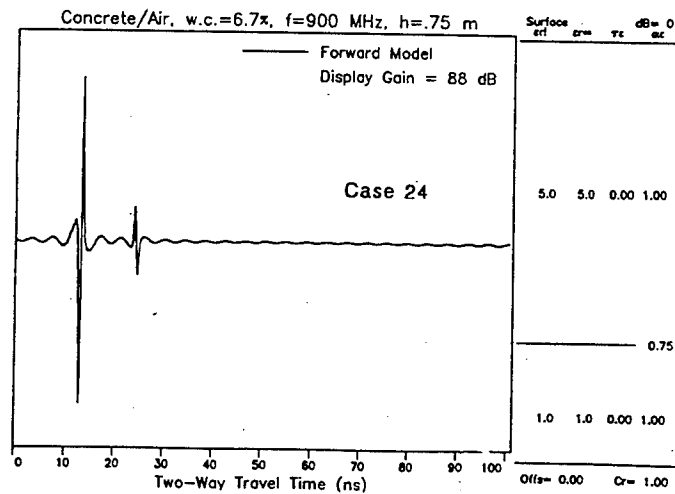
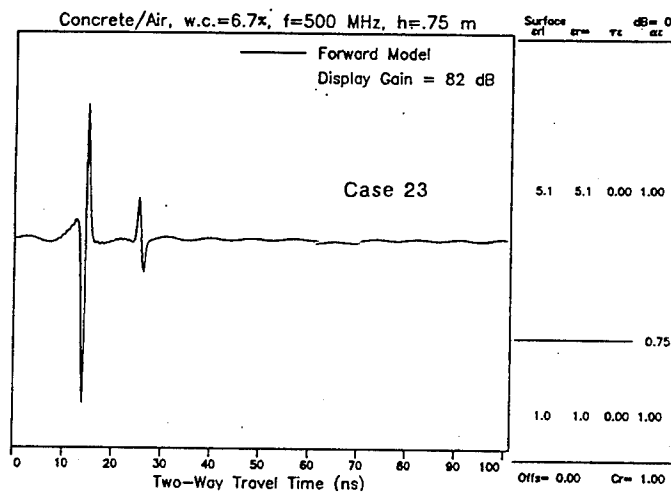
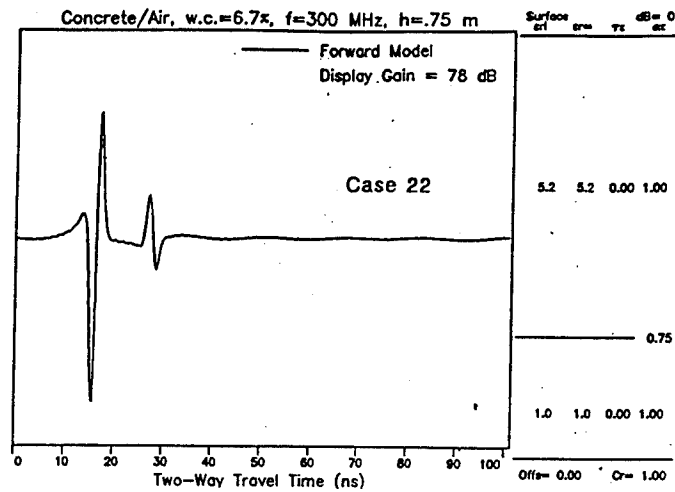


Figure B8. GPR model calculation results, Cases 22-24

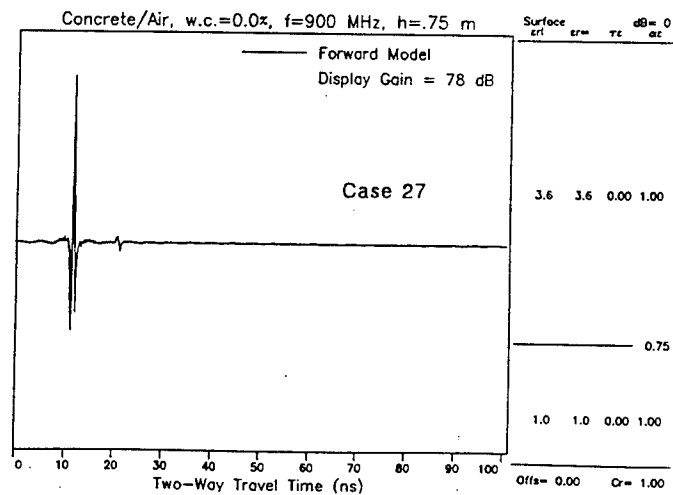
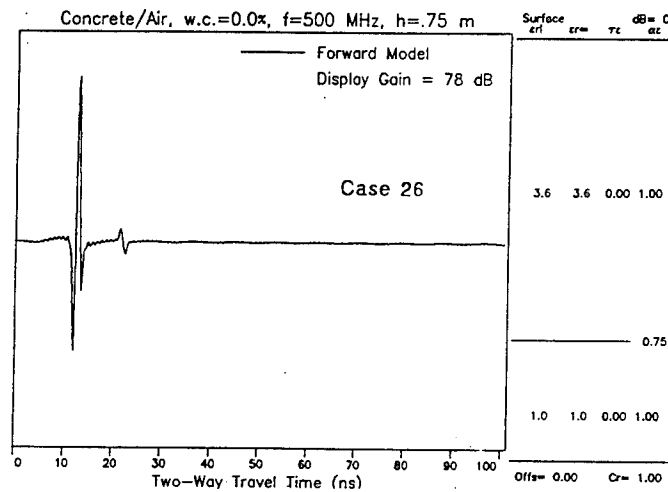
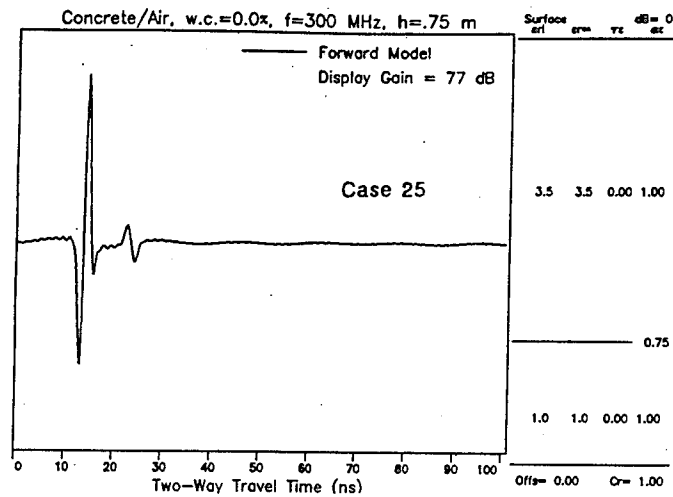


Figure B9. GPR model calculation results, Cases 25-27

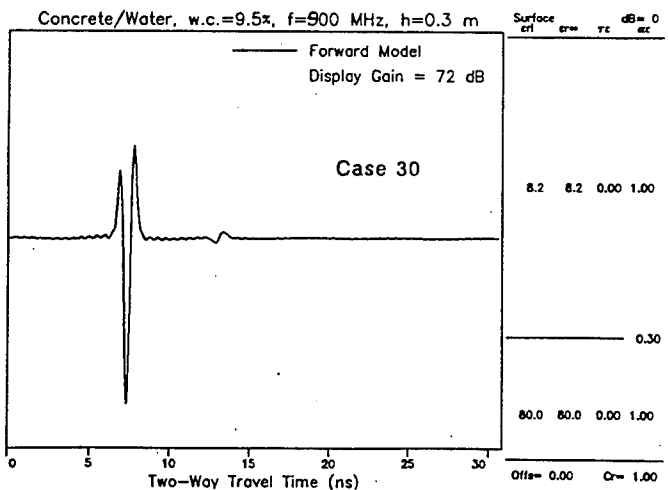
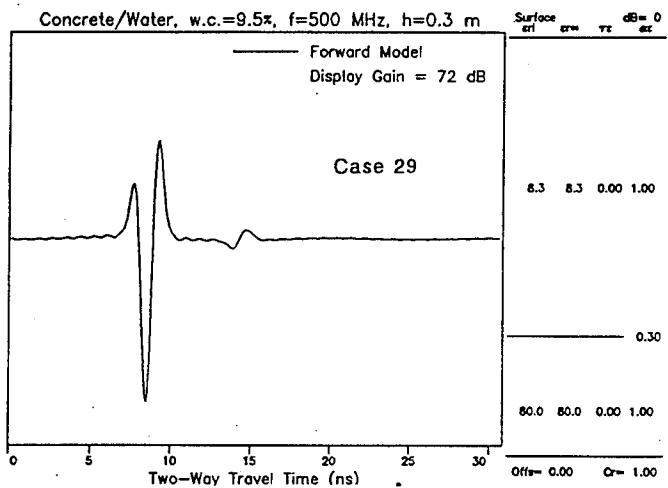
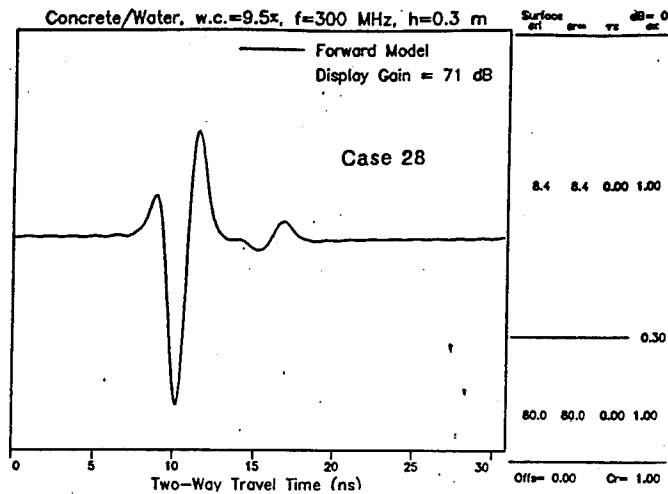


Figure B10. GPR model calculation results, Cases 28-30

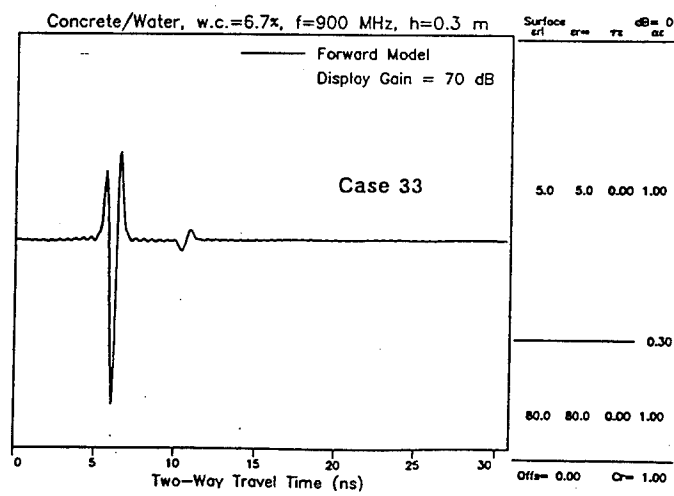
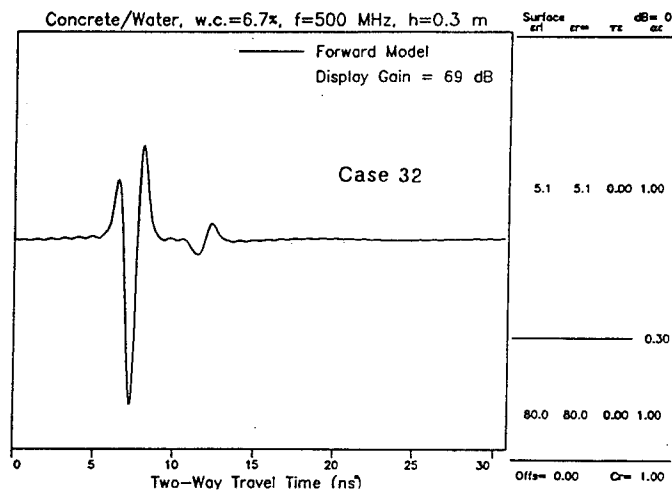
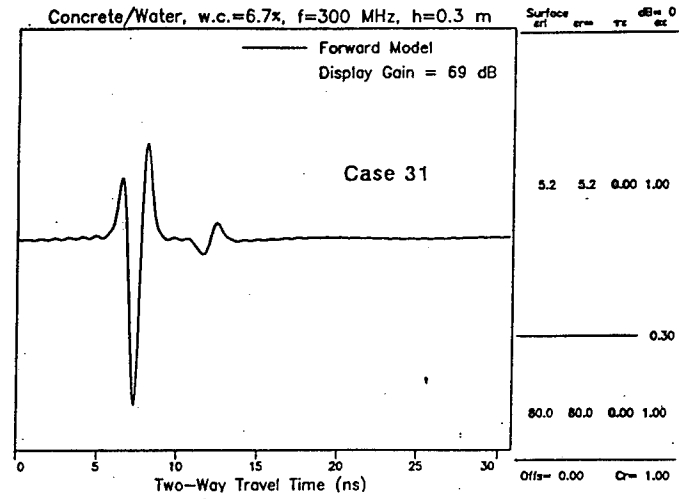


Figure B11. GPR model calculation results, Cases 31-33

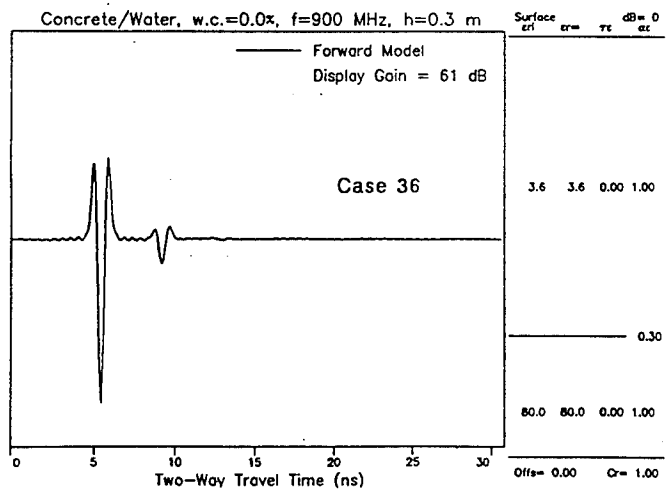
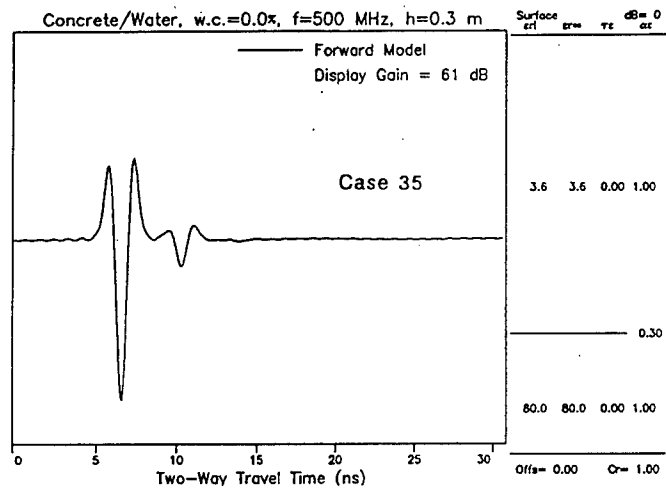
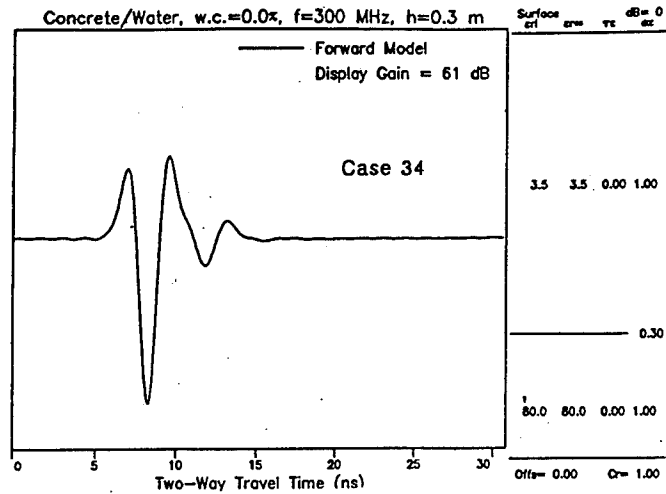


Figure B12. GPR model calculation results, Cases 34-36

Appendix C

GPRMODv2 Forward Modeling Results for Problem Set 2

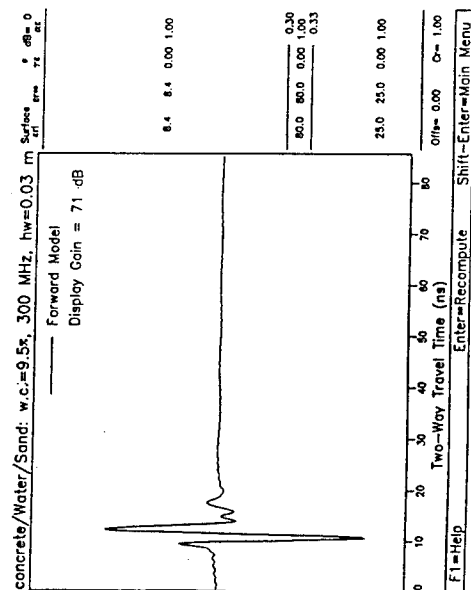
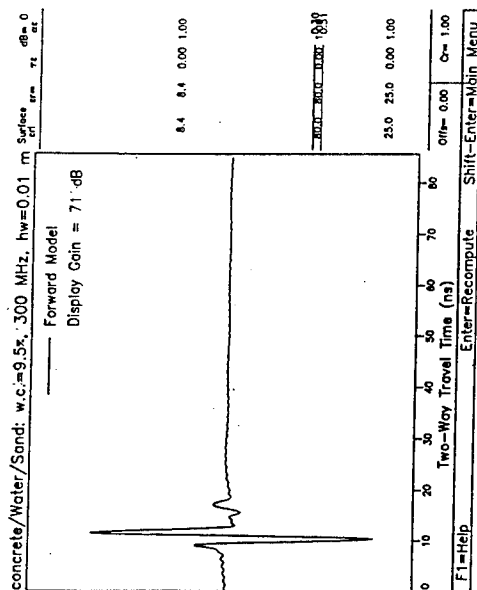
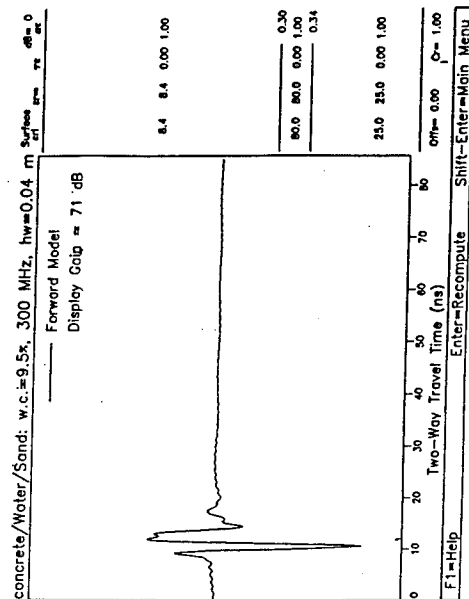
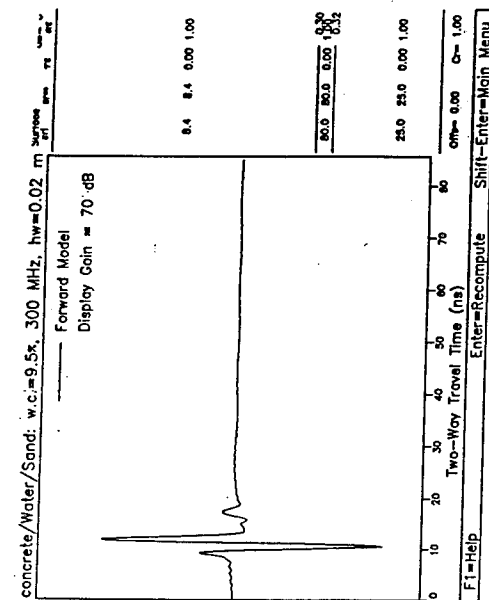
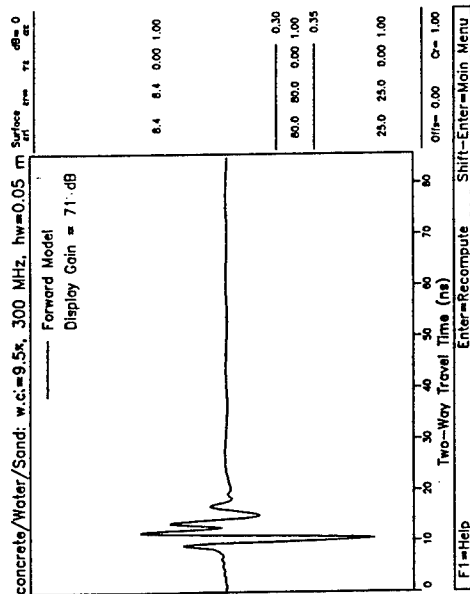
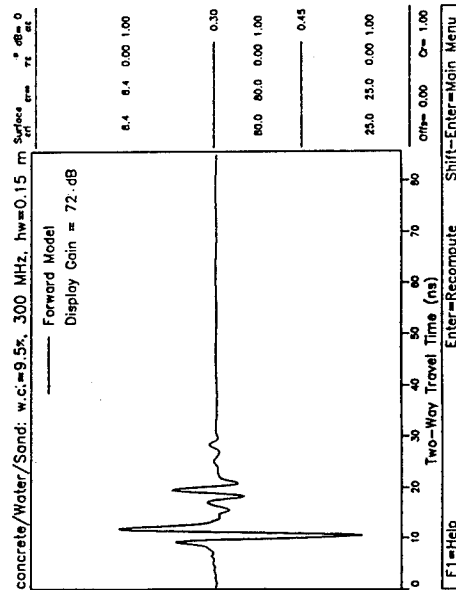


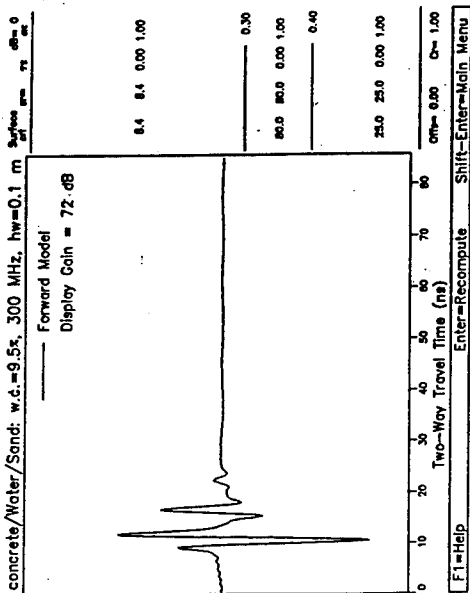
Figure C1. Problem Set 2, Cases 37-40, multiples



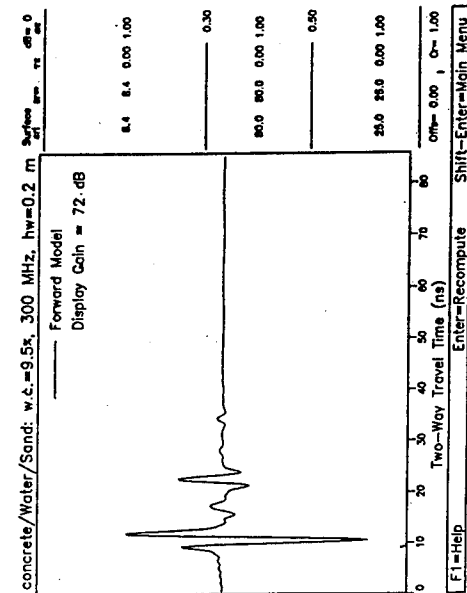
Case 41



Case 43

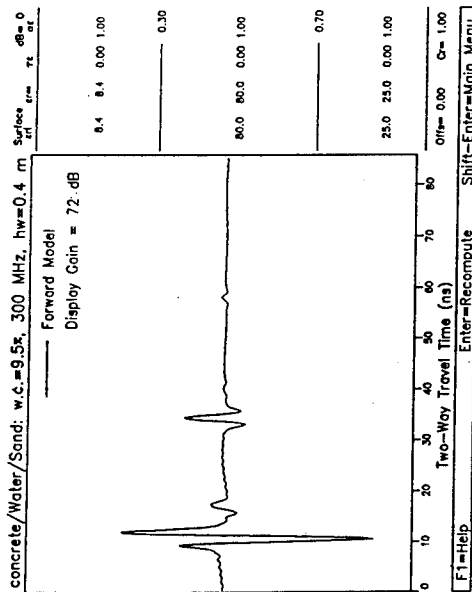


Case 42

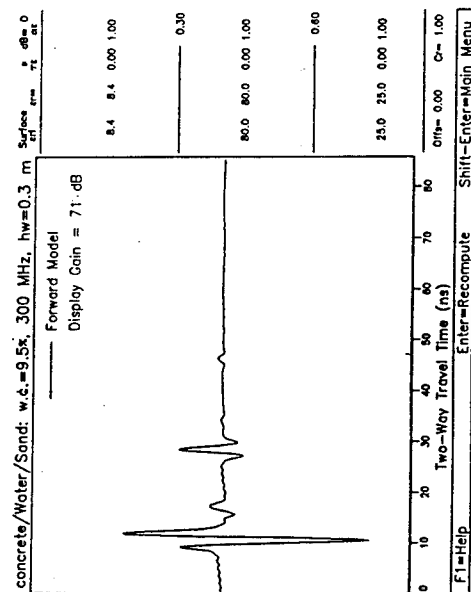


Case 44

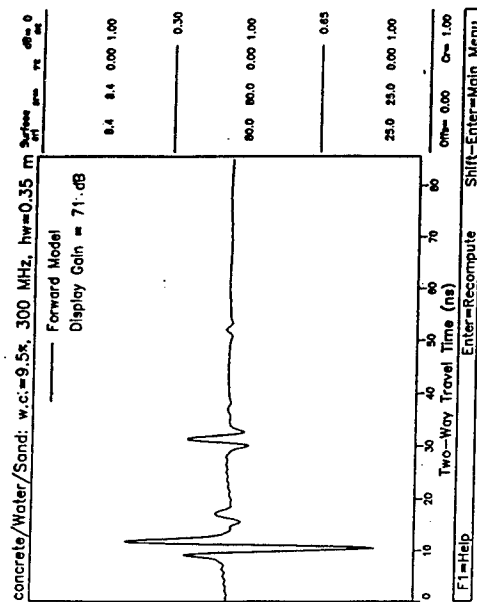
Figure C2. Problem Set 2, Cases 41-44, multiples



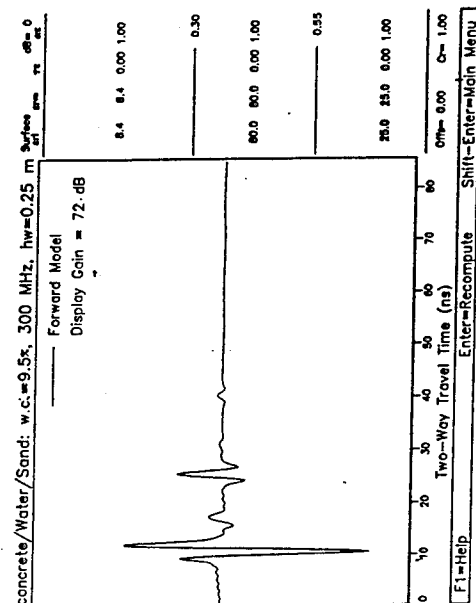
Case 45



Case 47

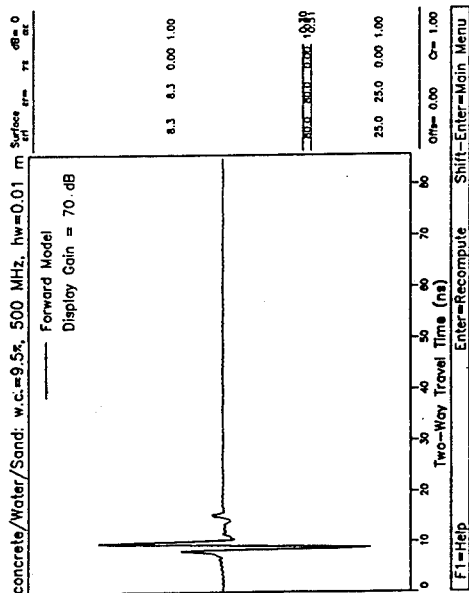


Case 46

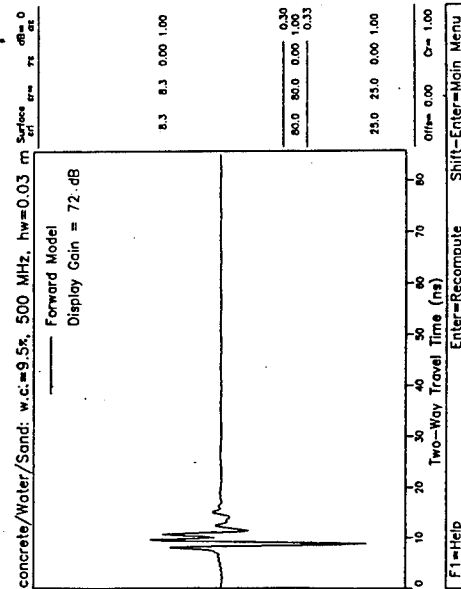


Case 48

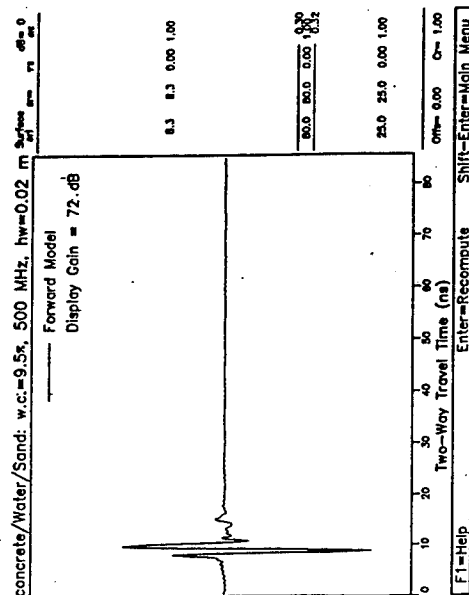
Figure C3. Problem Set 2, Cases 45-48, multiples



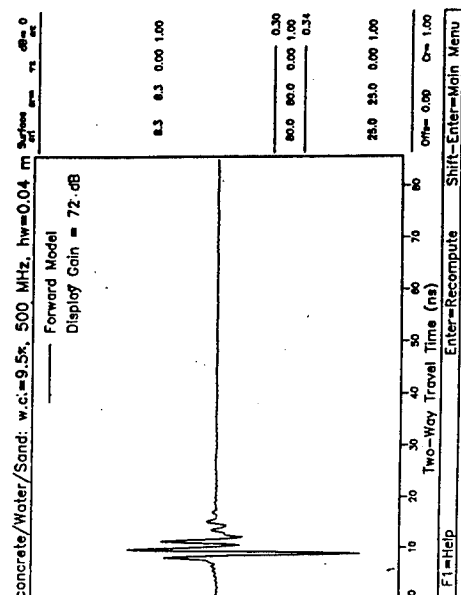
Case 49



Case 51

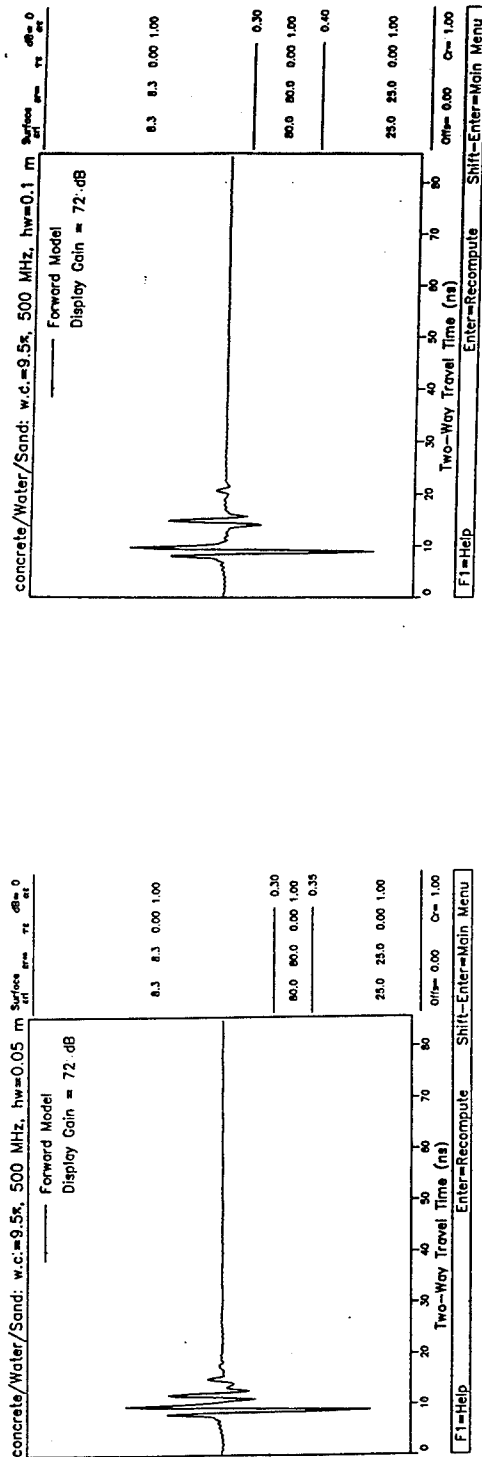


Case 50

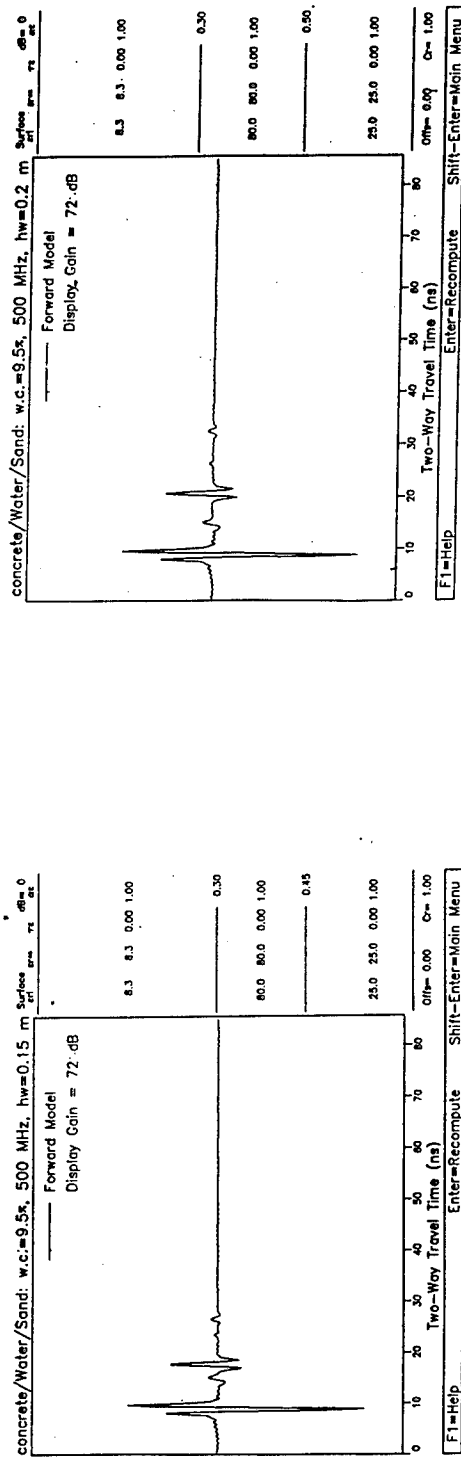


Case 52

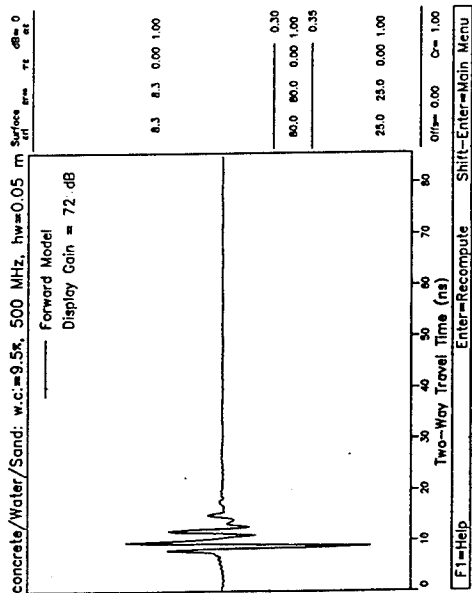
Figure C4. Problem Set 2, Cases 49-52, multiples



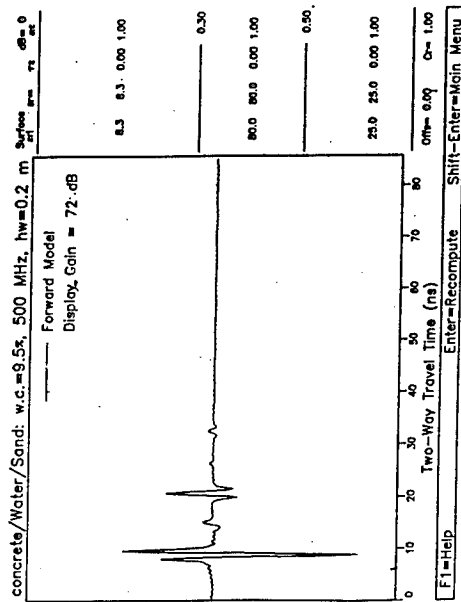
Case 53



Case 54

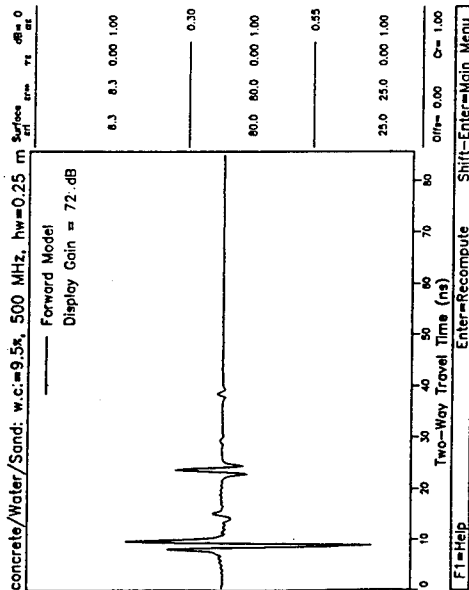


Case 55

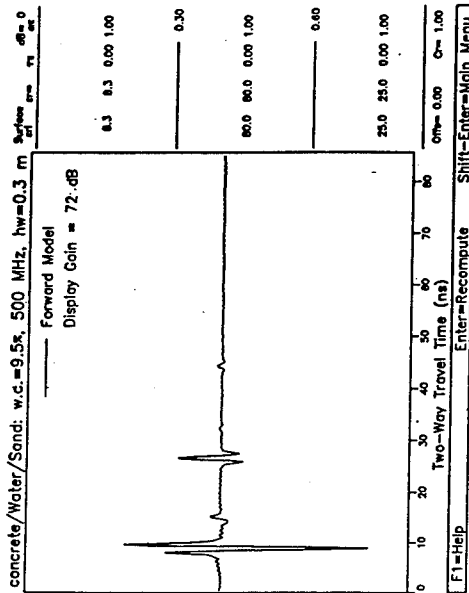


Case 56

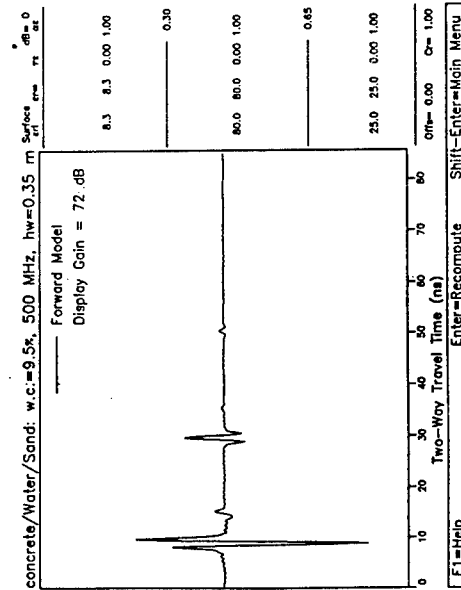
Figure C5. Problem Set 2, Cases 53-56, multiples



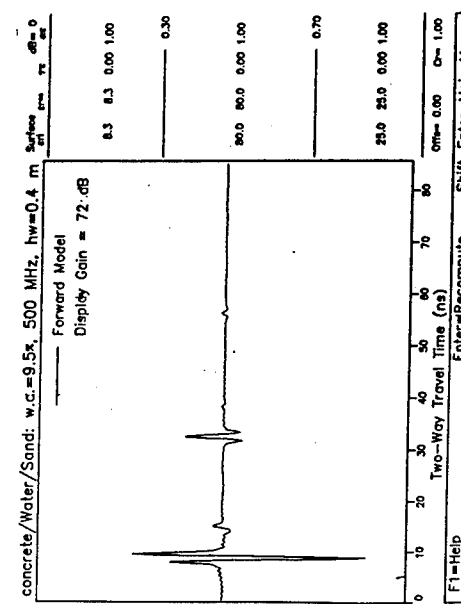
Case 57



Case 58

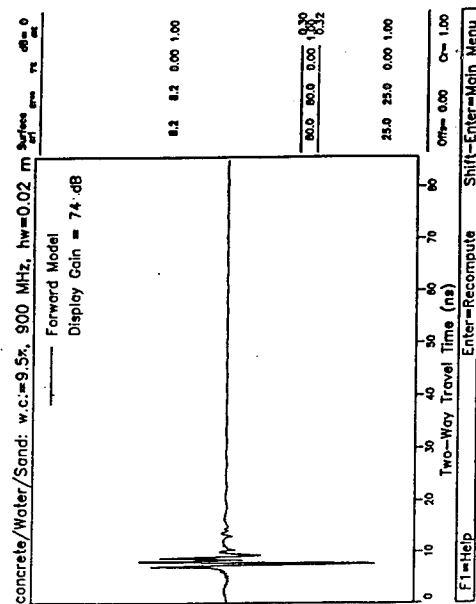


Case 59

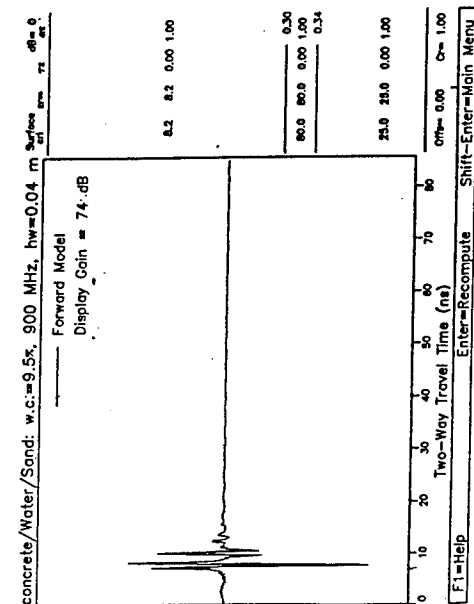


Case 60

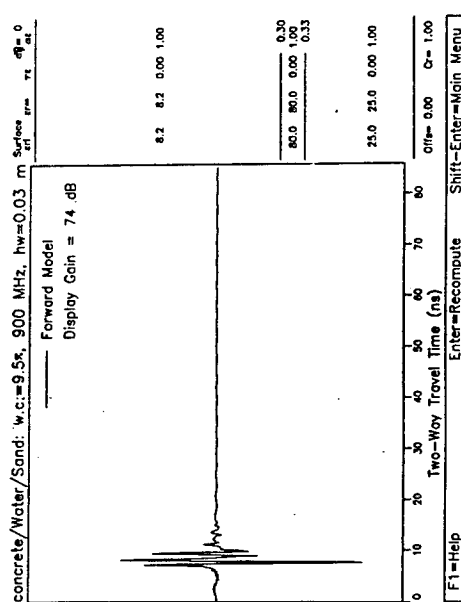
Figure C6. Problem Set 2, Cases 57-60, multiples



Case 61



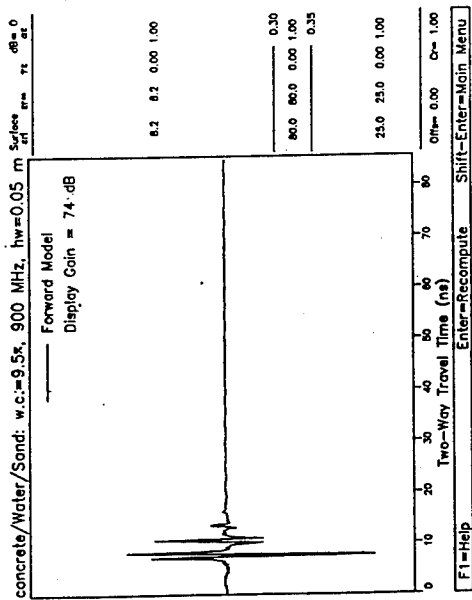
Case 62



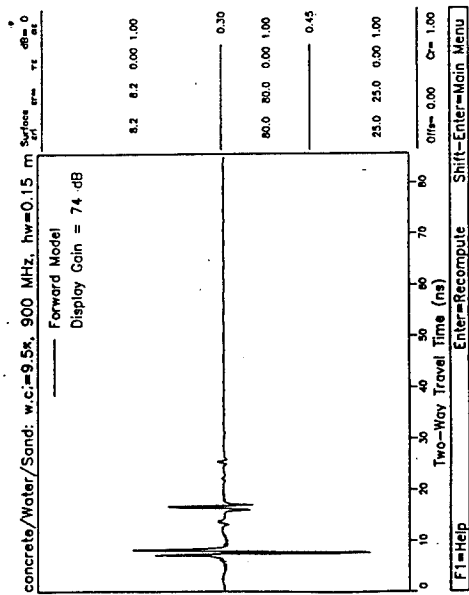
Case 63

Case 64

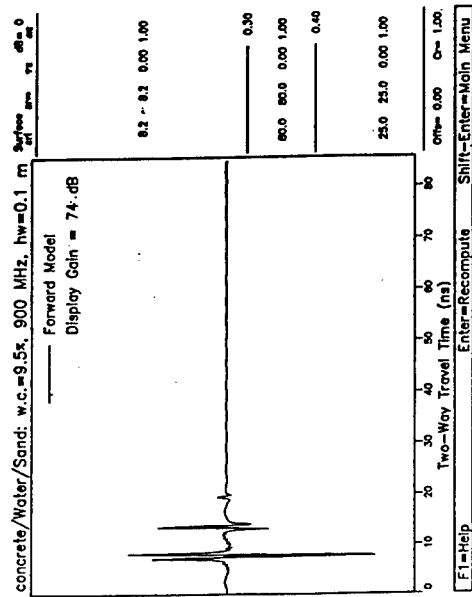
Figure C7. Problem Set 2, Cases 61-64, multiples



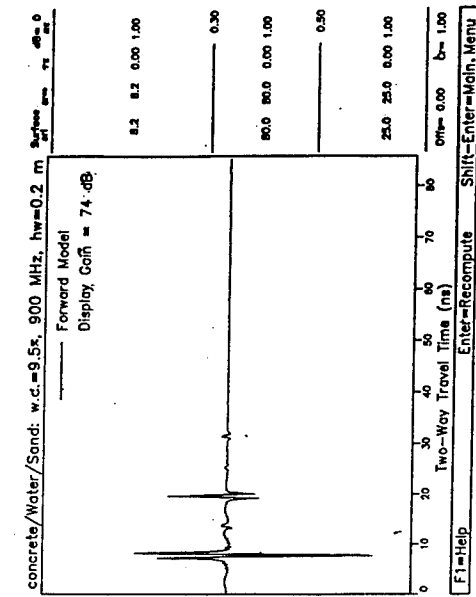
Case 65



Case 67

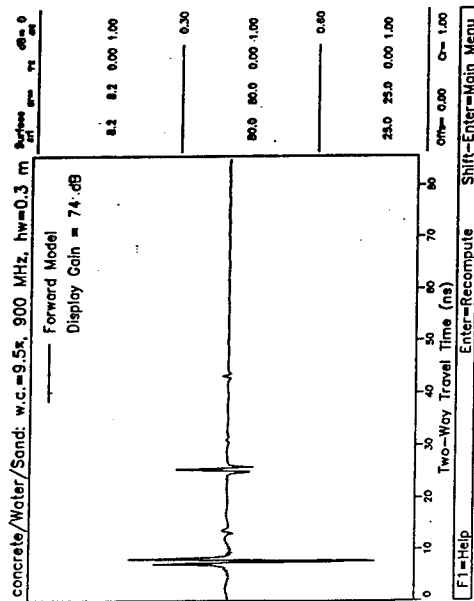


Case 66



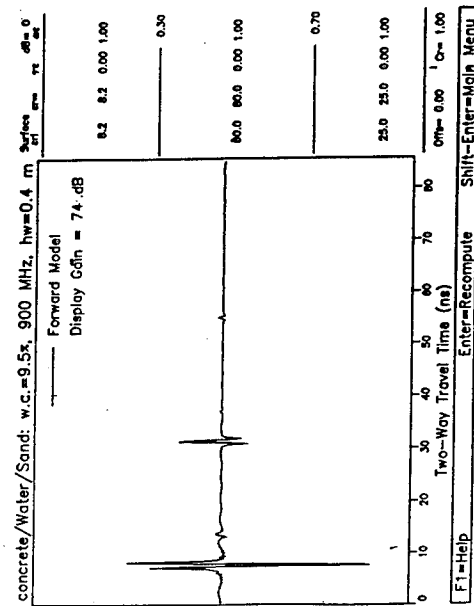
Case 68

Figure C8. Problem Set 2, Cases 65-68, multiples



Case 69

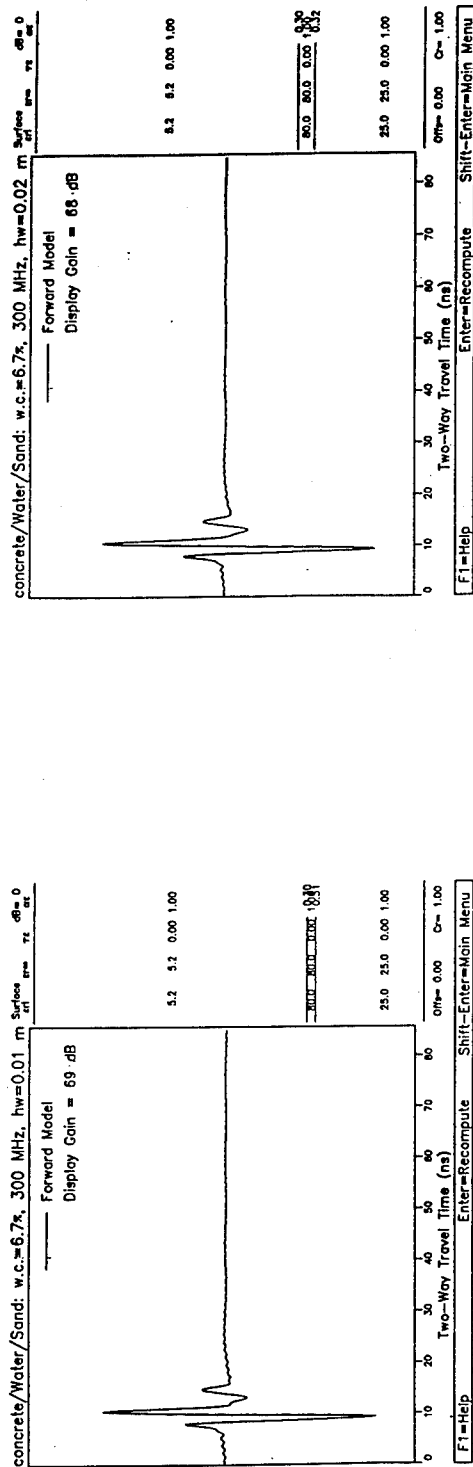
Case 70



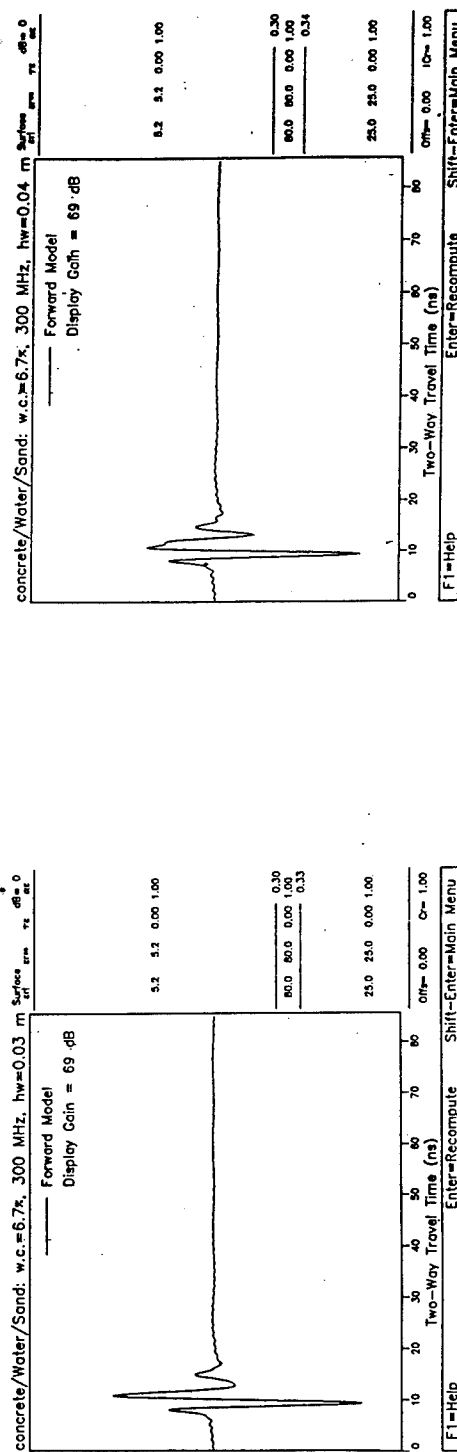
Case 71

Case 72

Figure C9. Problem Set 2, Cases 69-72, multiples

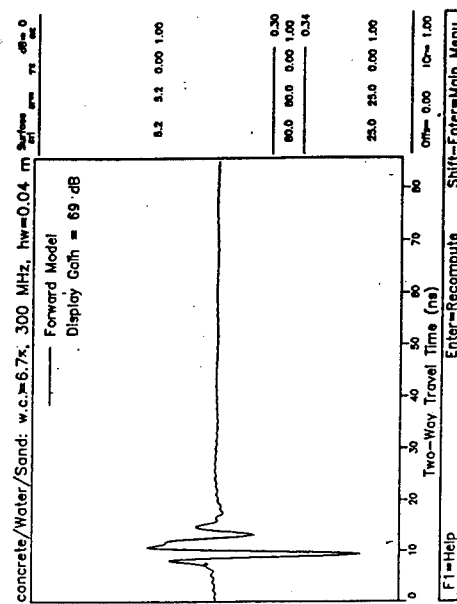


Case 73



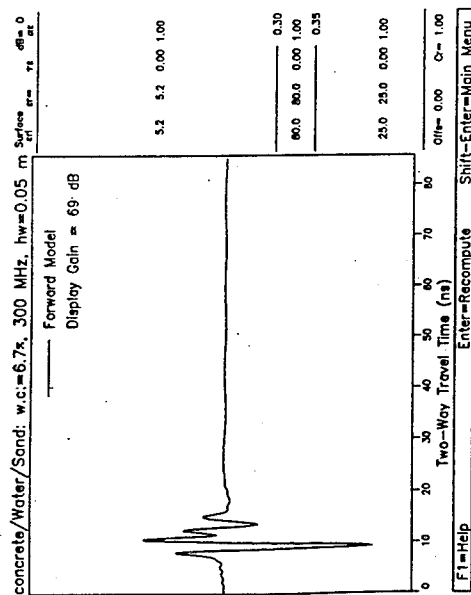
Case 75

Case 74

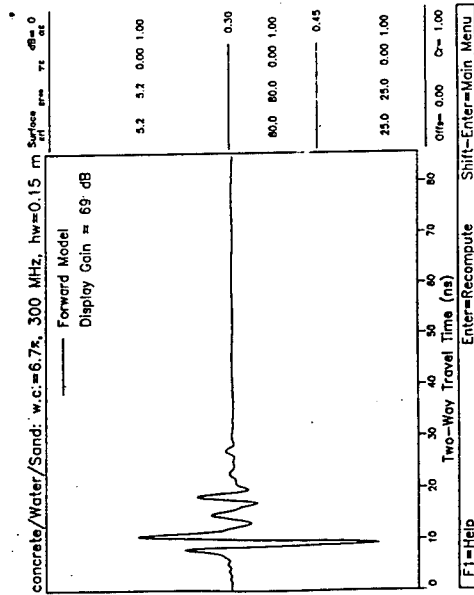


Case 76

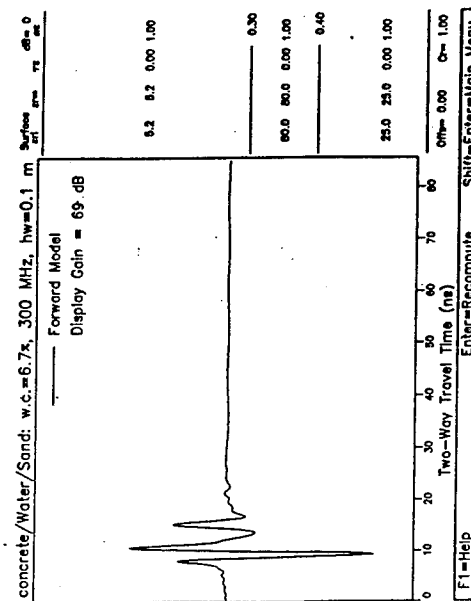
Figure C10. Problem Set 2, Cases 73-76, multiples



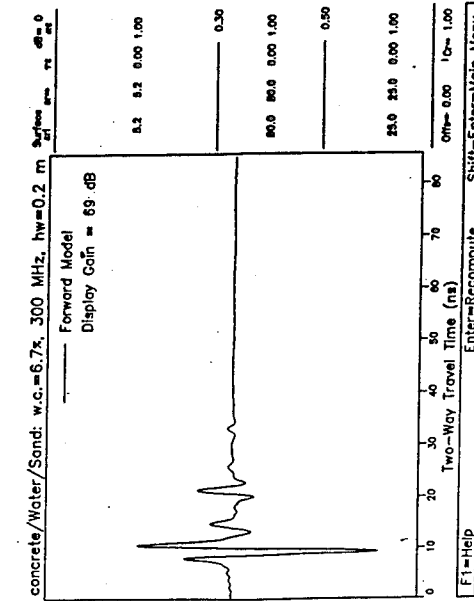
Case 77



Case 79

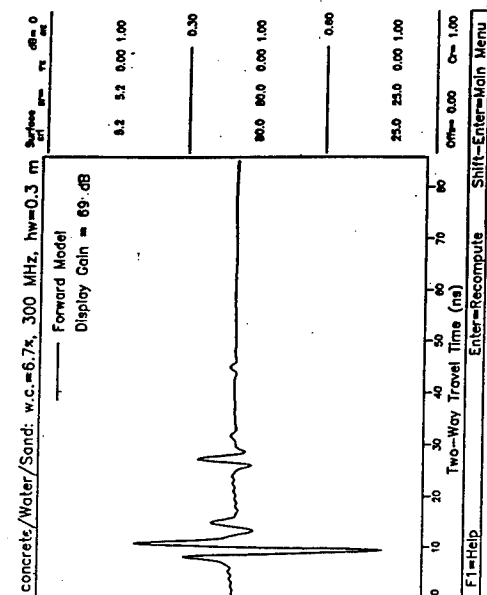


Case 78

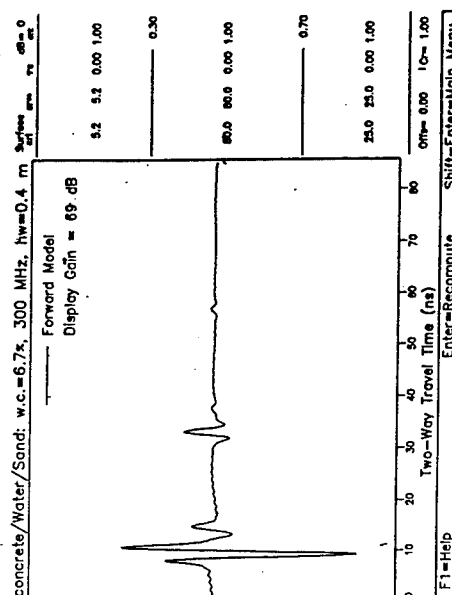


Case 80

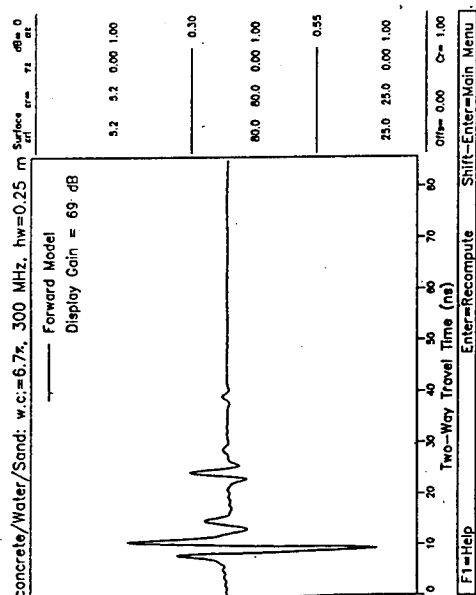
Figure C11. Problem Set 2, Cases 77-80, multiples



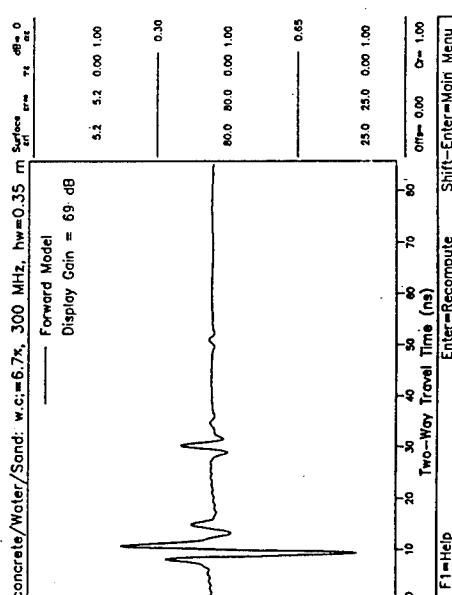
Case 82



Case 84

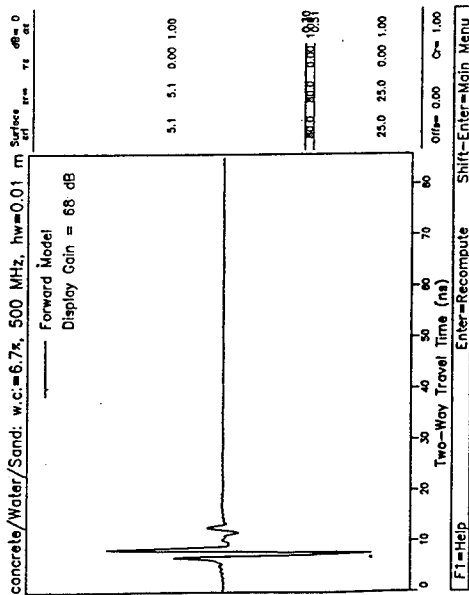


Case 81



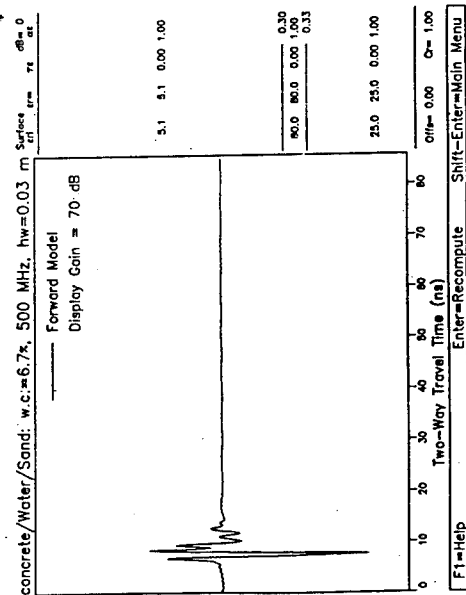
Case 83

Figure C12. Problem Set 2, Cases 81-84, multiples

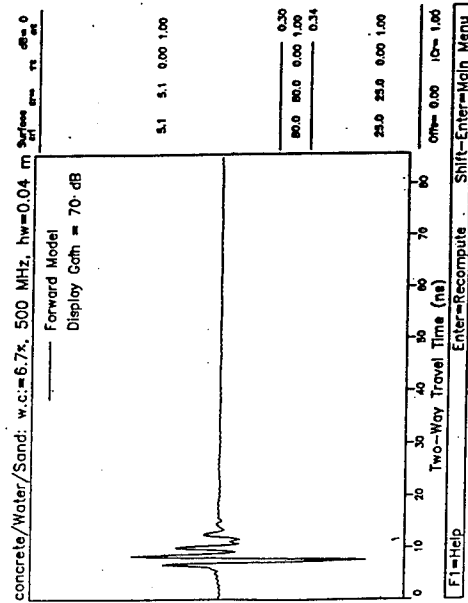


Case 85

Case 86

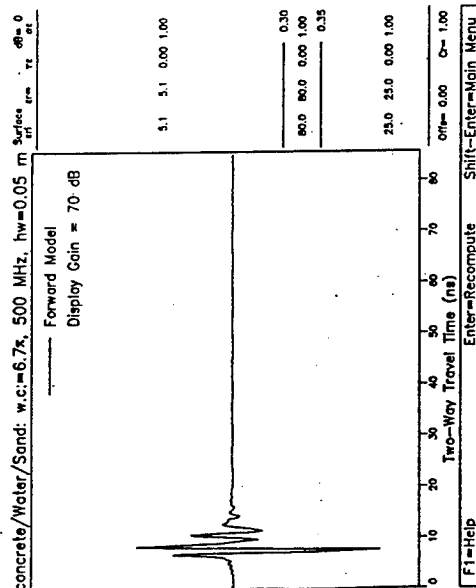


Case 87

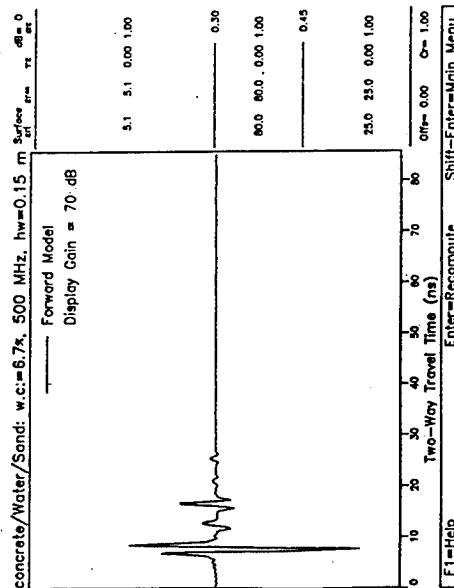


Case 88

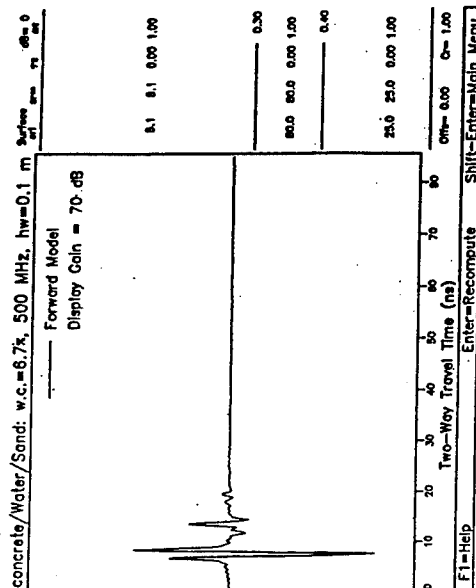
Figure C13. Problem Set 2, Cases 85-88, multiples



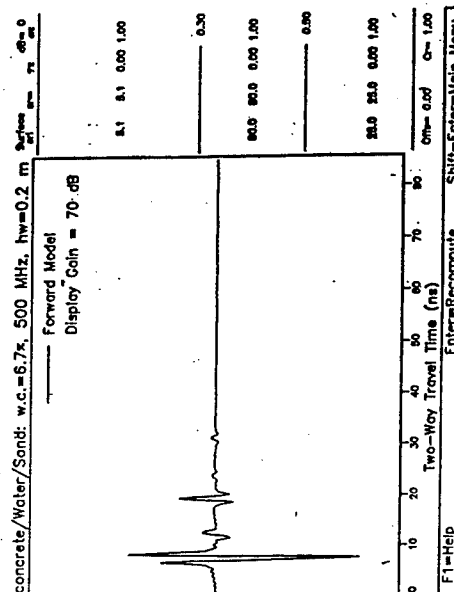
Case 89



Case 91

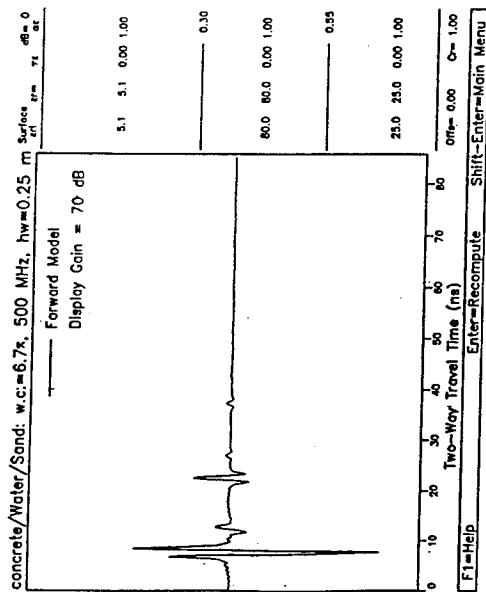


Case 90



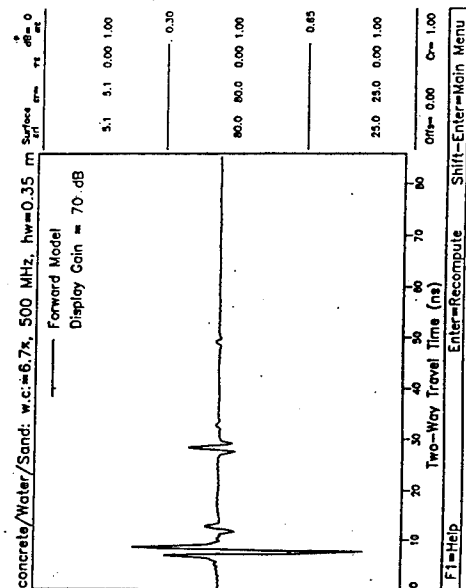
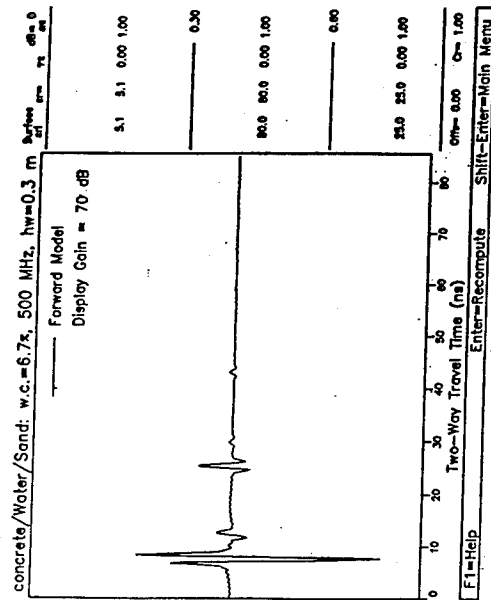
Case 92

Figure C14. Problem Set 2, Cases 89-92, multiples



Case 93

Case 94



Case 95

Case 96

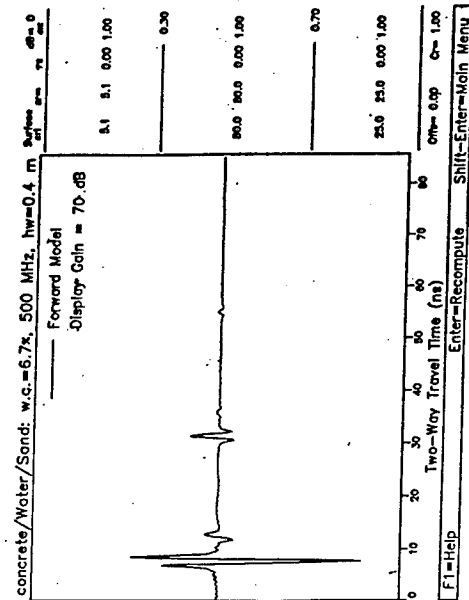
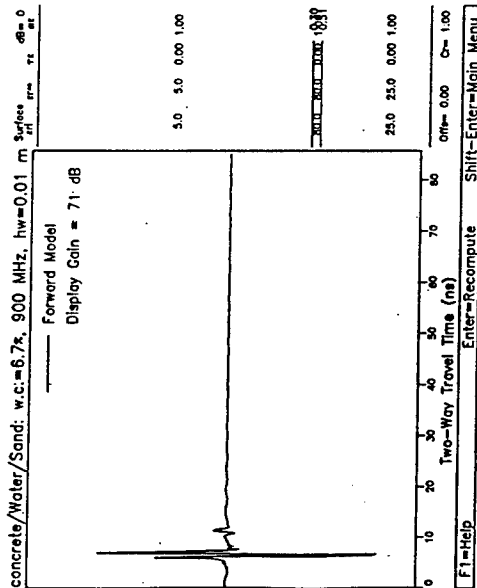
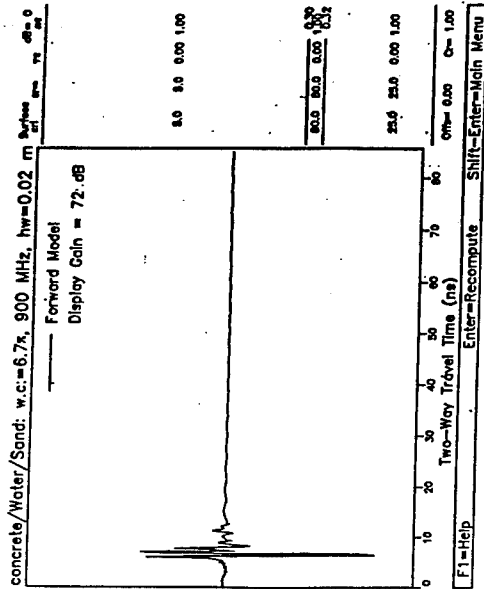


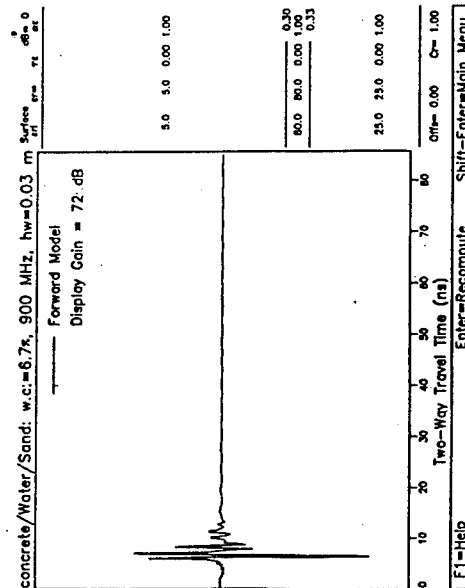
Figure C15. Problem Set 2, Cases 93-96, multiples



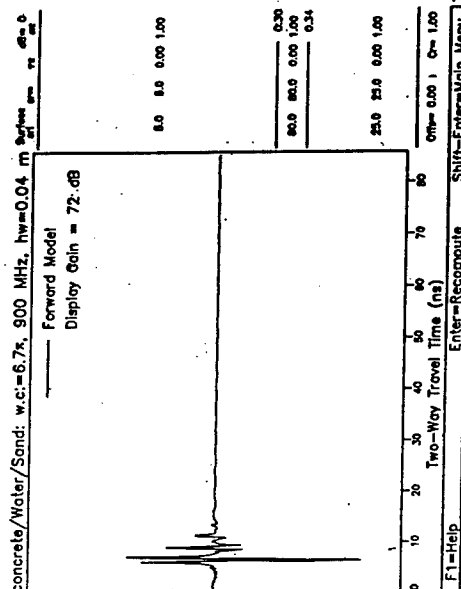
Case 97



Case 98

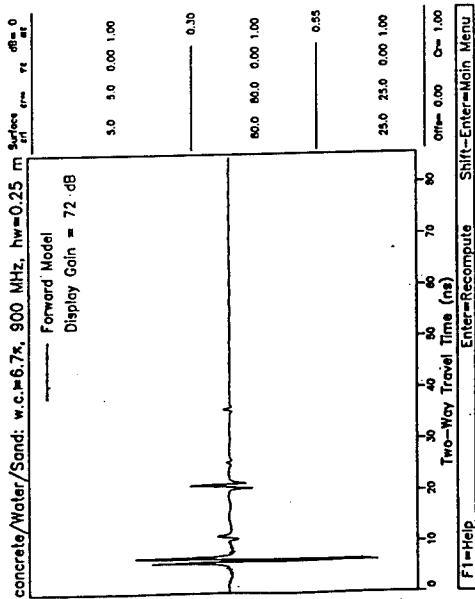


Case 99

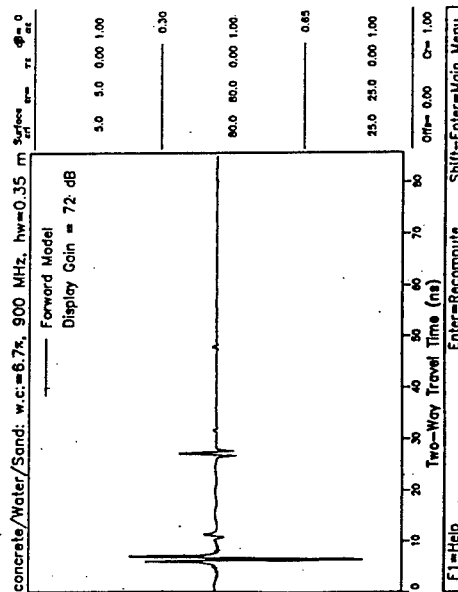


Case 100

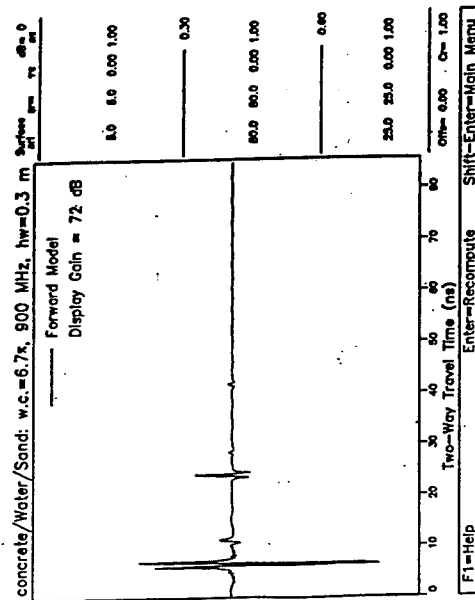
Figure C16. Problem Set 2, Cases 97-100, multiples



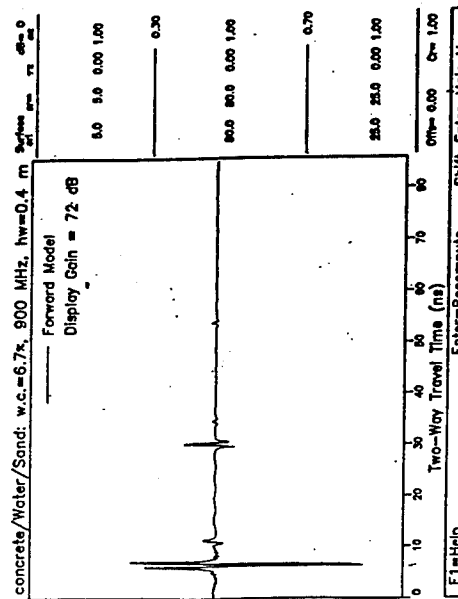
Case 105



Case 107



Case 106



Case 108

Figure C18. Problem Set 2, Cases 105-108, multiples

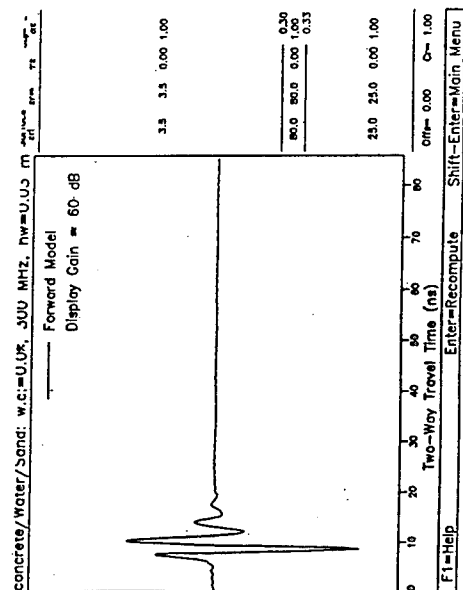
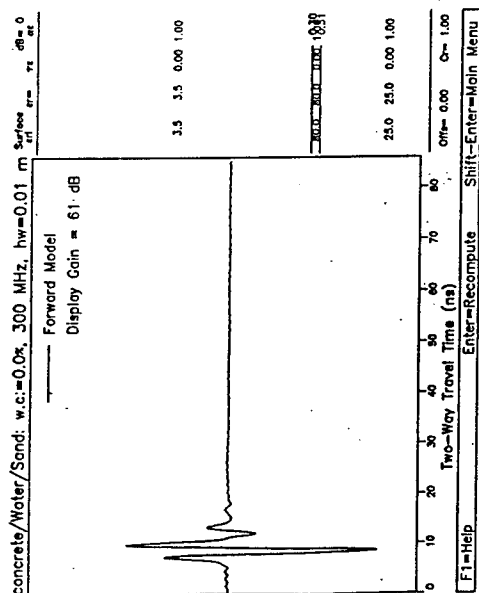
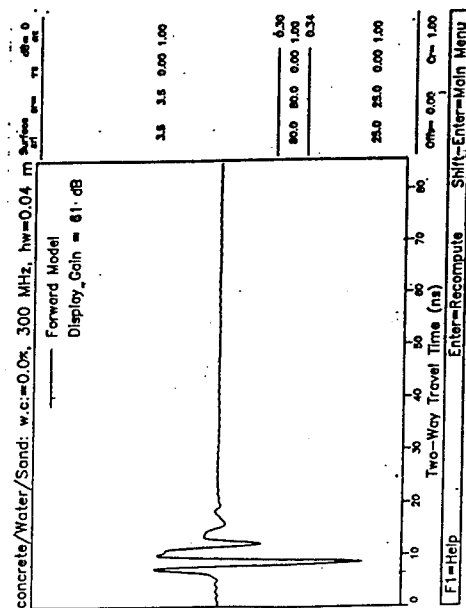
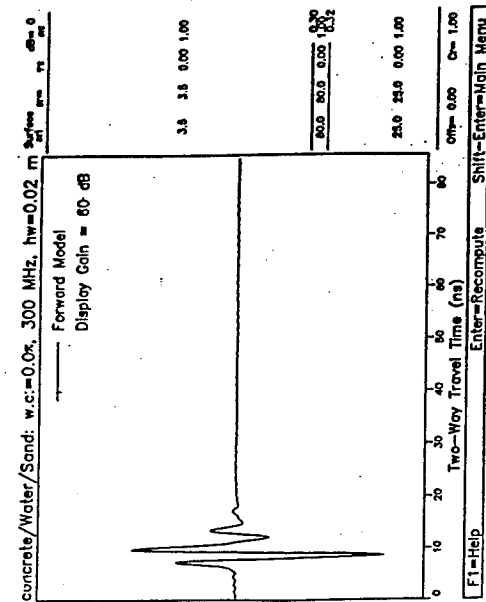


Figure C19. Problem Set 2, Cases 109-112, multiples

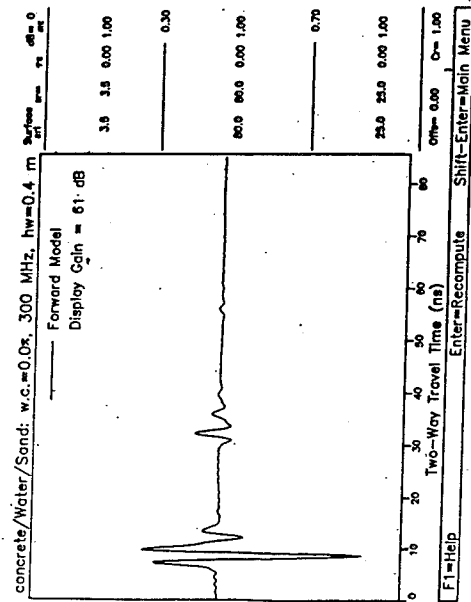
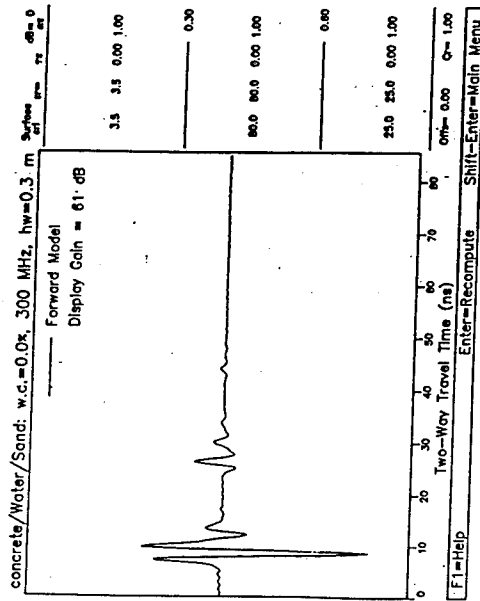
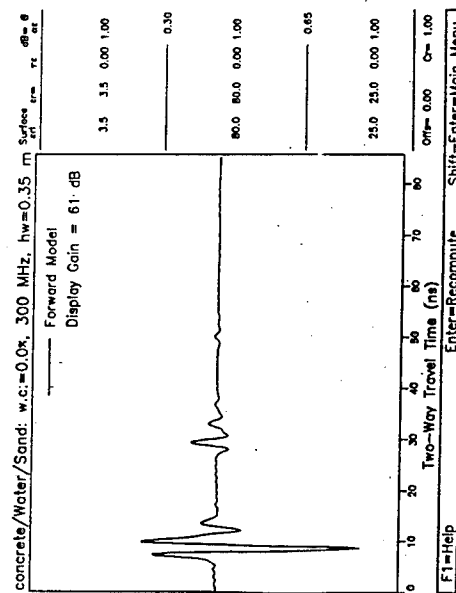
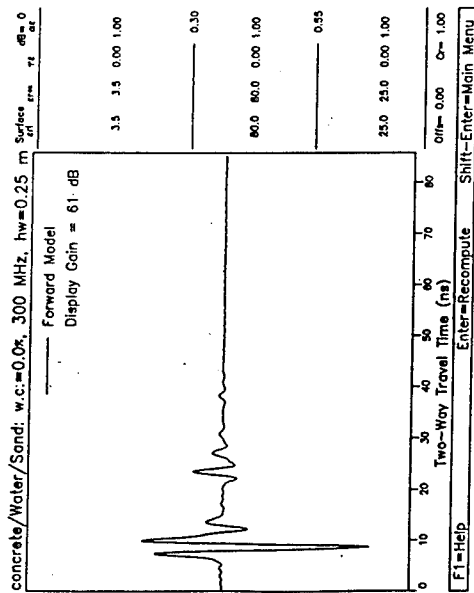
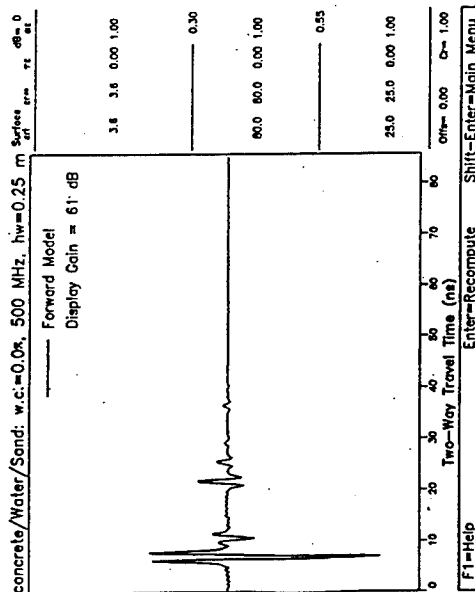
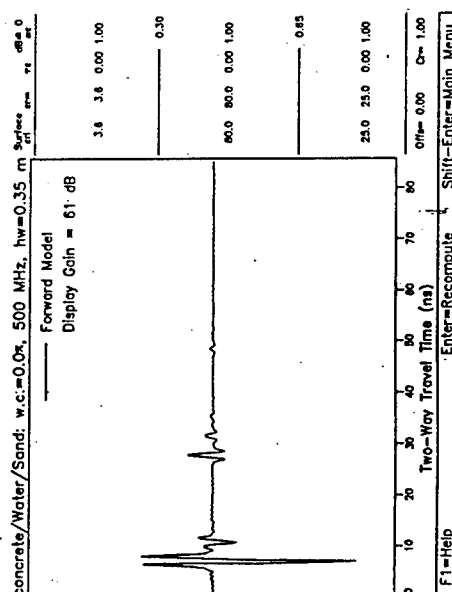


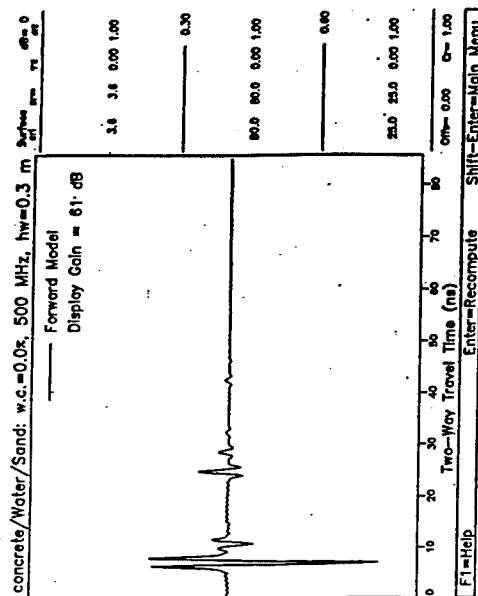
Figure C21. Problem Set 2, Cases 117-120, multiples



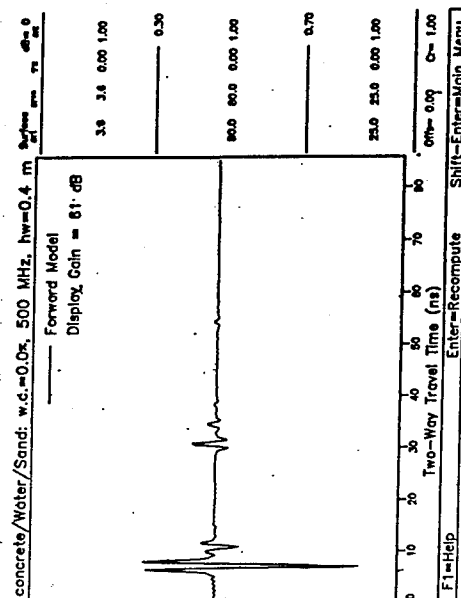
Case 121



Case 123

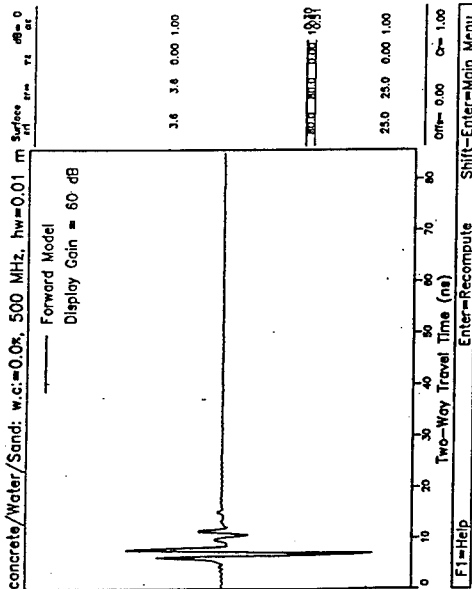


Case 122

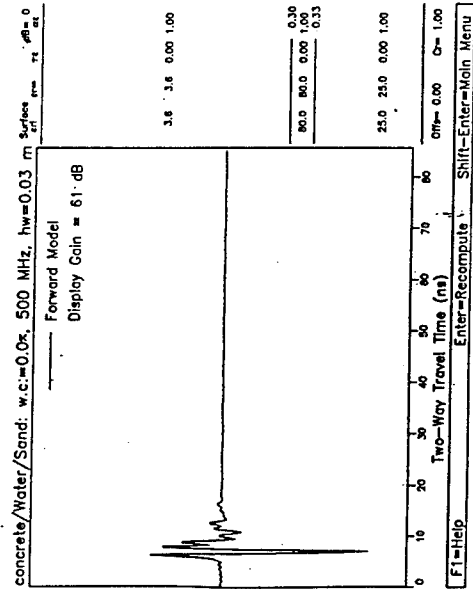


Case 124

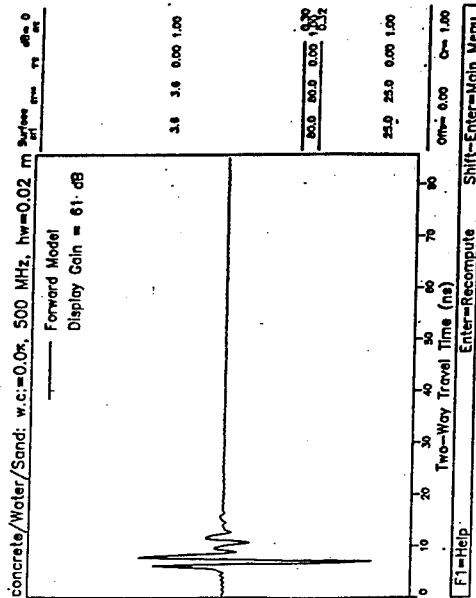
Figure C22. Problem Set 2, Cases 121-124, multiples



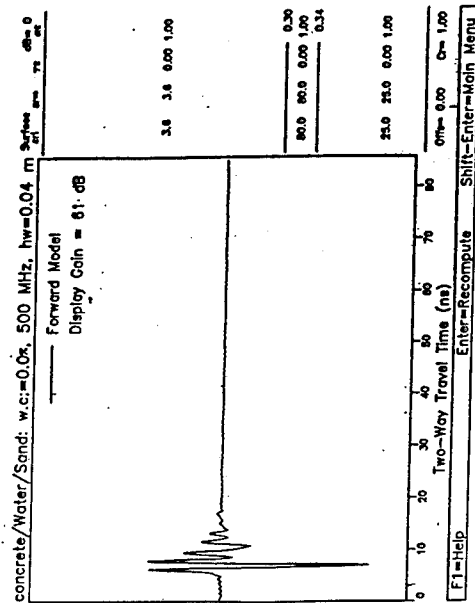
Case 125



Case 127

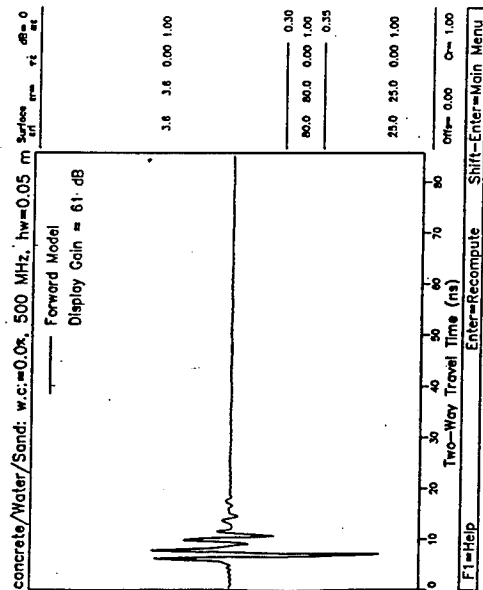


Case 126

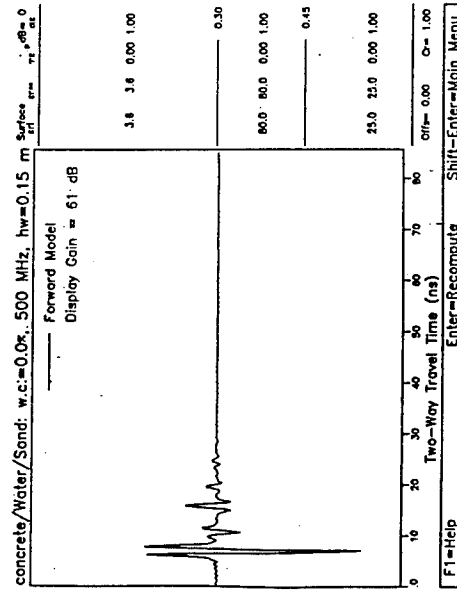


Case 128

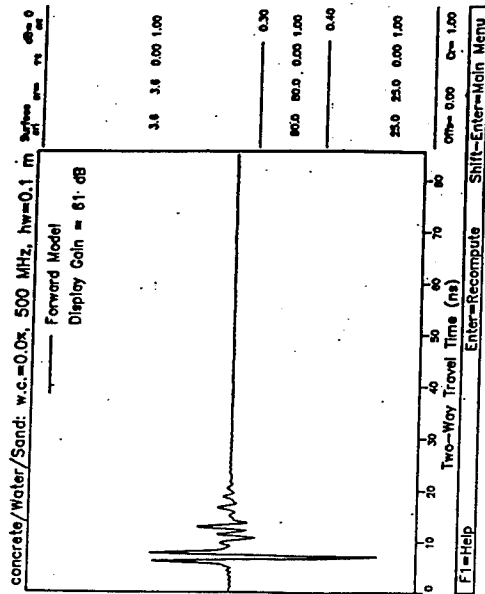
Figure C23. Problem Set 2, Cases 125-128, multiples



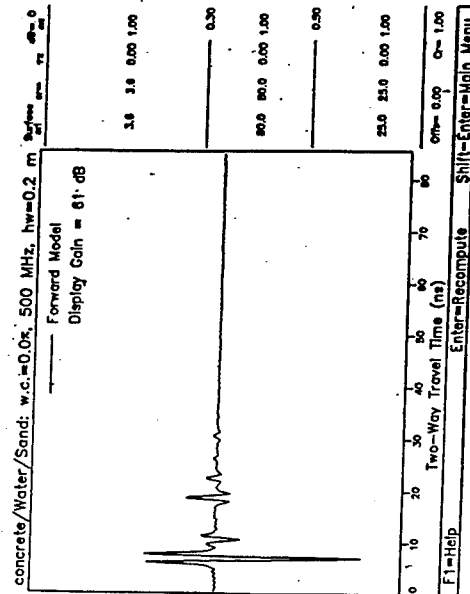
Case 129



Case 131

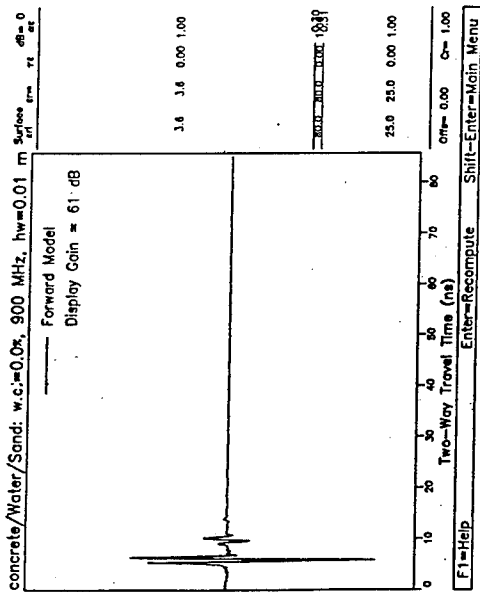


Case 130



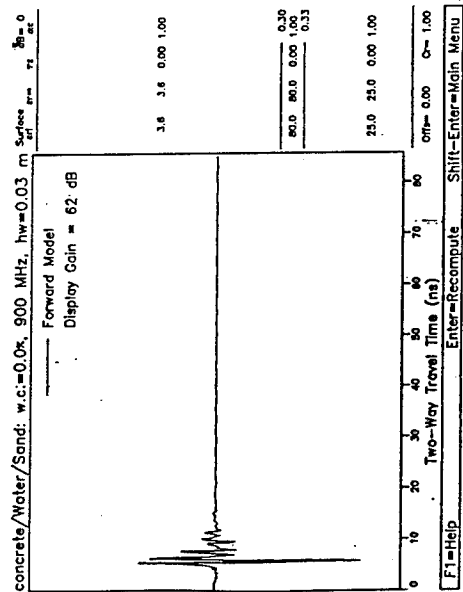
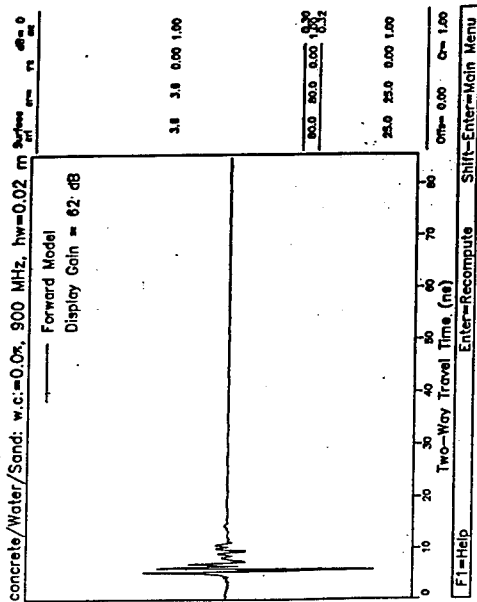
Case 132

Figure C24. Problem Set 2, Cases 129-132, multiples



Case 133

Case 134



Case 135

Case 136

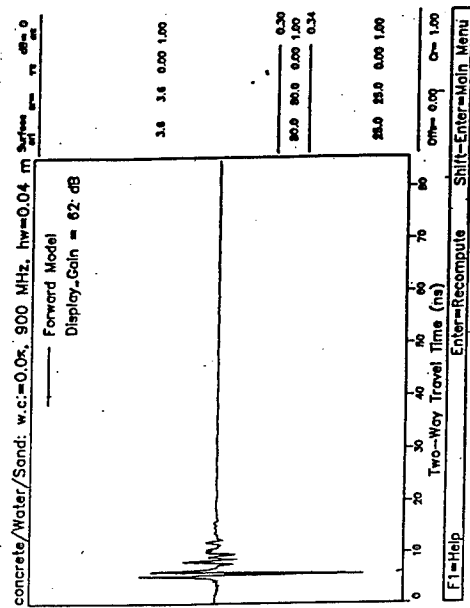
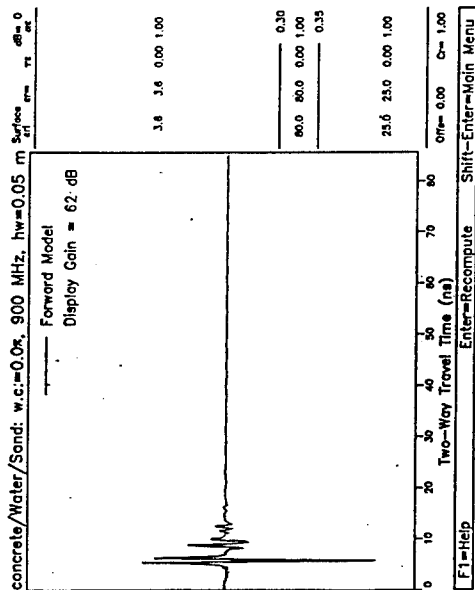
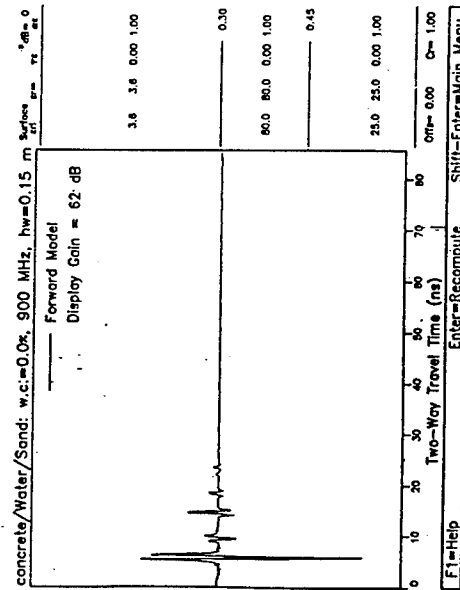


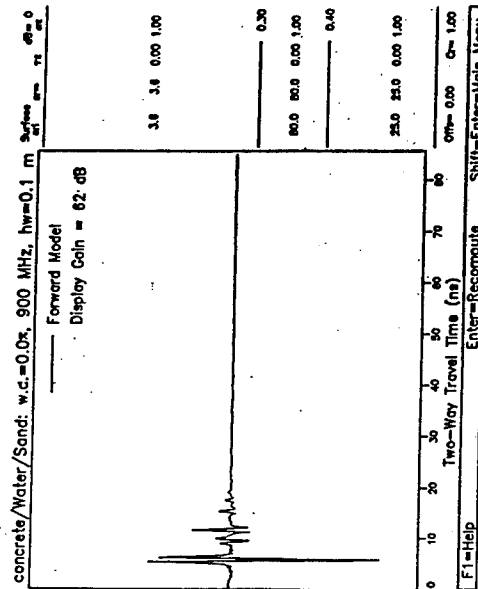
Figure C25. Problem Set 2, Cases 133-136, multiples



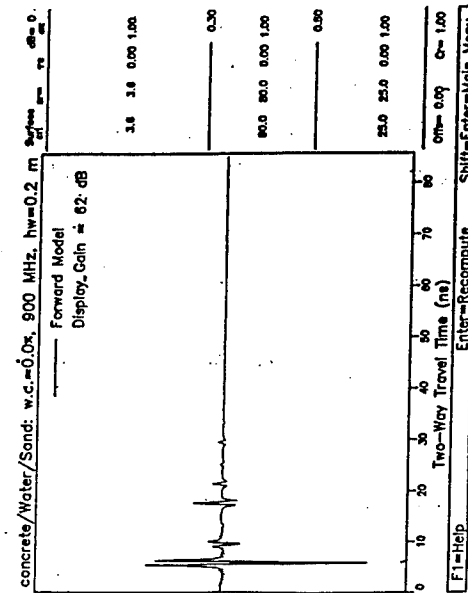
Case 137



Case 139

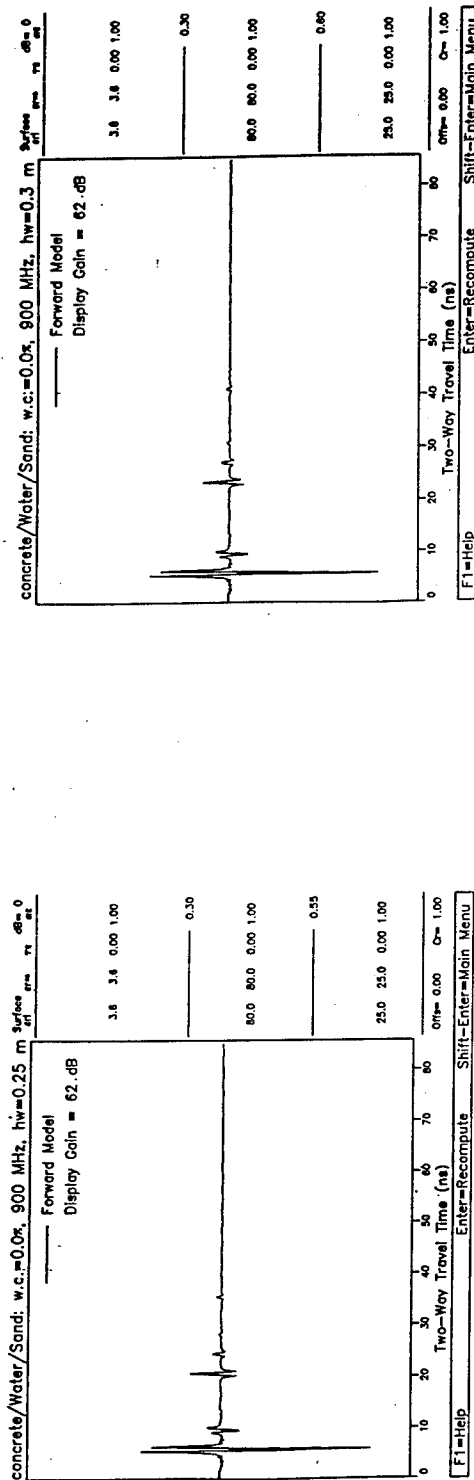


Case 138

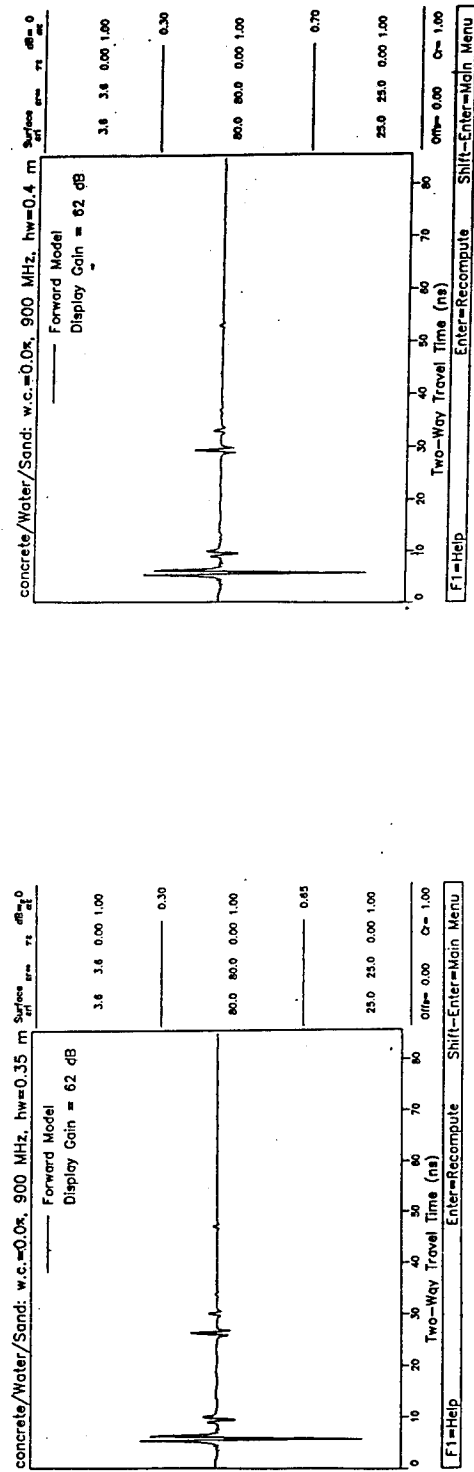


Case 140

Figure C26. Problem Set 2, Cases 137-140, multiples

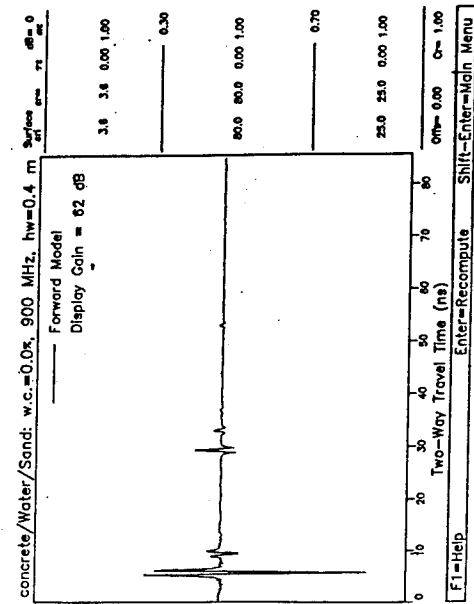


Case 141



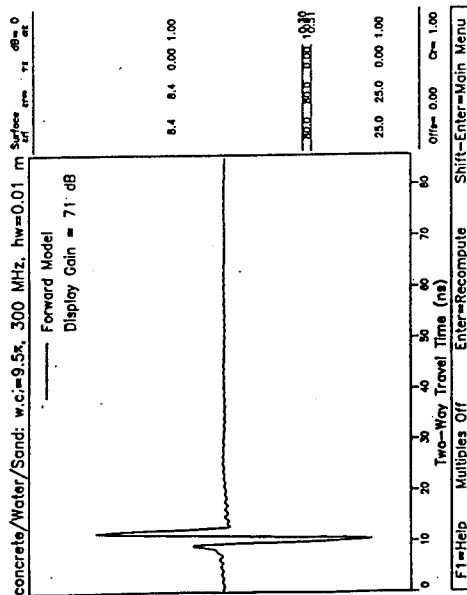
Case 143

Case 142

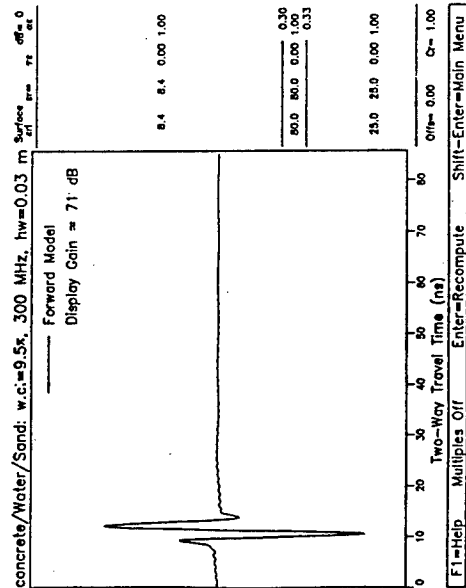


Case 144

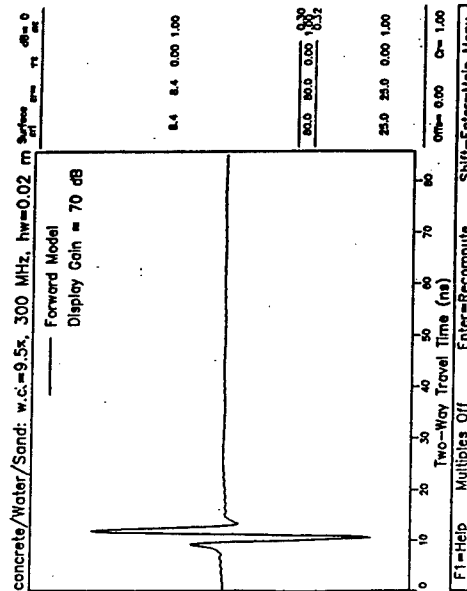
Figure C27. Problem Set 2, Cases 141-144, multiples



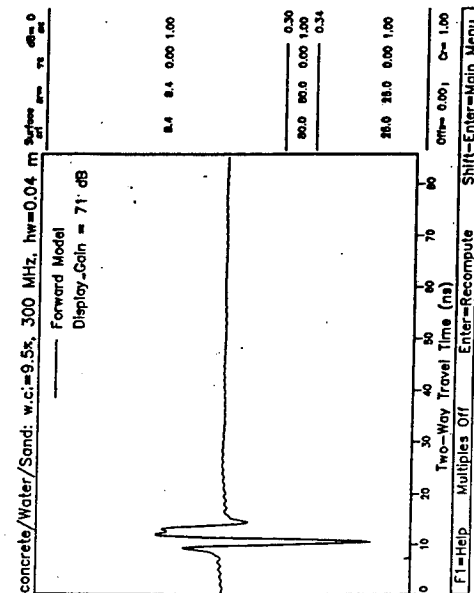
Case 145



Case 147

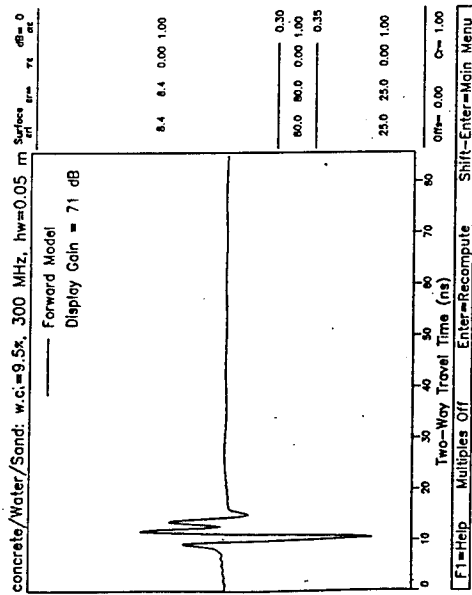


Case 146



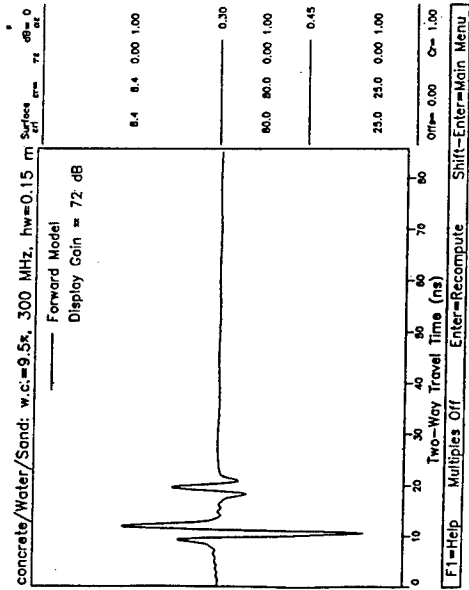
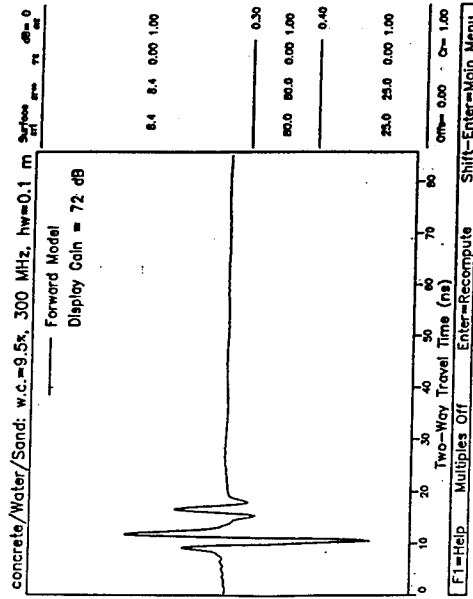
Case 148

Figure C28. Problem Set 2, Cases 145-148, no multiples



Case 149

Case 150



Case 151

Case 152

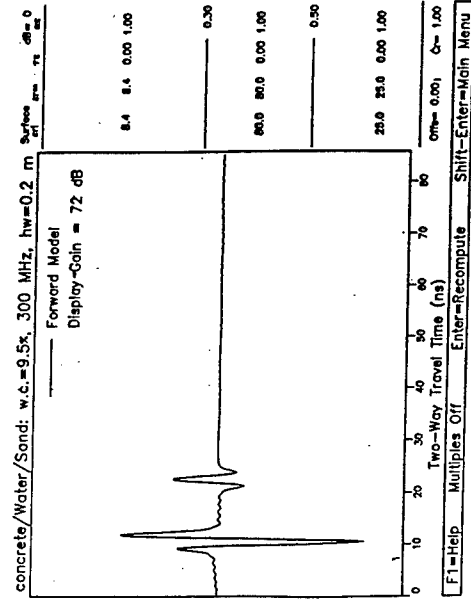
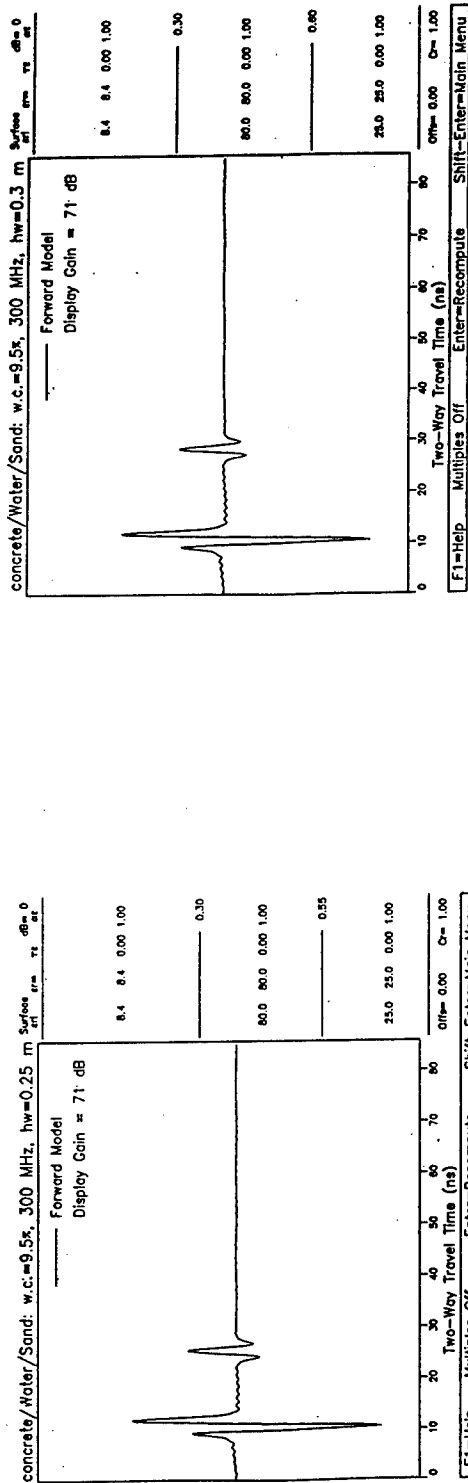
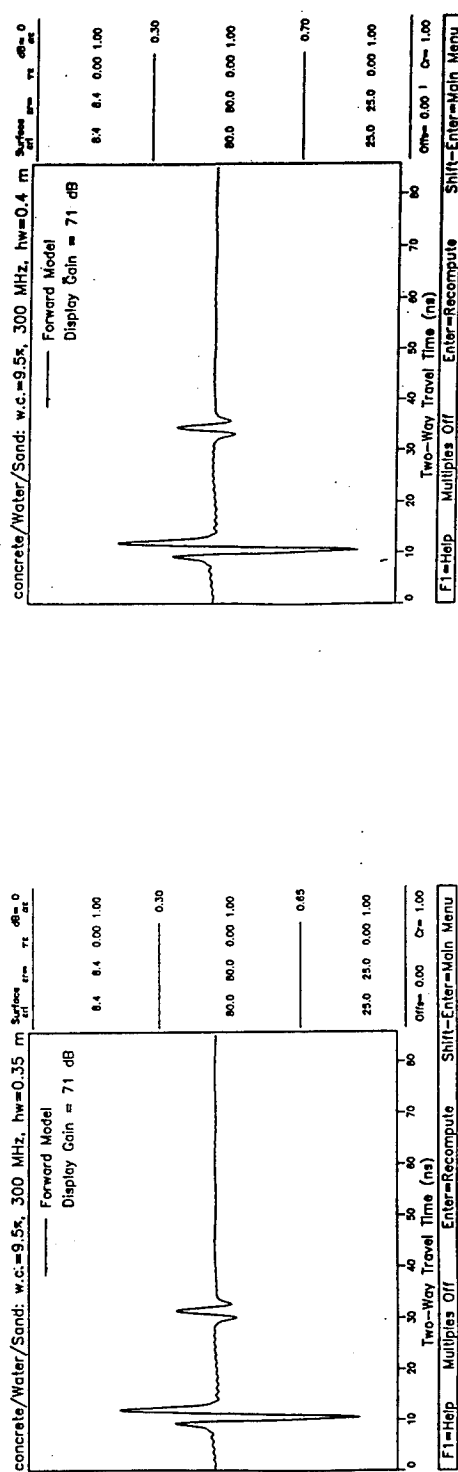


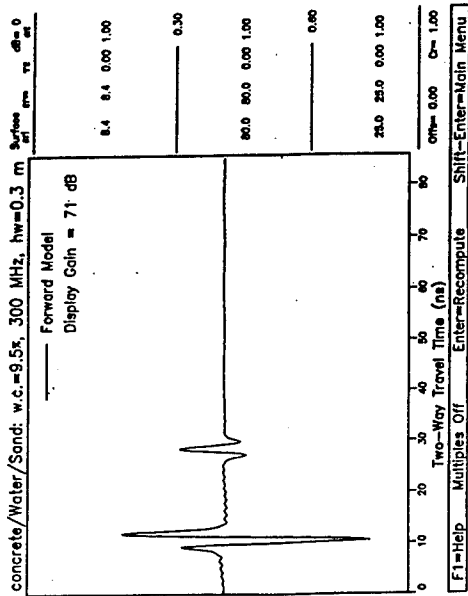
Figure C29. Problem Set 2, Cases 149-152, no multiples



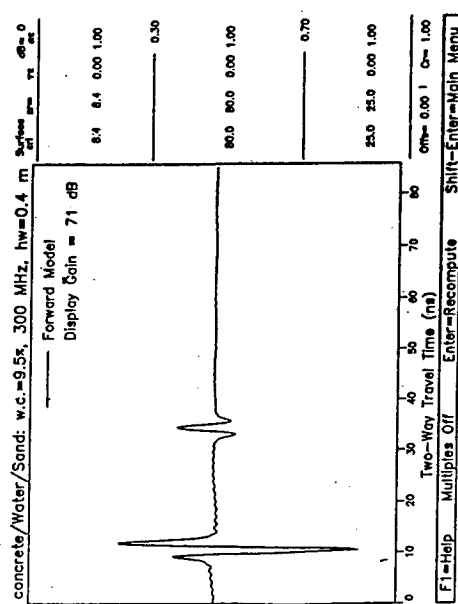
Case 153



Case 155

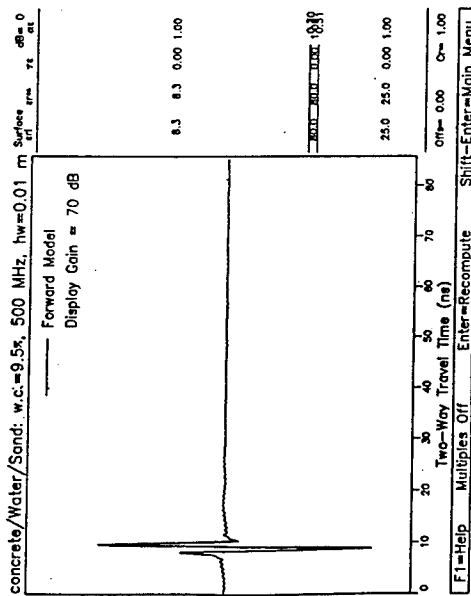


Case 154

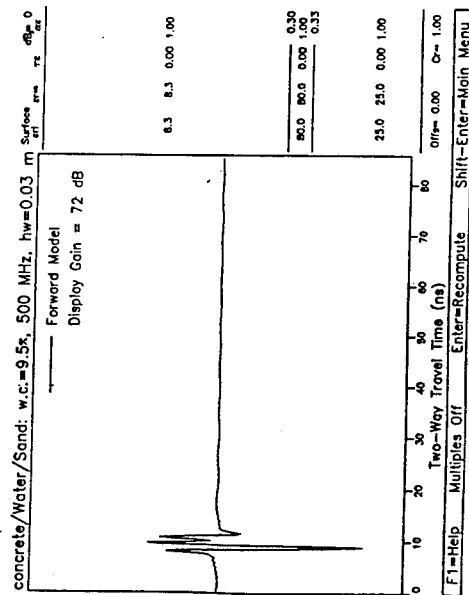


Case 156

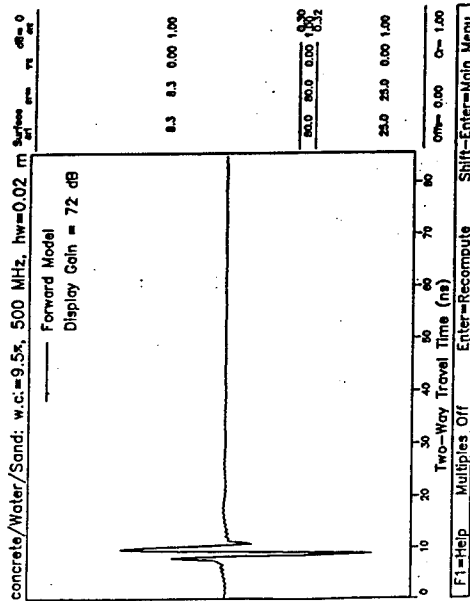
Figure C30. Problem Set 2, Cases 153-156, no multiples



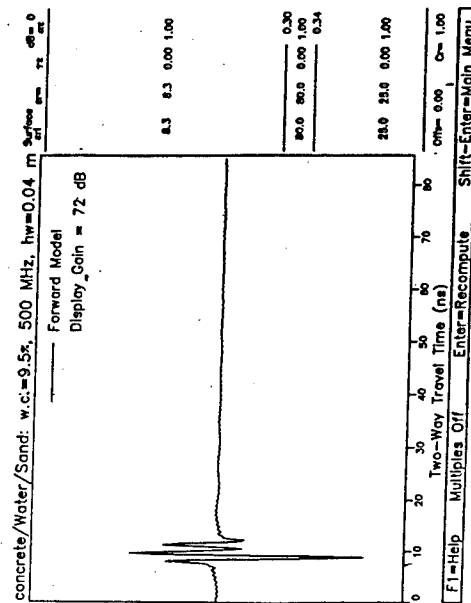
Case 157



Case 159

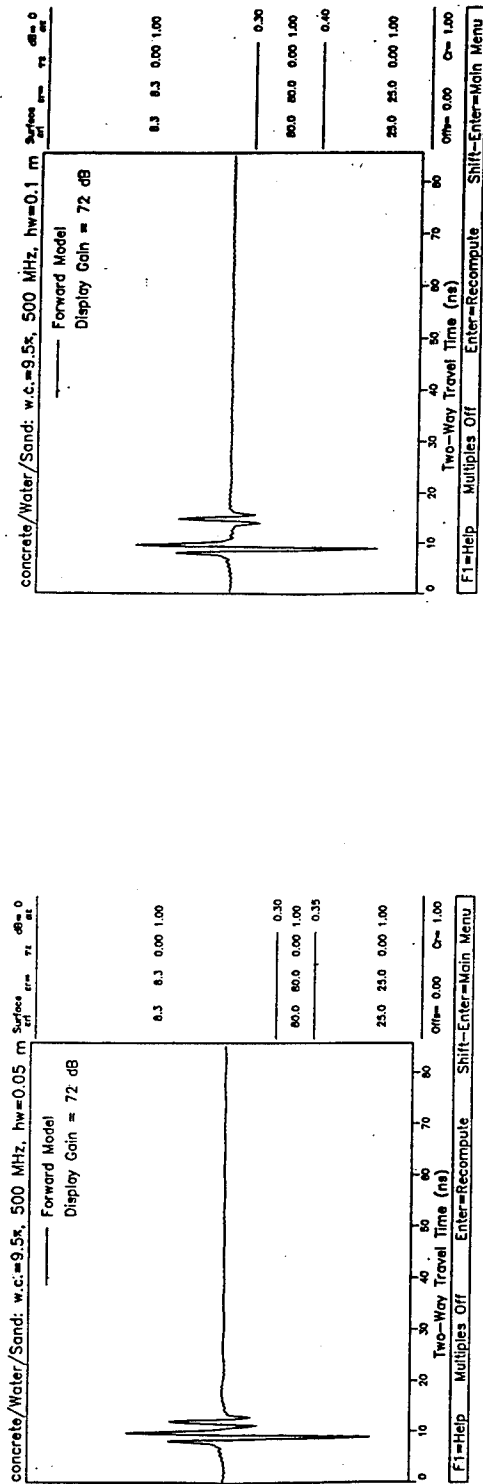


Case 158



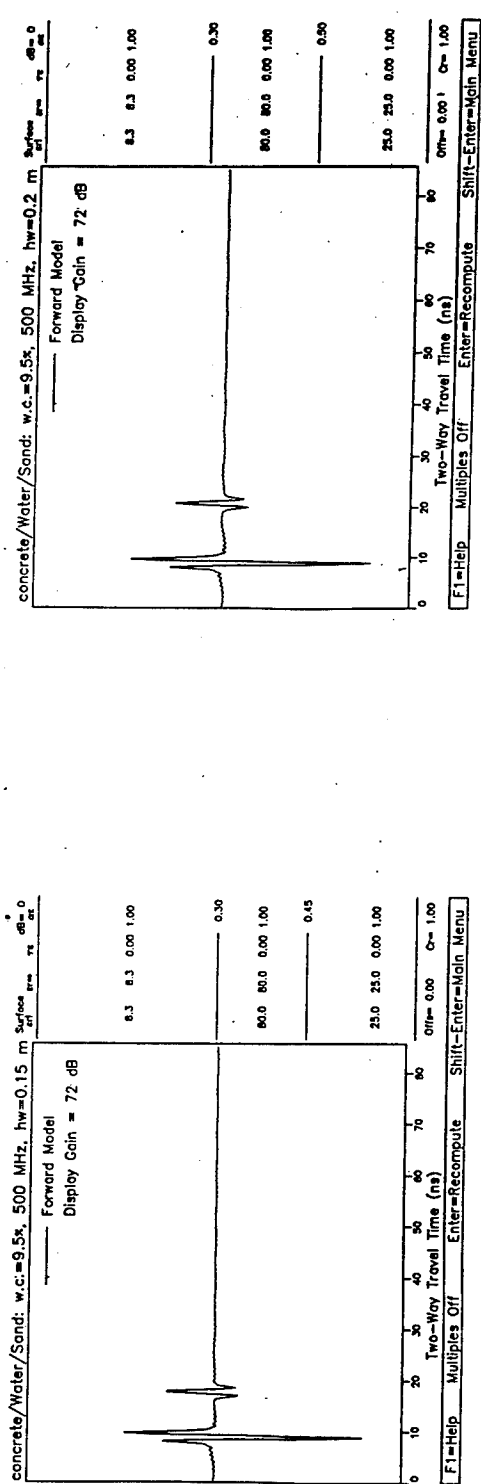
Case 160

Figure C31. Problem Set 2, Cases 157-160, multiples



Case 161

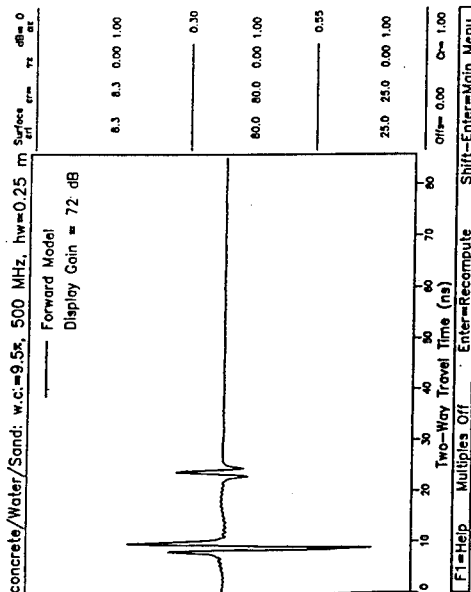
Case 162



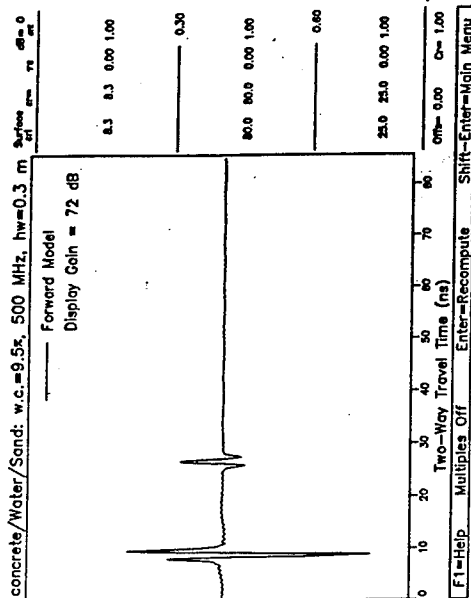
Case 163

Case 164

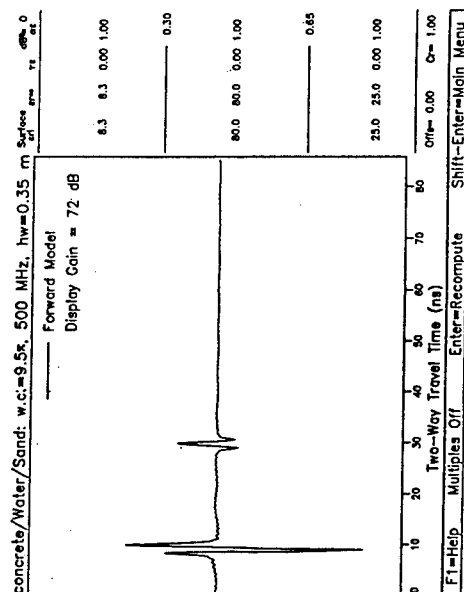
Figure C32. Problem Set 2, Cases 161-164, multiples



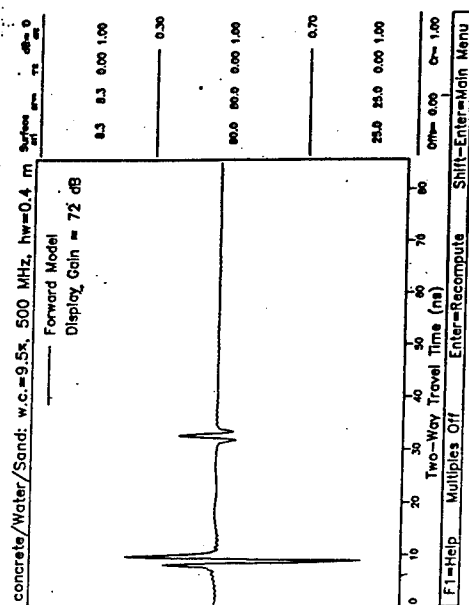
Case 165



Case 166

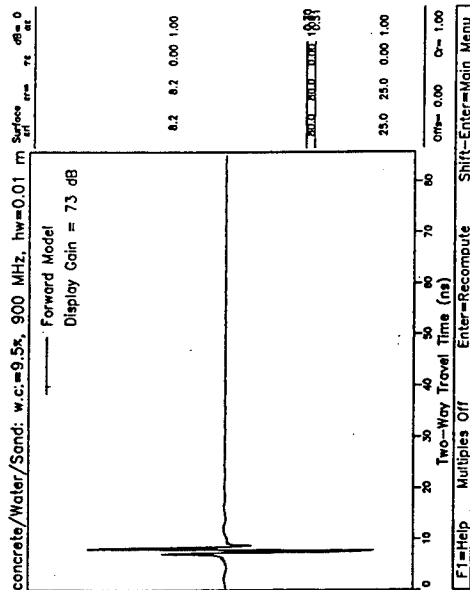


Case 167

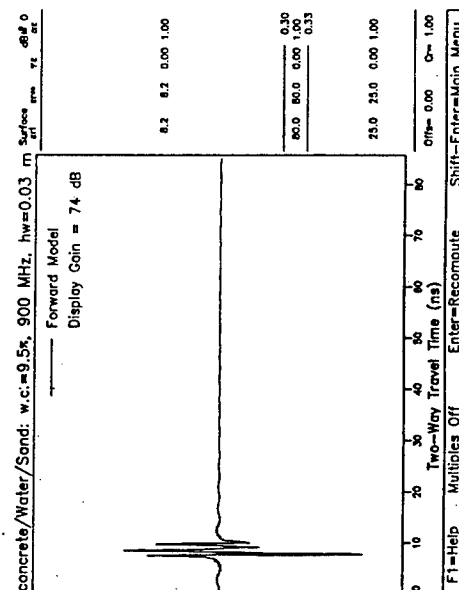


Case 168

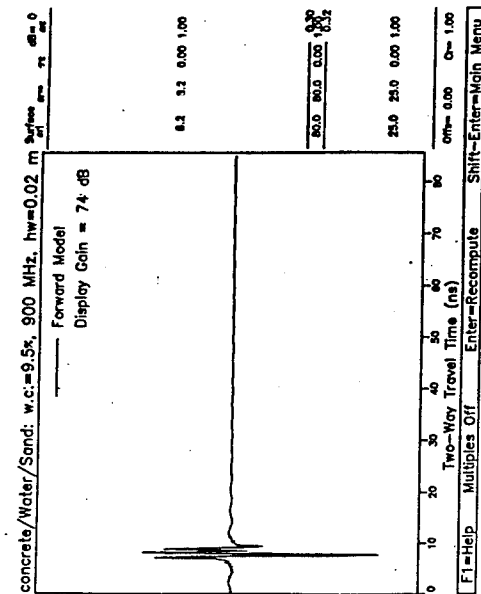
Figure C33. Problem Set 2, Cases 165-168, multiples



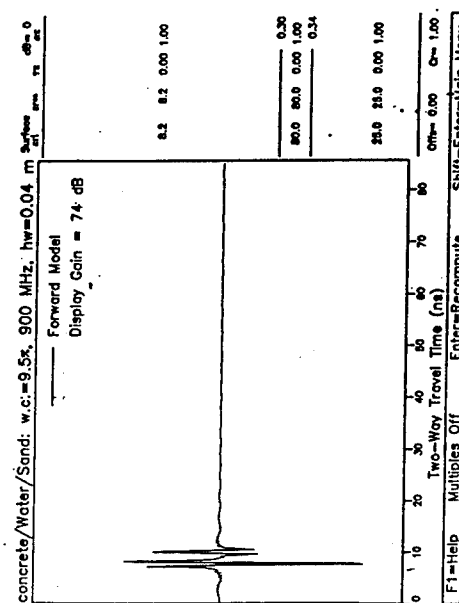
Case 169



Case 170

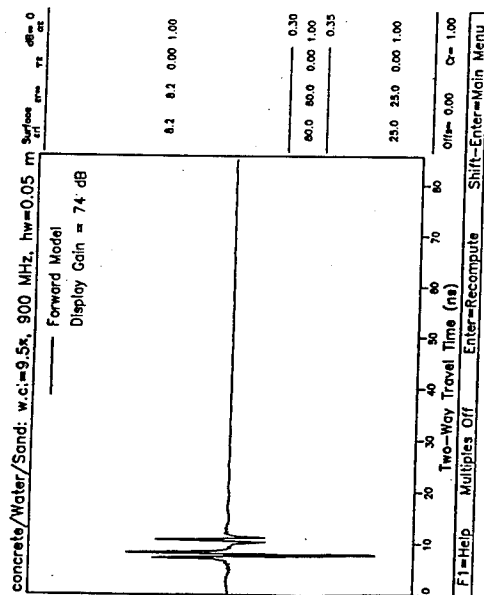


Case 171

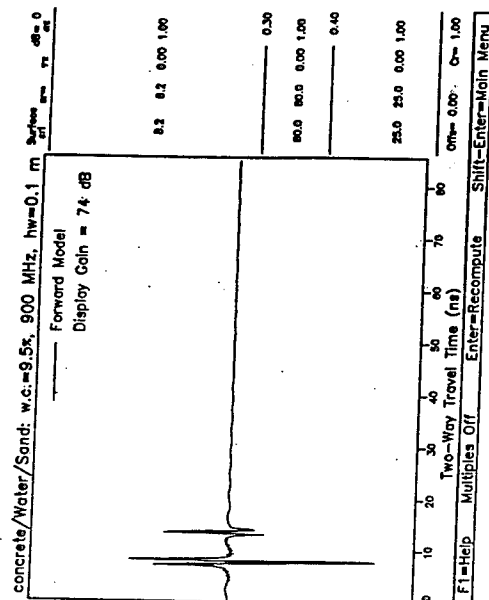


Case 172

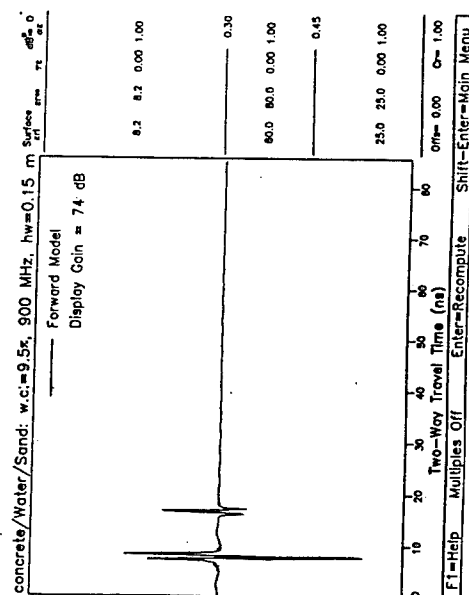
Figure C34. Problem Set 2, Cases 169-172, multiples



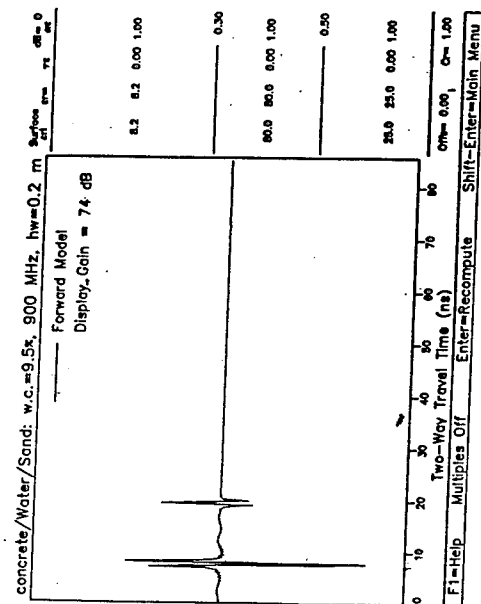
Case 173



Case 174

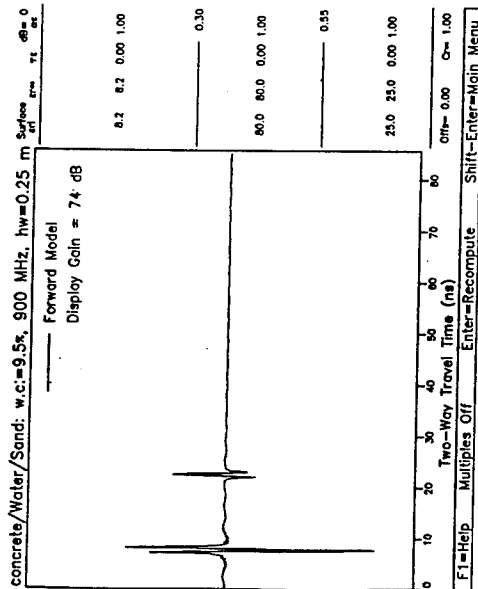


Case 175

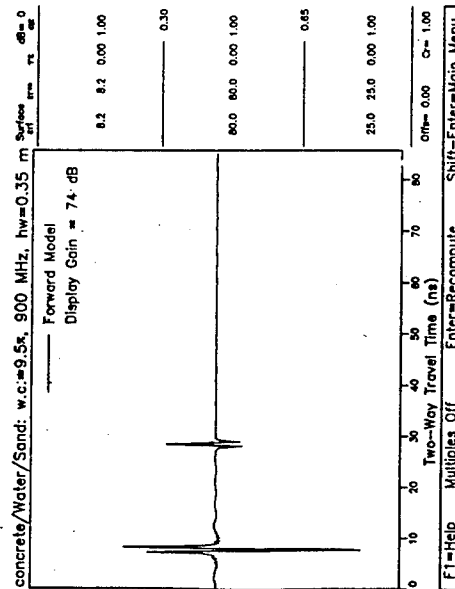


Case 176

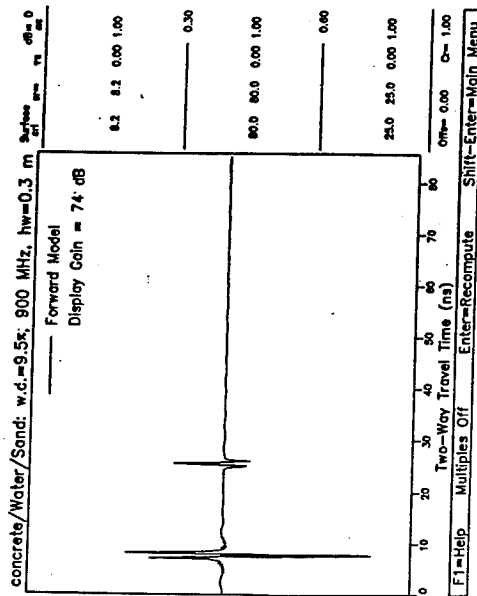
Figure C35. Problem Set 2, Cases 173-176, multiples



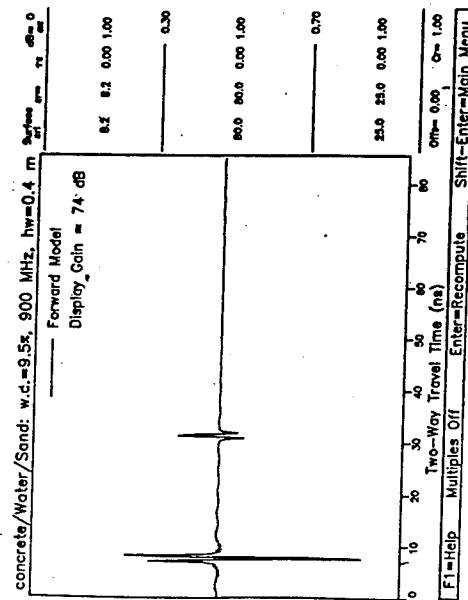
Case 177



Case 179

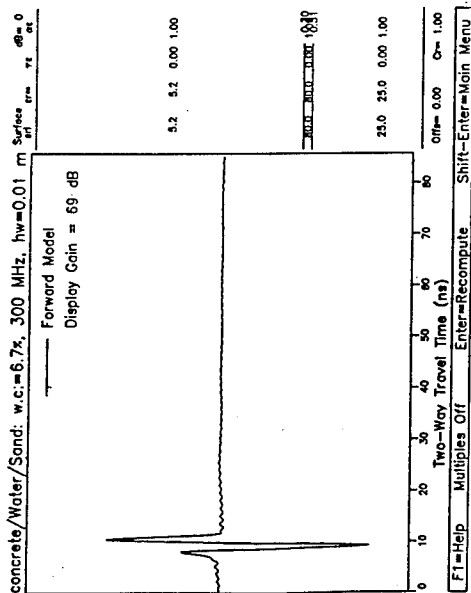


Case 178



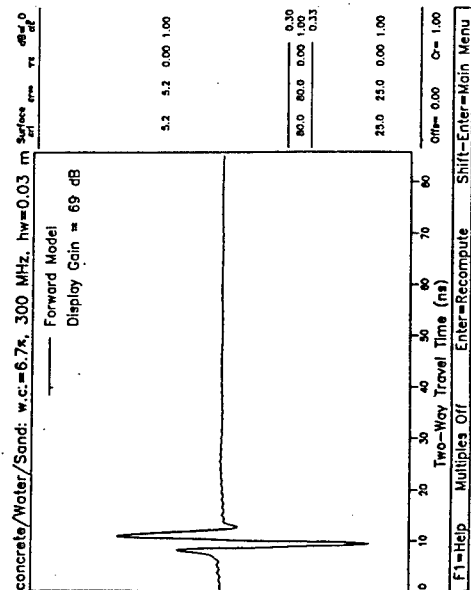
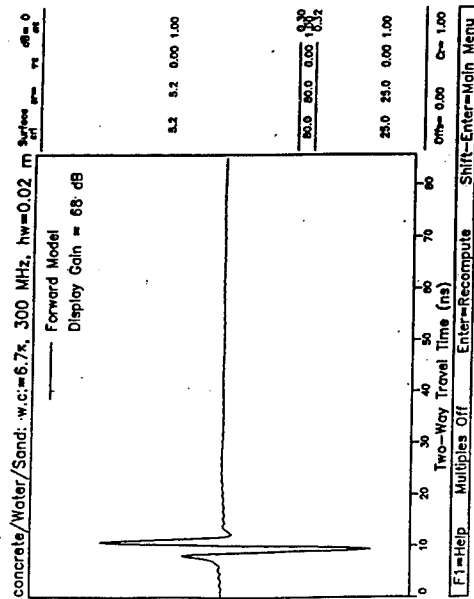
Case 180

Figure C36. Problem Set 2, Cases 177-180, multiples

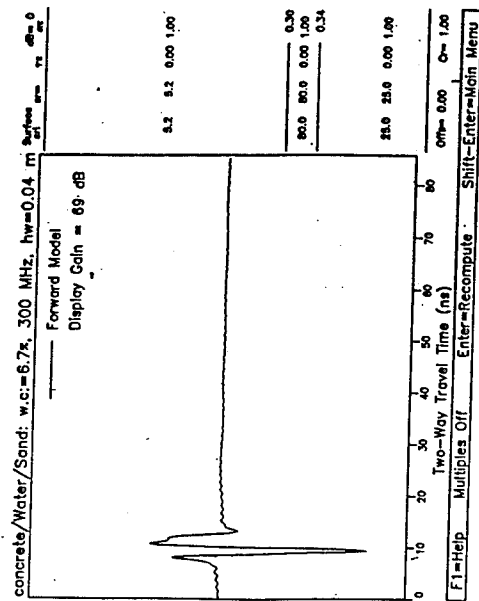


Case 181

Case 182

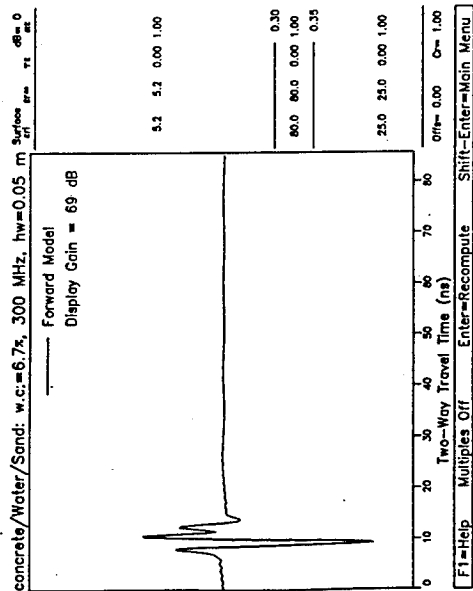


Case 183

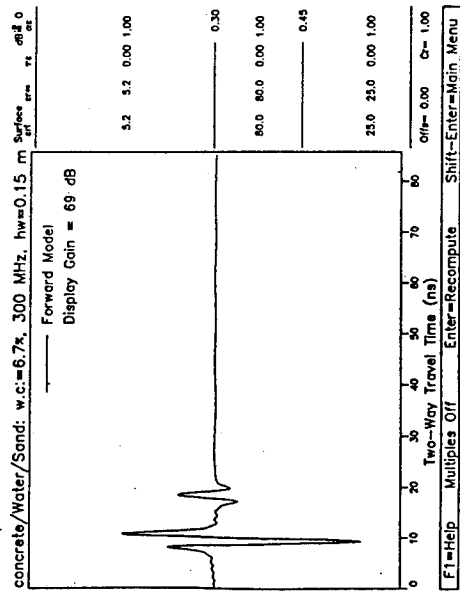


Case 184

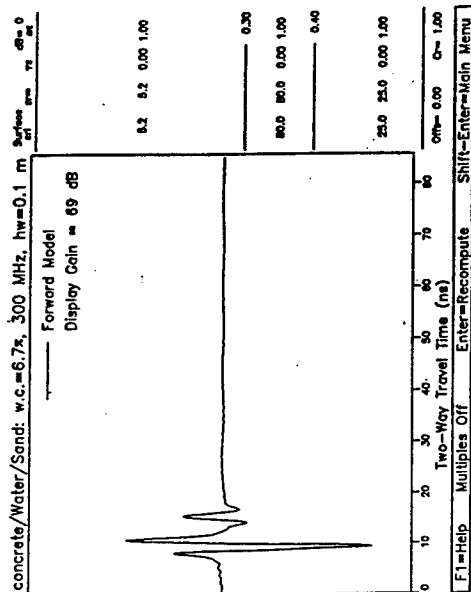
Figure C37. Problem Set 2, Cases 181-184, multiples



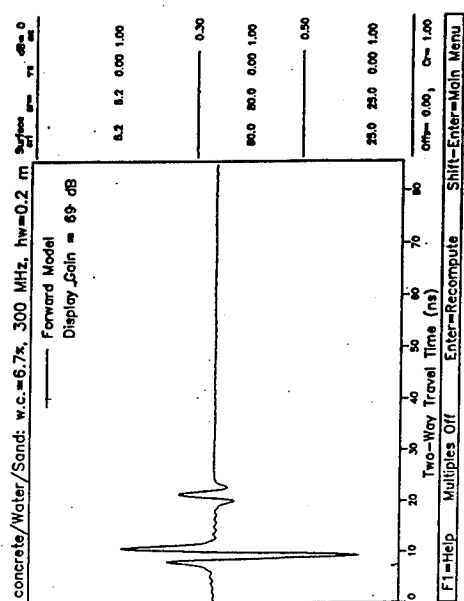
Case 185



Case 187

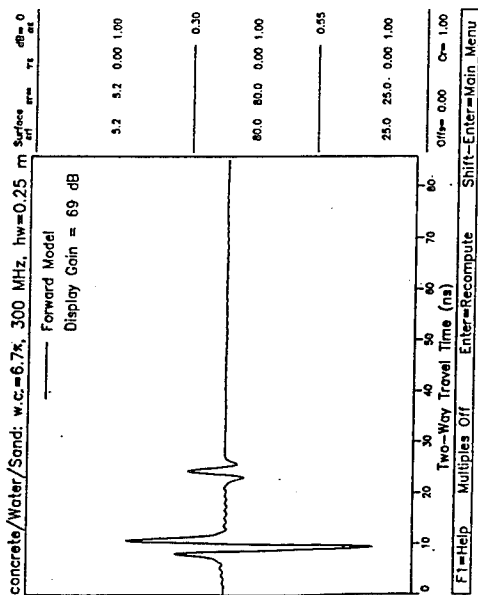


Case 186



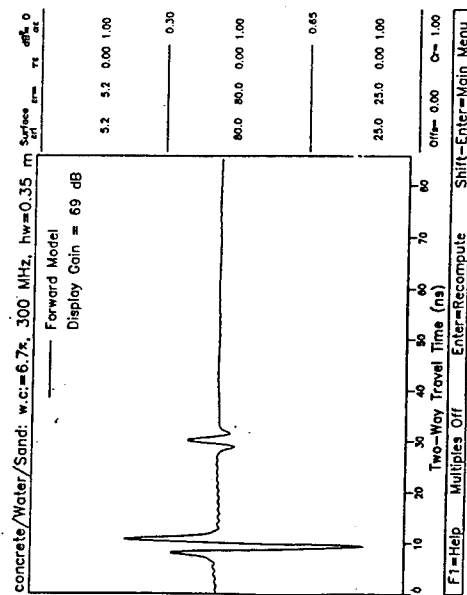
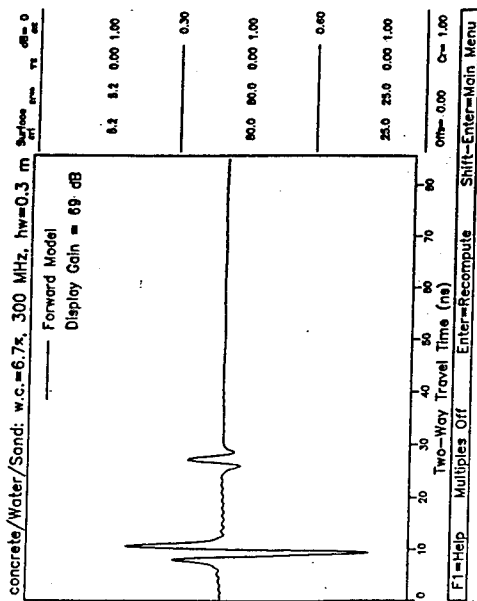
Case 188

Figure C38. Problem Set 2, Cases 185-188, multiples

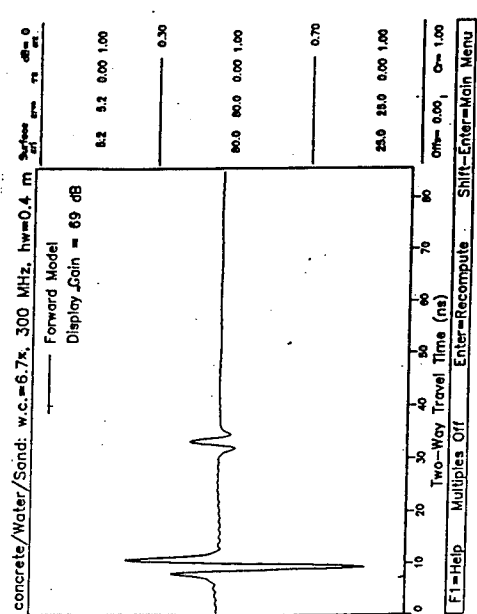


Case 189

Case 190

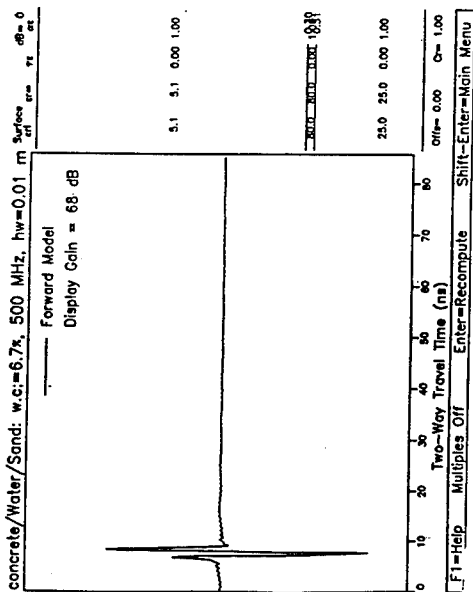


Case 191



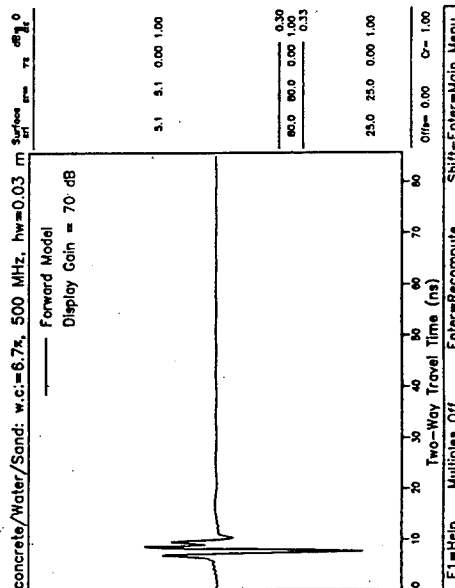
Case 192

Figure C39. Problem Set 2, Cases 189-192, multiples



Case 193

Case 194



Case 195

Case 196

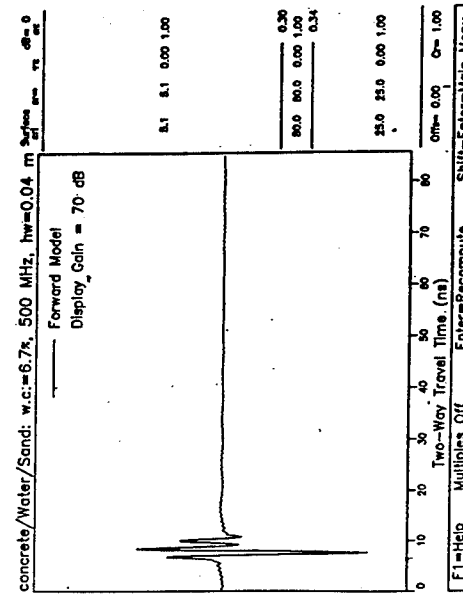
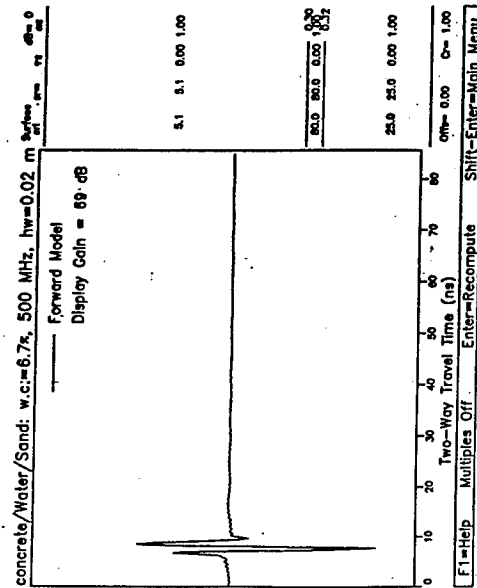


Figure C40. Problem Set 2, Cases 193-196, multiples

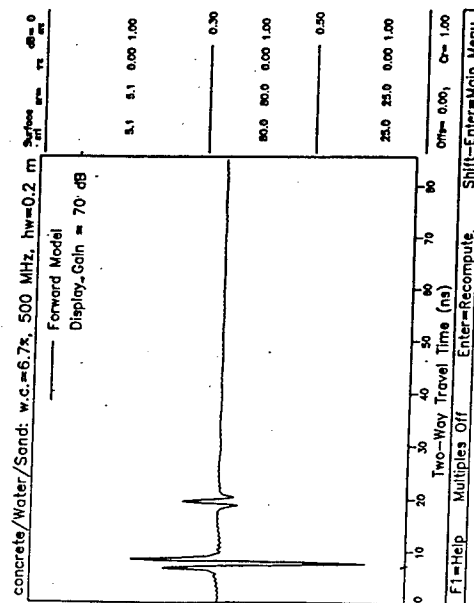
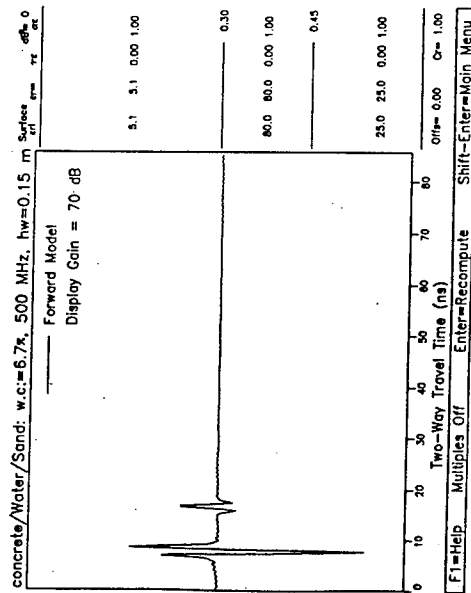
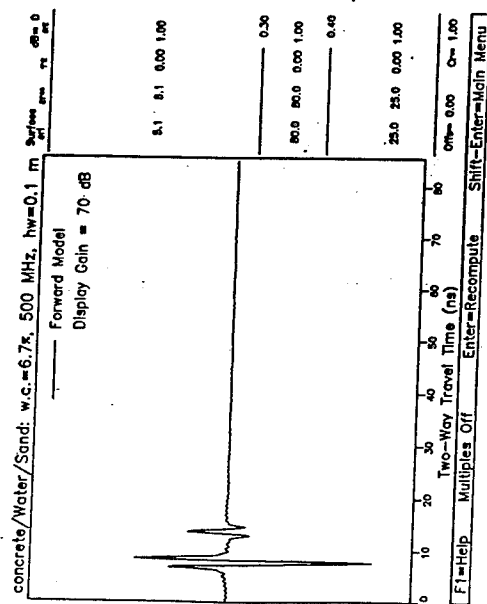
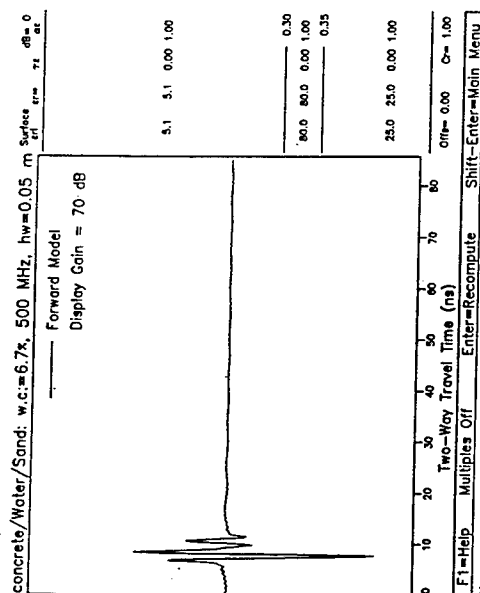
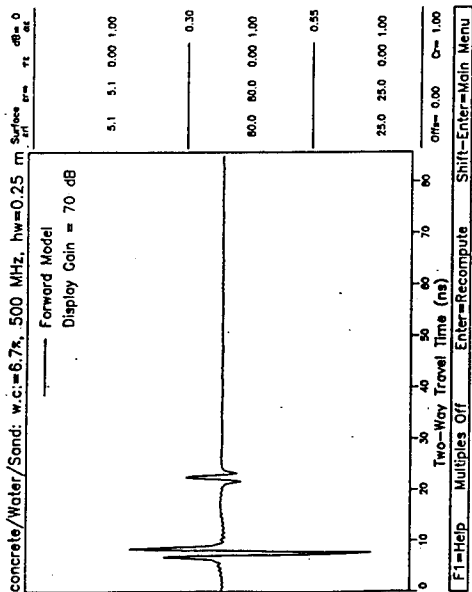
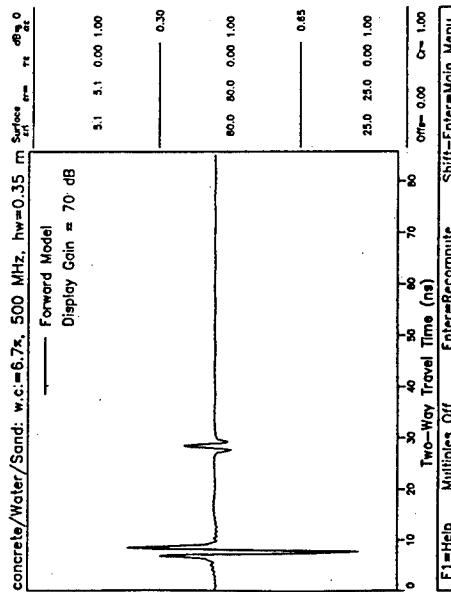


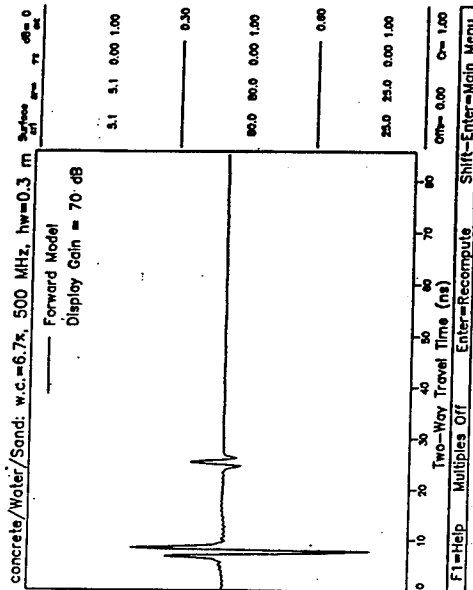
Figure C41. Problem Set 2, Cases 197-200, multiples



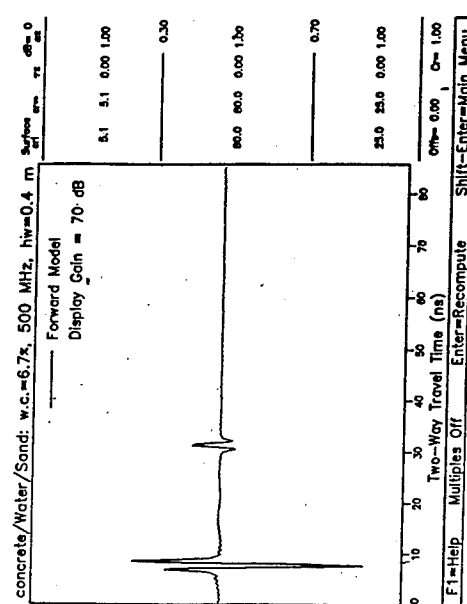
Case 201



Case 203

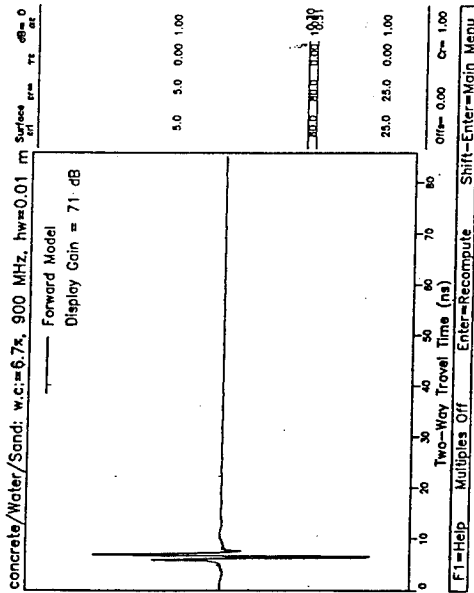


Case 202

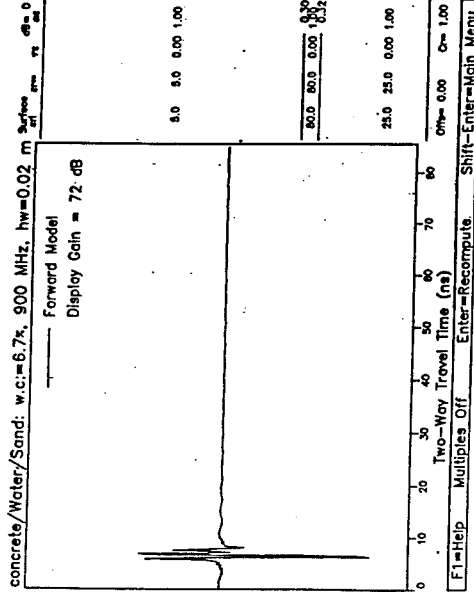


Case 204

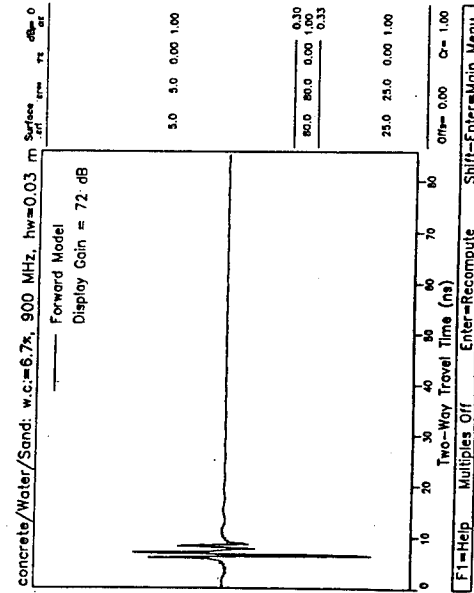
Figure C42. Problem Set 2, Cases 201-204, multiples



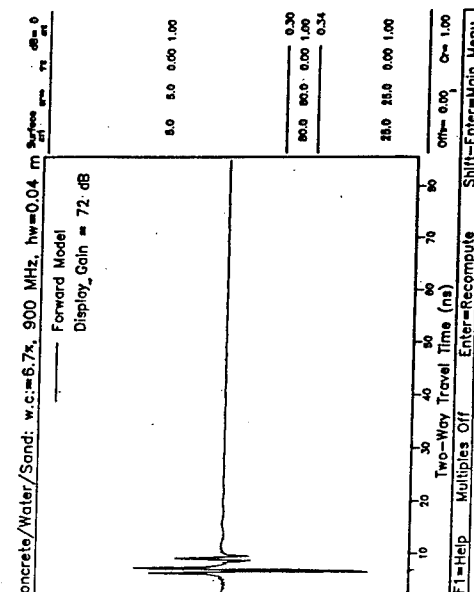
Case 205



Case 206

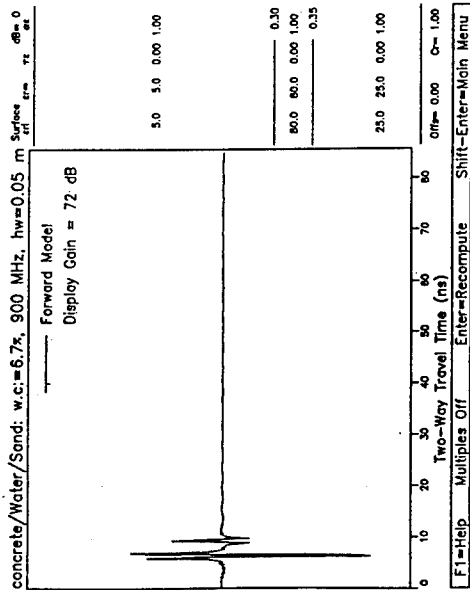


Case 207



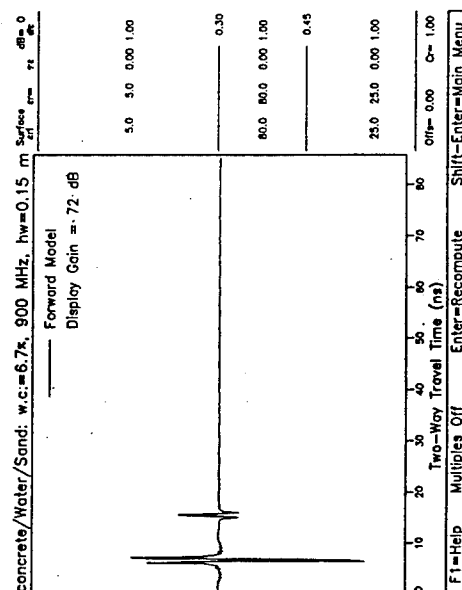
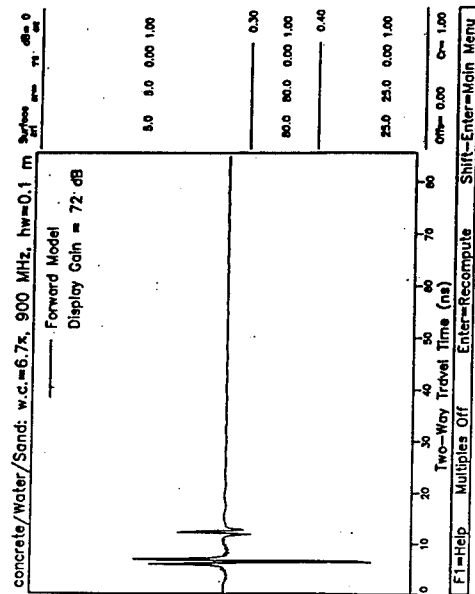
Case 208

Figure C43. Problem Set 2, Cases 205-208, multiples



Case 209

Case 210



Case 211

Case 212

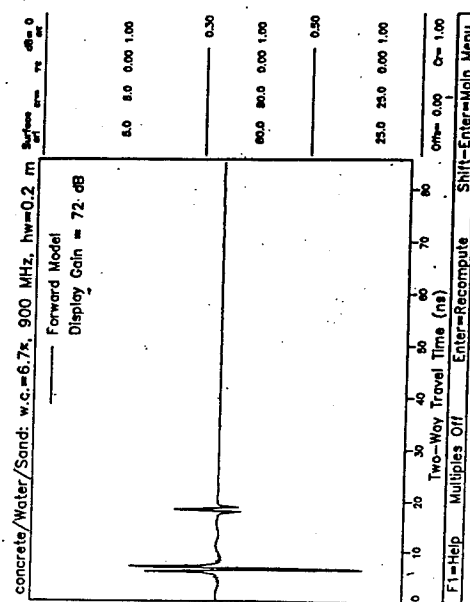


Figure C44. Problem Set 2, Cases 209-212, multiples

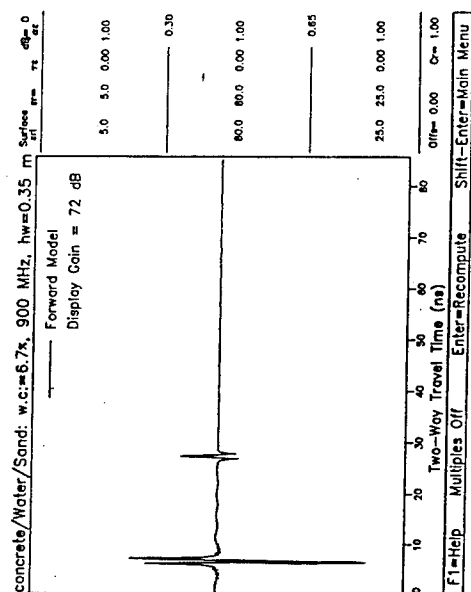
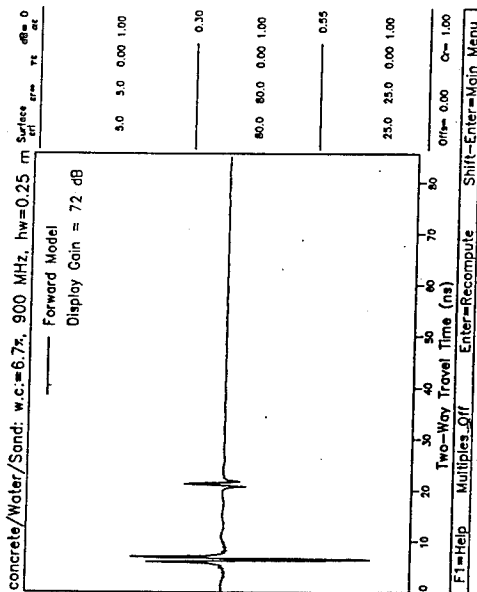
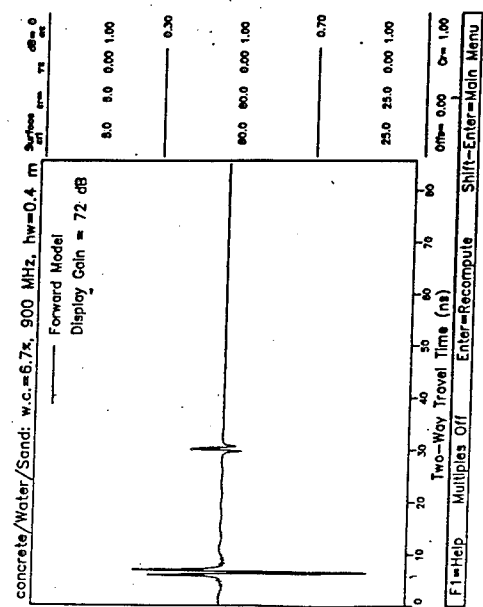
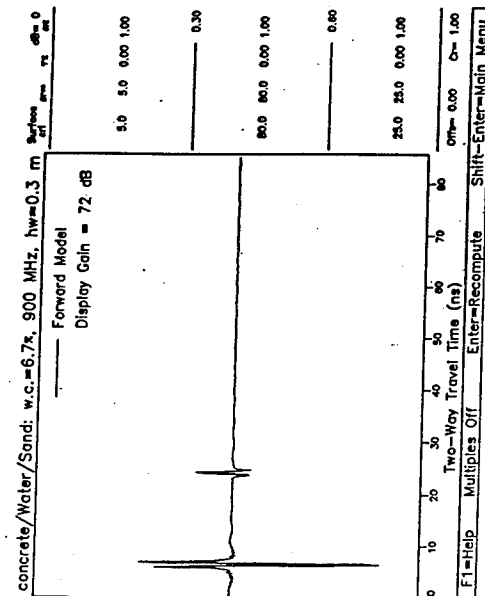
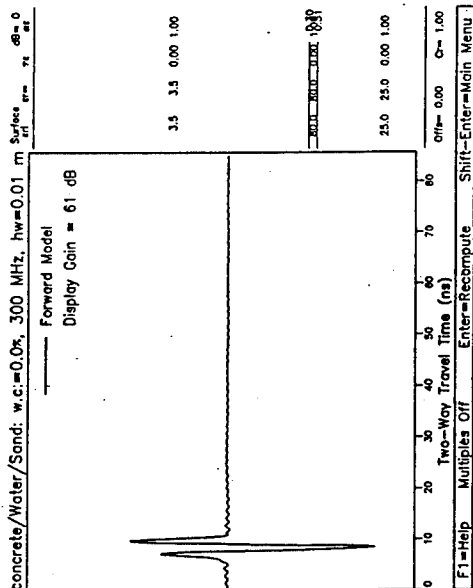
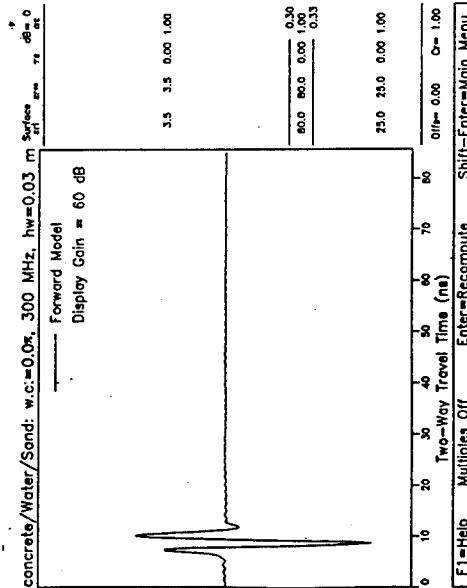


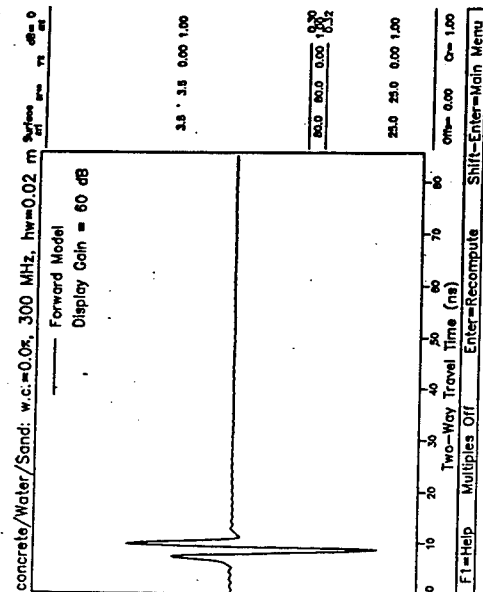
Figure C45. Problem Set 2, Cases 213-216, multiples



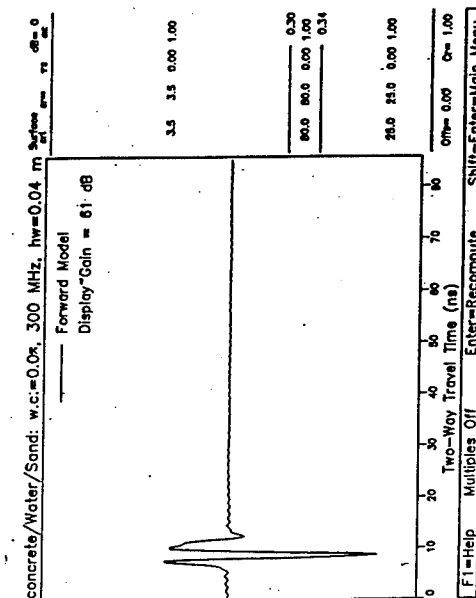
Case 217



Case 219

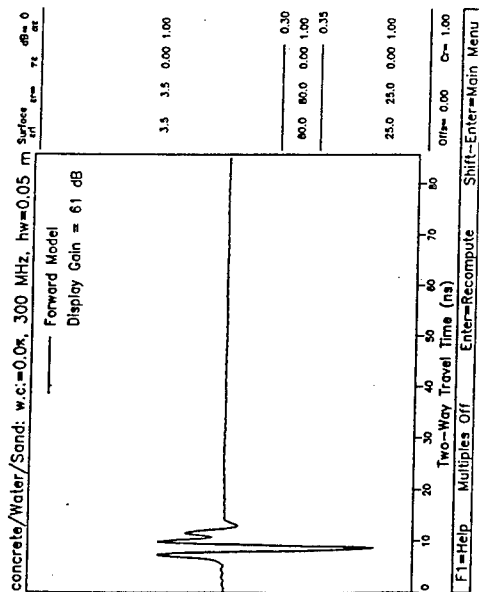


Case 218

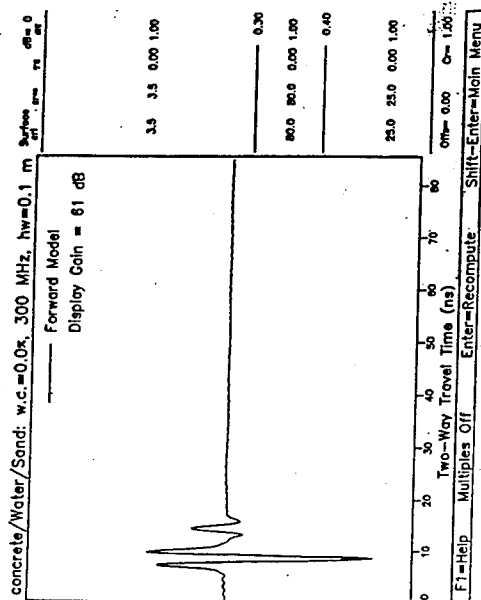


Case 220

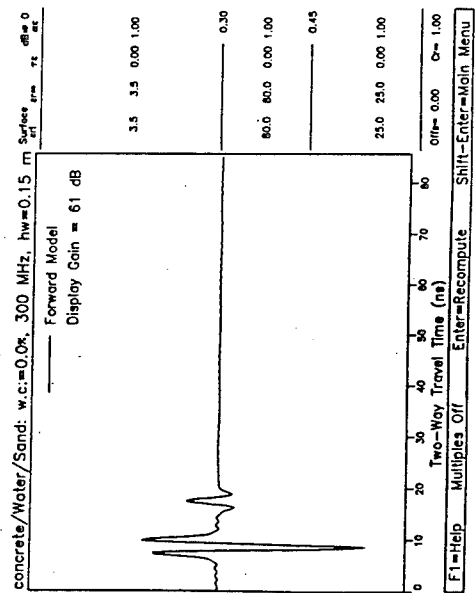
Figure C46. Problem Set 2, Cases 217-220, multiples



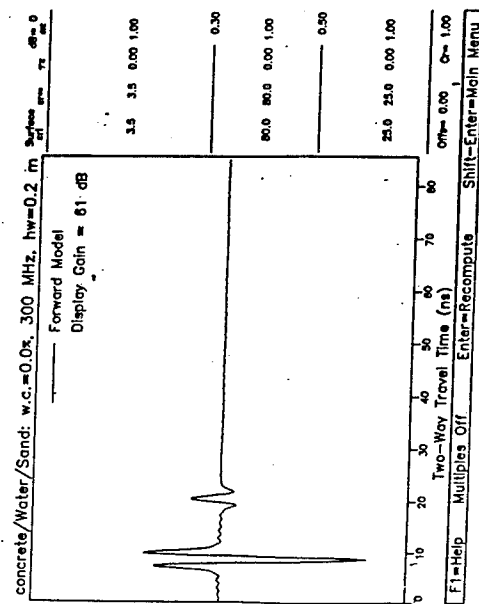
Case 221



Case 222

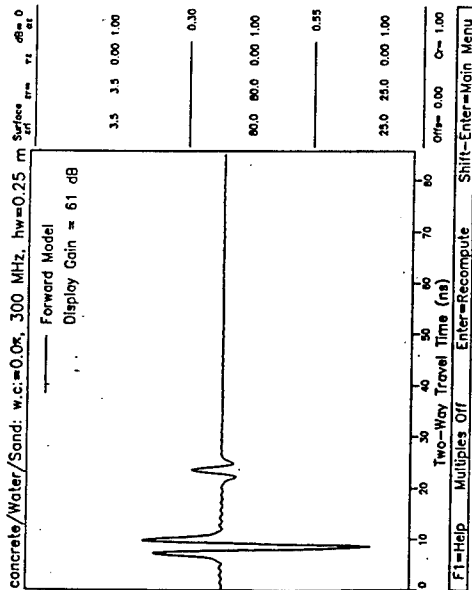


Case 223

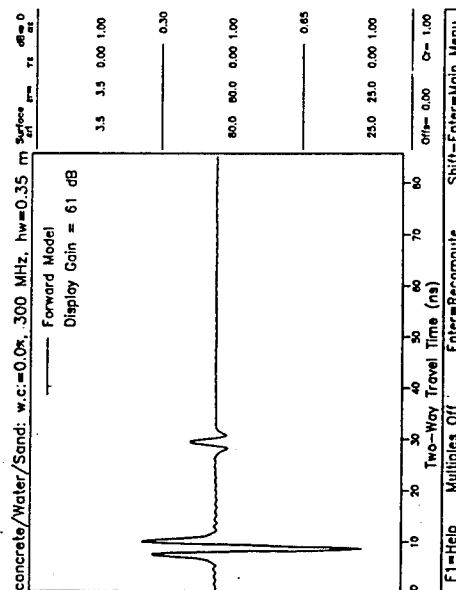


Case 224

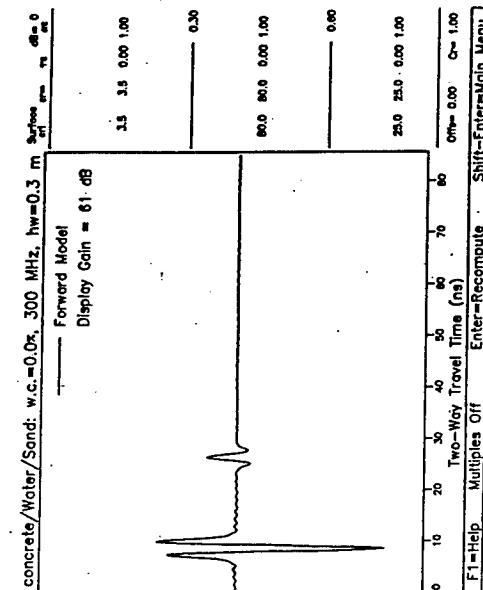
Figure C47. Problem Set 2, Cases 221-224, multiples



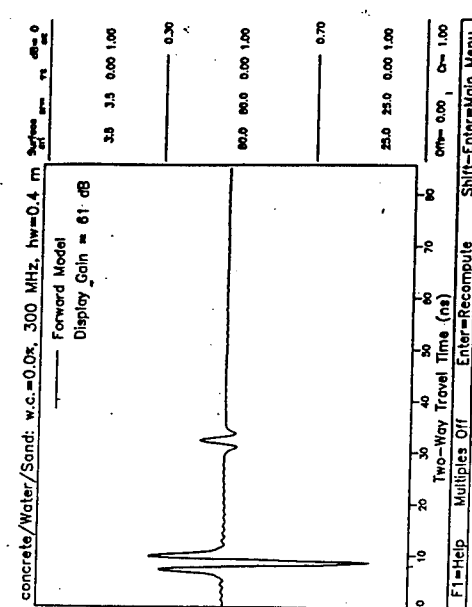
Case 225



Case 227

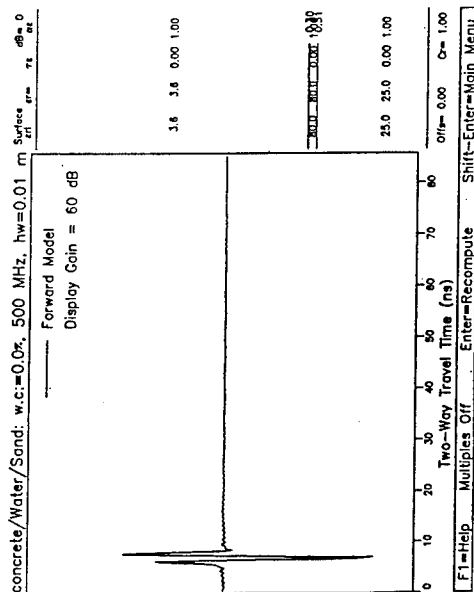


Case 226

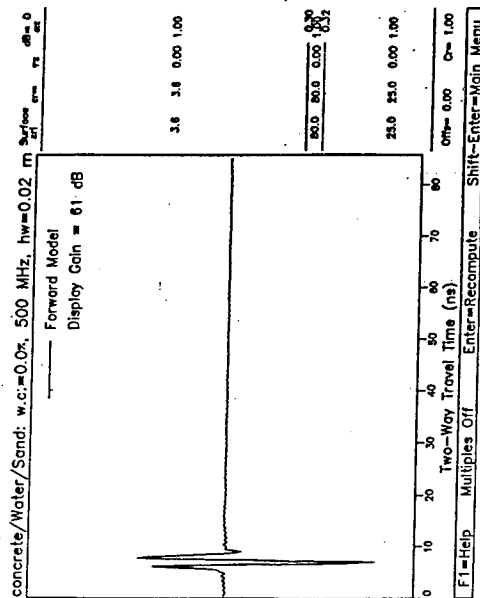


Case 228

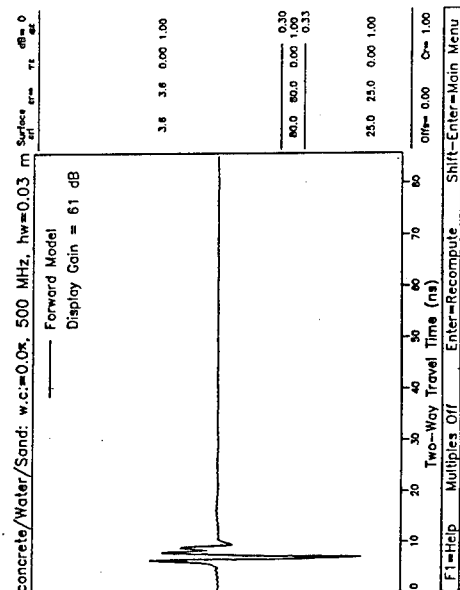
Figure C48. Problem Set 2, Cases 225-228, multiples



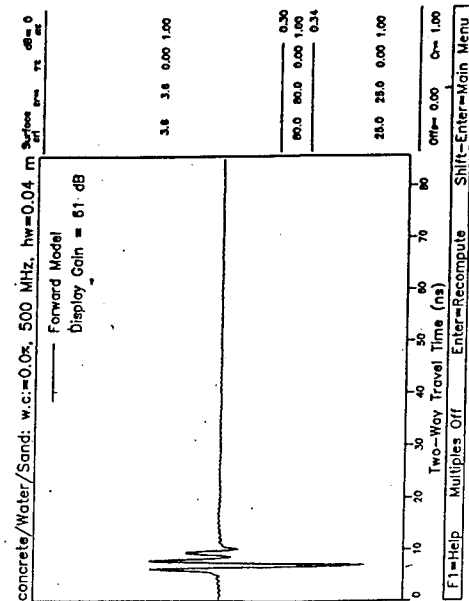
Case 229



Case 230

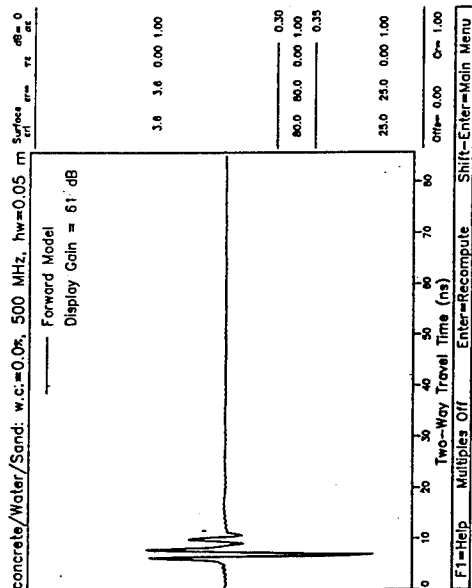


Case 231

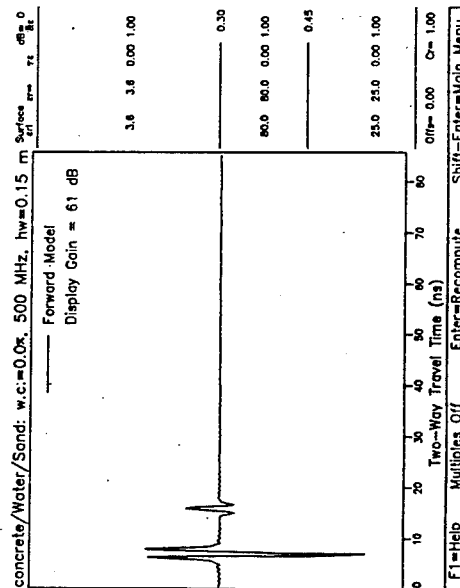


Case 232

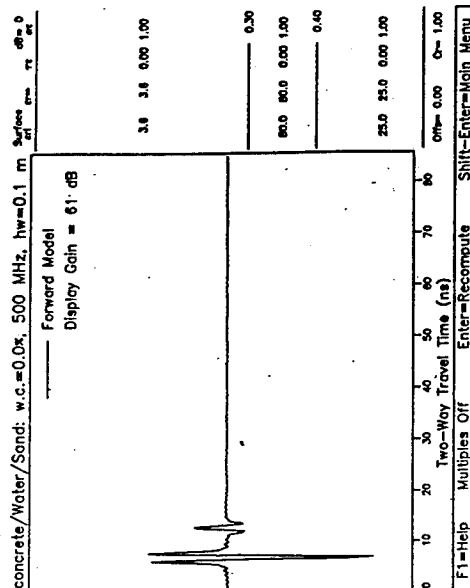
Figure C49. Problem Set 2, Cases 229-232, multiples



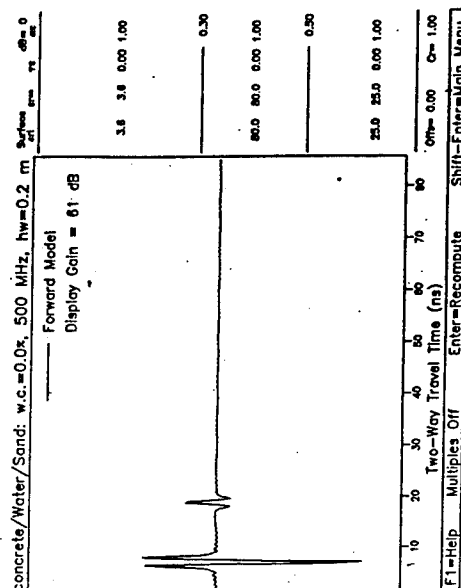
Case 233



Case 235

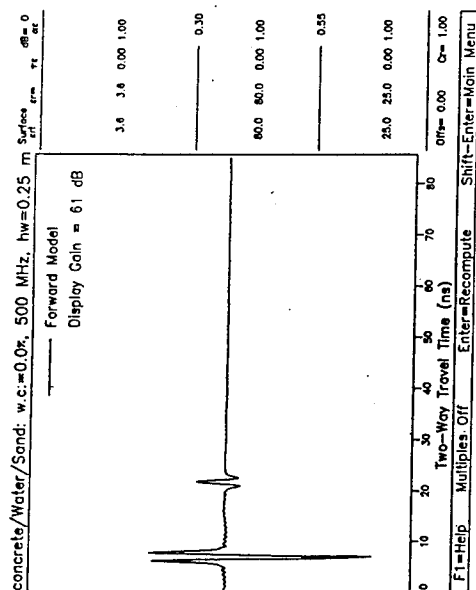


Case 234



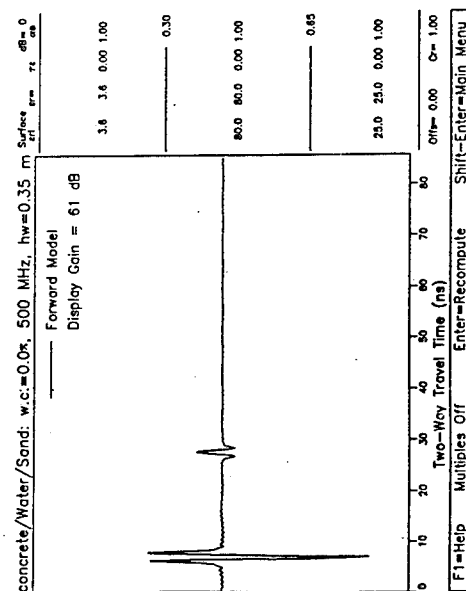
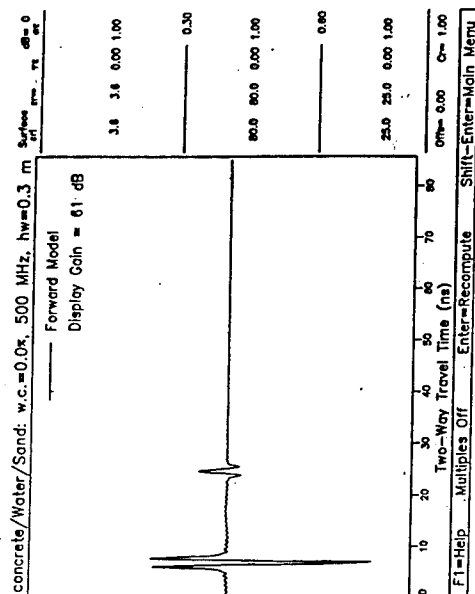
Case 236

Figure C50. Problem Set 2, Cases 233-236, multiples



Case 237

Case 238



Case 239

Case 240

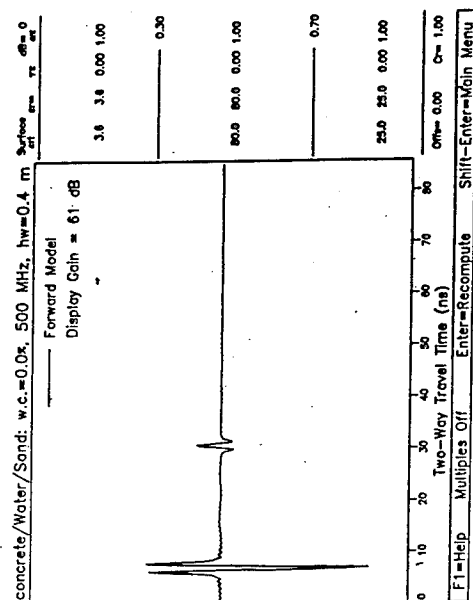
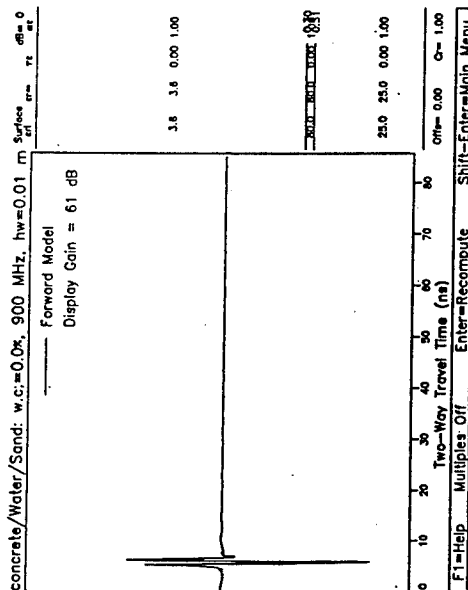
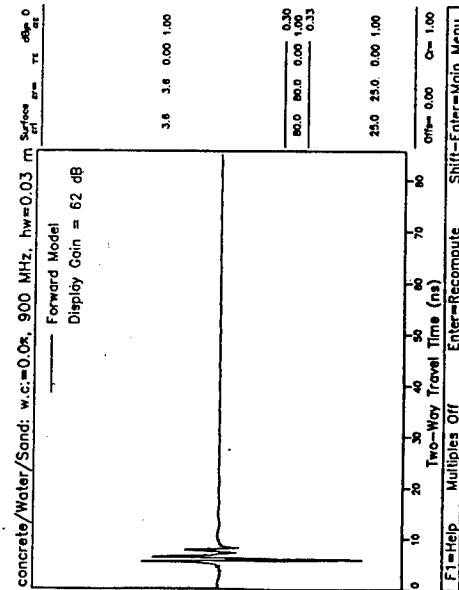


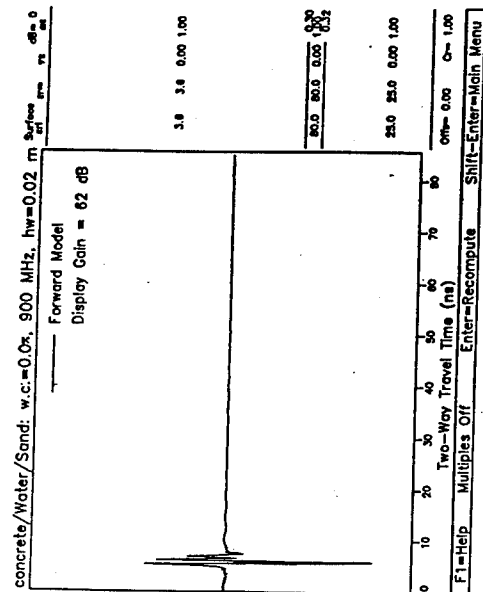
Figure C51. Problem Set 2, Cases 237-240, multiples



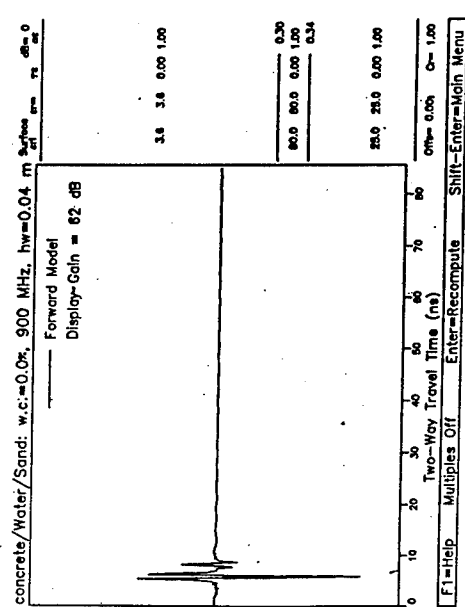
Case 241



Case 243

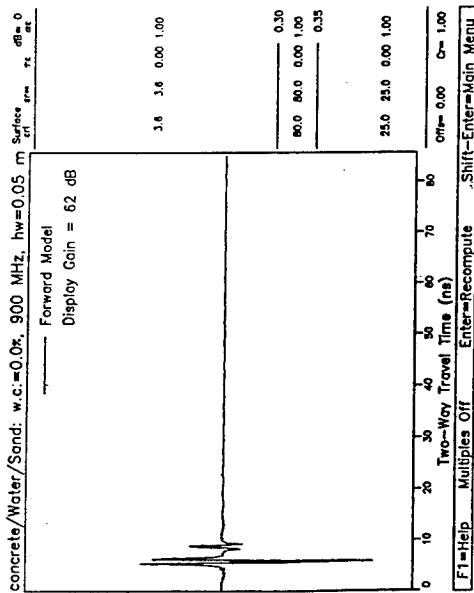


Case 242



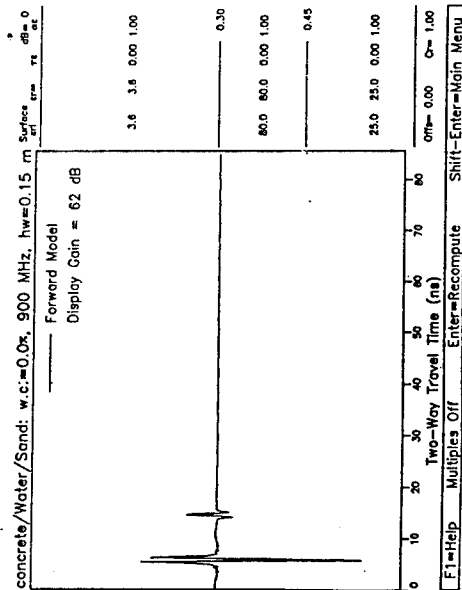
Case 244

Figure C52. Problem Set 2, Cases 241-244, multiples



Case 245

Case 246



Case 247

Case 248

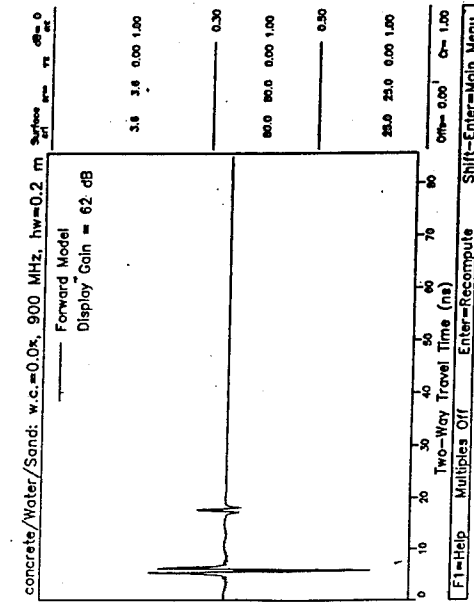
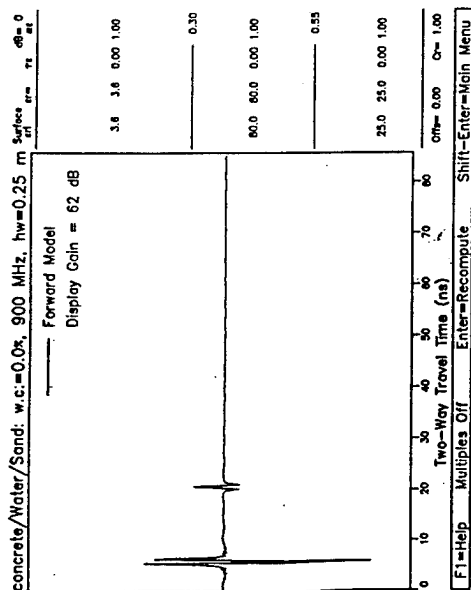
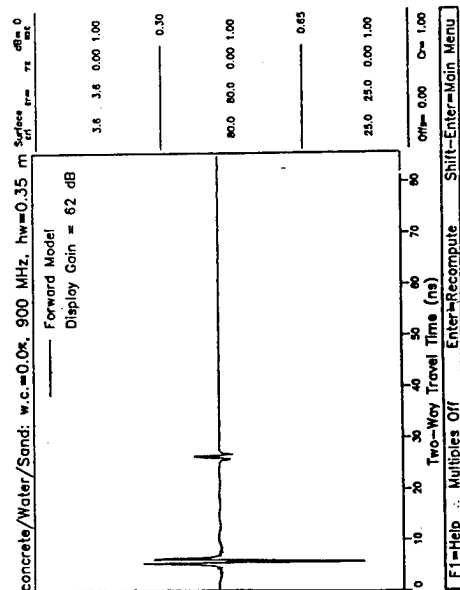


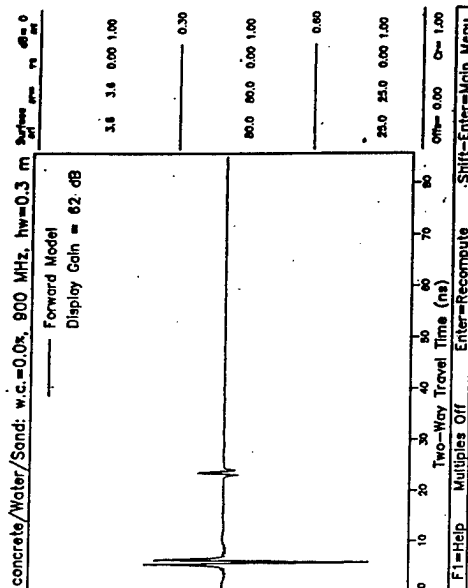
Figure C53. Problem Set 2, Cases 245-248, multiples



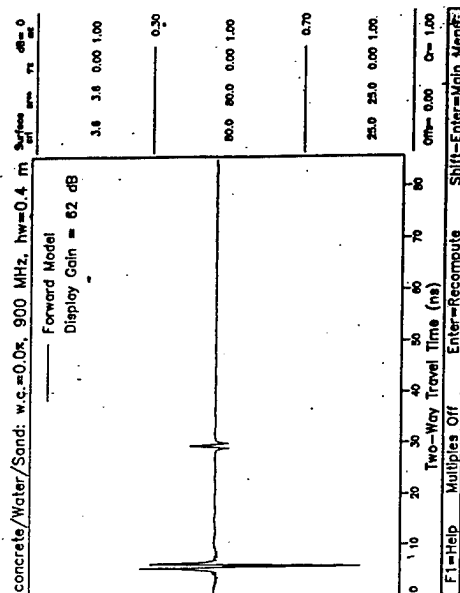
Case 249



Case 251



Case 250



Case 252

Figure C54. Problem Set 2, Cases 249-252, multiples

REPORT DOCUMENTATION PAGE

Form Approved
OMB No. 0704-0188

Public reporting burden for this collection of information is estimated to average 1 hour per response, including the time for reviewing instructions, searching existing data sources, gathering and maintaining the data needed, and completing and reviewing the collection of information. Send comments regarding this burden estimate or any other aspect of this collection of information, including suggestions for reducing this burden, to Washington Headquarters Services, Directorate for Information Operations and Reports, 1215 Jefferson Davis Highway, Suite 1204, Arlington, VA 22202-4302, and to the Office of Management and Budget, Paperwork Reduction Project (0704-0188), Washington, DC 20503.

1. AGENCY USE ONLY (Leave blank)		2. REPORT DATE September 1995		3. REPORT TYPE AND DATES COVERED Final report	
4. TITLE AND SUBTITLE Full Waveform Inverse Modeling of Ground Penetrating Radar Data: An Initial Approach				5. FUNDING NUMBERS	
6. AUTHOR(S) Janet E. Simms, Dwain K. Butler, Michael H. Powers					
7. PERFORMING ORGANIZATION NAME(S) AND ADDRESS(ES) U.S. Army Engineer Waterways Experiment Station, 3909 Halls Ferry Road, Vicksburg, MS 39180-6199; U.S. Geological Survey, Box 25046, MS 964, Denver, CO 80225-0046				8. PERFORMING ORGANIZATION REPORT NUMBER Miscellaneous Paper GL-95-4	
9. SPONSORING/MONITORING AGENCY NAME(S) AND ADDRESS(ES) Discretionary Research Program U.S. Army Engineer Waterways Experiment Station 3909 Halls Ferry Road, Vicksburg, MS 39180-6199				10. SPONSORING/MONITORING AGENCY REPORT NUMBER	
11. SUPPLEMENTARY NOTES Available from National Technical Information Service, 5285 Port Royal Road, Springfield, VA 22161.					
12a. DISTRIBUTION/AVAILABILITY STATEMENT Approved for public release; distribution is unlimited.				12b. DISTRIBUTION CODE	
13. ABSTRACT (Maximum 200 words) <p>Ground penetrating radar (GPR) surveys are often interpreted in a qualitative manner to identify anomalies. This method of interpretation is used to determine the existence of a feature when specific properties of the feature are of no interest. However, GPR data can also be interpreted quantitatively to give more definitive depths, geometry, and electromagnetic (EM) properties of the subsurface materials. Existing analysis procedures do not consider EM wave attenuation, dispersion, scattering, geometric spreading, or interface reflection/transmission losses. The aim of this research is to develop interpretation procedures which utilize the full GPR waveform for determining layer thicknesses and the EM properties of subsurface materials. The work consisted of three phases: 1) review existing capability for full waveform forward modeling of GPR signals, 2) develop a catalog of theoretical GPR receiver waveforms for representative layered models, and 3) examine the feasibility of developing an inverse modeling procedure to determine physical properties by comparing full waveform forward solutions to measured GPR signatures.</p>					
14. SUBJECT TERMS Geophysics Ground penetrating radar GPR Inverse modeling Inversion				15. NUMBER OF PAGES 133	
				16. PRICE CODE	
17. SECURITY CLASSIFICATION OF REPORT UNCLASSIFIED	18. SECURITY CLASSIFICATION OF THIS PAGE UNCLASSIFIED	19. SECURITY CLASSIFICATION OF ABSTRACT UNCLASSIFIED	20. LIMITATION OF ABSTRACT		